



Universidade Estadual de Campinas
Instituto de Geociências

JUAN SEBASTIAN LUNA OSORIO

3D GEOLOGICAL MODELING OF THE OLIGOCENE-MIOCENE TURBIDITE
SYSTEM IN THE EASTERN MARLIM OILFIELD, CAMPOS BASIN, BRAZIL

MODELAGEM GEOLÓGICA 3D DO SISTEMA TURBIDITICO OLIGOCENO-
MIOCENO NO CAMPO MARLIM LESTE, BACIA DE CAMPOS, BRASIL.

CAMPINAS

2017

JUAN SEBASTIAN LUNA OSORIO

3D GEOLOGICAL MODELING OF THE OLIGOCENE-MIOCENE TURBIDITE
SYSTEM IN THE EASTERN MARLIM OILFIELD, CAMPOS BASIN, BRAZIL

MODELAGEM GEOLÓGICA 3D DO SISTEMA TURBIDITICO OLIGOCENO-
MIOCENO NO CAMPO MARLIM LESTE, BACIA DE CAMPOS, BRASIL.

THESIS PRESENTED TO THE INSTITUTE OF
GEOSCIENCES OF THE UNIVERSITY OF CAMPINAS TO
OBTAIN THE DEGREE OF MASTER OF SCIENCE IN
GEOSCIENCES IN THE AREA OF GEOLOGY AND
NATURAL RESOURCES

DISSERTAÇÃO APRESENTADA AO INSTITUTO DE
GEOCIÊNCIAS DA UNIVERSIDADE ESTADUAL DE
CAMPINAS PARA OBTENÇÃO DO TÍTULO DE MESTRE
EM GEOCIÊNCIAS NA ÁREA DE GEOLOGIA E
RECURSOS NATURAIS

SUPERVISOR / ORIENTADOR: PROF. DR. ALESSANDRO BATEZELLI

ESTE EXEMPLAR CORRESPONDE À VERSÃO FINAL
DA DISSERTAÇÃO DEFENDIDA PELO ALUNO JUAN
SEBASTIAN LUNA OSORIO E ORIENTADO PELO
PROF. DR. ALESSANDRO BATEZELLI

CAMPINAS

2017

Agência(s) de fomento e nº(s) de processo(s): CNPq, 155607/2015-4

ORCID: <http://orcid.org/0000-0001-7367-3845>

Ficha catalográfica
Universidade Estadual de Campinas
Biblioteca do Instituto de Geociências
Marta dos Santos - CRB 8/5892

L971t Luna Osorio, Juan Sebastian, 1987-
3D Geological Modeling of the Oligocene-Miocene Turbidite System in the Eastern Marlim Oilfield, Campos Basin, Brazil / Juan Sebastian Luna Osorio. – Campinas, SP : [s.n.], 2017.

Orientador: Alessandro Batezelli.

Dissertação (mestrado) – Universidade Estadual de Campinas, Instituto de Geociências.

1. Campos petrolíferos - Campos, Bacia de (RJ). 2. Modelagem 3D. 3. Modelagem geológica. I. Batezelli, Alessandro, 1972-. II. Universidade Estadual de Campinas. Instituto de Geociências. III. Título.

Informações para Biblioteca Digital

Título em outro idioma: Modelagem Geológica 3D do Sistema Turbidítico Oligoceno-Mioceno no Campo Marlim Leste, Bacia de Campos, Brasil

Palavras-chave em inglês:

Oil fields - Campos Basin (Brazil)

3D modeling

Geological modeling

Área de concentração: Geologia e Recursos Naturais

Titulação: Mestre em Geociências

Banca examinadora:

Alessandro Batezelli [Orientador]

Emilson Pereira Leite

Lucas Verissimo Warren

Data de defesa: 16-08-2017

Programa de Pós-Graduação: Geociências



UNICAMP

**UNIVERSIDADE ESTADUAL DE CAMPINAS
INSTITUTO DE GEOCIÊNCIAS**

AUTOR: Juan Sebastian Luna Osorio

Modelagem geológica 3D do sistema turbidítico oligoceno – mioceno no campo
Marlim Leste, Bacia de Campos, Brasil

ORIENTADOR: Prof. Dr. Alessandro Batezelli

Aprovado em: 16 / 08 / 2017

EXAMINADORES:

Prof. Dr. Alessandro Batezelli - Presidente

Prof. Dr. Emilson Pereira Leite

Prof. Dr. Lucas Verissimo Warren

***A Ata de Defesa assinada pelos membros da Comissão Examinadora,
consta no processo de vida acadêmica do aluno.***

Campinas, 16 de agosto de 2017.

*“To my beloved wife Alexandra. For your
patience and understanding, for your kindness
and sacrifice you inspired me to be a better
person, thank you for always being by my side”*

ACKNOWLEDGMENTS

I would like to express my gratitude to my supervisor Prof. Dr. Alessandro Batezelli for his useful comments, remarks, and engagement through the learning process of this master thesis. Furthermore, I would like to thank Prof. Dr. Emilson Pereira Leite, Prof. Dr. Alessandra Davolio, and Prof. Dr. Lucas Warren for their valuable suggestions pointing towards to improve my MSc thesis.

As well, my special thanks to the Brazilian National Council for Scientific and Technological Development (CNPq) for the financial support, and the National Agency of Petroleum, Gas, and Biofuels of Brazil (ANP) for providing the dataset used in the current research.

I would like to thank my friends Wilmar Andres de la Hoz, Oscar Javier Acevedo, Taynah Buratto Rebelo, César Eduardo Herrera Quintero and Claudio Marinho for their feedback, cooperation and of course friendship. In addition, I would like to express my gratitude to the staff of the Institute of Geosciences for the last minute favors.

Last but not least, I would like to thank my family, my parents Hernando and Maria Helena, my sisters Helena and Sandra, and my brother Andres for supporting me spiritually throughout writing this thesis and my life in general.

BIOGRAPHY

Juan S. Luna O.

Geologist of the Industrial University of Santander (UIS) in Colombia (2012). Throughout his career, he has conducted different geological studies related to the oil and gas industry. In his undergraduate thesis project, he carried out an investigation entitled “Hydrocarbon potential of the Basal Calcareous Group in the Villanueva village, province of Santander, Colombia”; in association with the Research Group on Hydrocarbon and Coal Geology (GIGHC) of which he was a member since 2011 to 2013. The mentioned investigation was presented in a poster presentation at the International Conference and Exhibition of the American Association of Petroleum Geologists (AAPG–ICE) in Cartagena, Colombia, 2013. He worked at the same research group as a junior geologist until 2013 on a research project entitled “Geological model of the Campo Escuela Colorado oilfield, MMV, Colombia” where he developed seismic and well log interpretation, structural and stratigraphic correlations, and reservoir modeling aiming to develop a 3D reservoir characterization. The results of the mentioned investigation were presented in national conferences and one paper was published in a specialized index Geological Journal of Colombia. Furthermore, he developed different petroleum geochemical laboratory techniques such as analysis of Total Organic Carbon (%TOC), Rock Eval Pyrolysis and Vitrinite Reflectance (%Ro) in the same research group for different oil companies.

Later, he worked as a consultant at the Colombian Petroleum Institute of Ecopetrol S.A as a junior geologist in two research projects entitled “Occurrence, Distribution and Character of Hydrocarbon Source Kitchens in the Southern Foredeep of the Llanos Basin, Colombia”, and “Use of new technologies in the evaluation of the potential of heavy crude oil. Pilot study – Llanos Basin”, where he investigated the hydrocarbon potential of different source rocks in the Llanos and Eastern Cordillera sedimentary basins.

In 2014, he was selected in the “Young talents program” of Ecopetrol S.A, working in in the exploration department as seismic interpreter giving support to different research projects and developing tasks such as 2D-3D seismic and well log interpretation, petroleum systems modeling and petroleum geochemistry characterization in Llanos and Catatumbo sedimentary basins in Colombia.

In 2015, he started his MSc studies in Geosciences at the University of Campinas consolidating his knowledge in petroleum geology and geological modeling. Aiming to explain how it works the Oligocene-Miocene turbidite system in the Eastern Marlim oilfield located in the Campos Basin in Brazil; he carried out the application of sequence and seismic stratigraphy, 3D reservoir modeling and hydrocarbon volume calculations through the interpretation of seismic, stratigraphic and structural information; achieving a 3D model, which honored the geological setting of the study area

RESUMO

O campo petrolífero de Marlim Leste está localizado no nordeste da Bacia de Campos, e faz parte do Complexo de Marlim, uma das mais importantes acumulações de petróleo já descobertas no Brasil. Esta pesquisa apresenta métodos para caracterizar sistemas turbidíticos de águas profundas através de interpretações sedimentológicas e estratigráficas baseadas em correlações de poços, mapas de proporção e distribuição de areia, análise petrofísica, interpretação sísmica e de perfis de poços, e a partir da integração destas informações a criação de um modelo geológico 3D. Comumente, diferentes abordagens matemáticas e estatísticas são empregadas na modelagem estática de reservatórios, e apesar de apresentarem bons resultados carecem de informações geológicas. Sendo assim, o objetivo do presente trabalho foi obter um modelo geológico 3D levando em consideração diversas informações geológicas advindas da interpretação de diferentes dados visando atingir um resultado mais coerente com arcabouço estratigráfico da unidade e assim alcançar uma abordagem mais realista. A seção do Oligoceno-Mioceno estudada nesta pesquisa pertence à sequência E74 de Winter *et al.* (2007), que foi considerada uma sequência de segunda ordem no presente trabalho e que, por sua vez, faz parte do trato de sistema de mar alto (*HST*) de primeira ordem da Bacia de Campos. Como resultado, quatro principais litofácies foram identificadas em toda a seção. As fácies arenosas (Sm e Smcf) foram consideradas fácies reservatório e as demais, depósitos lamíticos (Sh) e calcário (M), constituem as fácies não-reservatório. A partir da análise de marcadores elétricos e/ou litológicos foram definidas três diferentes zonas denominadas de arenito inferior (LS), arenito médio (MS) e arenito superior (US). O arenito inferior (LS) marca os estágios iniciais de um ciclo de *HST*, instaurado após a formação da superfície de máxima inundação (MFS) que equivale ao chamado Marco Azul, um marco estratigráfico regional na Bacia de Campos. A zona referente arenito médio (MS) exhibe canais lateralmente amalgamados e verticalmente atribuídos a fluxos de turbidez de alta densidade que marcam os principais estágios do *HST*. Por fim, a zona do arenito superior (US), é representada por arenitos lateralmente amalgamados, que terminam em *pinch out* em direção à parte central e leste do campo, marcando os estágios finais do *HST*. Os mapas de proporção de areia e de distribuição das zonas definidas mostram feição na forma de lobo e estruturas de canais discretos. Ao longo do eixo dos canais estão as zonas de maior espessura dos arenitos, representando os canais de alimentação dos lobos distais. Assim, a presente pesquisa sugere pelo menos dois fluxos turbidíticos bipartidos que representam diferentes estágios de deposição relacionados a uma sequência turbidítica de águas profundas, inserida em um complexo de lobo submarino. Os corpos de arenitos turbidíticos amalgamados, maciços, não consolidados, exibem uma boa porosidade e continuidade lateral e vertical, representando excelentes reservatórios, como era esperado. Além disso, uma modelagem estrutural foi estabelecida mostrando que as feições seguem o estilo estrutural da bacia, sujeita a um regime de distensão associado à formação de falhas lítricas associadas à tectônica salina. Deste modo, todas as informações citadas foram incorporadas à modelagem geológica 3D (modelo estático), que se destaca pelo detalhamento das informações geológicas estabelecido nesta pesquisa, garantindo a confiabilidade, autodescrição e a qualidade dos métodos utilizados no atual estudo. Finalmente, os resultados desta pesquisa foram integrados com cálculos volumétricos de hidrocarbonetos, onde o modelo determinístico indicou pelo menos 3,774 bilhões de barris de óleo (Bbls) de volume original de óleo no reservatório (OOIP), e os modelos probabilísticos apontam valores variando entre 3.603 (P10), 3.678 (P50) e 3.763 Bbls (P90) exibindo uma ótima correspondência com as reservas comprovadas de hidrocarbonetos calculadas pela Agência Nacional de Petróleo, Gás Natural e Biocombustíveis (ANP).

Palavras-chave: Modelagem geológica 3D, Modelo estático, Campo de Marlim Leste, Complexo de Marlim, Bacia de Campos.

ABSTRACT

The Eastern Marlim oilfield located in the northeastern offshore of the Campos Basin is a portion of the Marlim Complex considered as one of the most important giant oil accumulations ever found in Brazil. This research presents findings and suggests methods for characterizing a deepwater turbidite system, offering sedimentological and stratigraphical interpretations based on well correlations, distribution and sand proportion maps, petrophysical analysis, well log and seismic interpretation, merged in a final 3D geological modeling. Commonly, different mathematical and statistical approaches are employed in static reservoir modeling, displaying excellent outcomes, but they need to be mixed with a strong geological background, aiming to firmly support the subsurface framework and achieve a more realistic approach. The Oligocene-Miocene section studied in this research belongs to the E74 sequence (second-order sequence in the present investigation) of Winter et al. (2007), which, in turn, is part of the first-order Highstand Systems Tract (HST) of the Campos Basin. As a result, four principal lithofacies were identified in the entire section, where two are eminently reservoir facies associated with sandy facies (Sm and Smcf lithofacies) and the remaining lithofacies are evidently non-reservoir facies represented by shaly and calcareous deposits (Sh and M lithofacies). As well, three different major zones were identified as Lower sandstone (LS), Middle sandstone (MS), and Upper sandstone (US), taking into account correlatable electric and/or lithological markers. The Lower Sandstone (LS) marks the early stages of an entire HST cycle, deposited after the deposition of the maximum flooding surface (MFS) associated with the regional Blue Marker of the Campos Basin. Regarding the MS, this zone displays laterally and vertically amalgamated channel features deposits attributed to high-density turbidity flows marking the principal stages of the HST. Lastly, the US zone, represented by laterally amalgamated sandstones, which pinch out toward the middle and eastern portion of the field, marking the final stages of the HST. The sand proportion and distribution maps of the mentioned zones exhibit lobe-shape features and discrete channelized structures. Along the axis of the channels, a thickest distribution of sandstones is present, representing distal lobes feeding channels. Thus, the current research suggests at least two bipartite turbiditic flows representing different stages of deposition related with a deep-water turbidite sequence, composing the elements of a submarine lobe complex. Turbiditic massive unconsolidated amalgamated sandstone bodies displaying very good porosity, as well as lateral and vertical continuity, represent most of this time interval representing excellent reservoirs, as it was expected. In addition, a structural modeling was established displaying and following the structural style of the Campos Basin, which is predominantly subject to a distensive regime, causing normal faults with listric geometry associated with salt tectonics. All the mentioned information was merged into a 3D geological modeling displaying outstanding accordance with the geological framework established in this research allowing for completeness, self-descriptiveness, and quality of standard descriptive methods conducted in the present oilfield. Finally, the outcomes of this investigation were integrated with volumetric hydrocarbon calculations to support the results. At least 3,774 billion barrels of oil (Bbls) of original oil in place (OOIP) were calculated by the deterministic model, and probabilistic models yields possibilities ranging from 3,603 (P10), 3,678 (P50), and 3,763 Bbls (P90) displaying a great match with the proven hydrocarbon reserves calculated by the Brazilian National Agency of Petroleum, Natural Gas and Biofuels (ANP).

Keywords: 3D geological modeling, static modeling, Eastern Marlim oilfield, Marlim Complex, Campos Basin.

TABLE OF FIGURES

Figure 1. Location map of the Marlim Complex in the Campos Basin, offshore, Brazil. Modified from Delgado (2017). A) Location map of the Campos Basin in the SE offshore Brazil displaying the localization of the Marlim Complex. B) Location map showing the three giant oilfields that compose the Marlim Complex (Marlim, Southern Marlim and Eastern Marlim, respectively).	20
Figura 2. Stratigraphic chart showing the three supersequences proposed by Winter et al. (2007) that compose the sedimentary fill of the Campos Basin.. In this work, the studied section contains amalgamated sandstones deposits overlying the Blue marker (Blue line in the chart) considered as a maximum flooding surface (MFS) in the entire Campos basin (Winter et al, 2007). As well, the studied interval is part of the first-order Highstand system tract (HST) (dashed red square) of the Campos Basin (Winter et al., 2007). The reservoirs studied in this article are of Early Oligocene to Early Miocene age, covering the entire time span of the E64 sequence (green square) proposed by winter et al. (2007) including the Ubatuba (Geribá Member), Carapebus, and Emborê (São Tomé and Grussaí Members) formations respectively. Modified from Winter et al., (2007).....	26
Figure 3. Regional setting of the Eastern Marlim oilfield, Campos Basin, Offshore, Brazil. Location of the Well-14 is shown in Figure 21. Total depth (TD) of the well: 4780 m, Aptian. Information used for the recognition of seismostratigraphic units and depositional surfaces includes unconformities, biostratigraphic ages, lithologies, well logs and stacking patterns.....	27
Figure 4. (A)Waning flow in which velocity (u) decreases with time (t). (B) Normal grading is the product of a waning flow from which deposition of coarse-grained material is followed by fine-grained material. Normal grading is the product of a single depositional event. Normal grading does not contain complex features, such as sudden vertical increase in grain size or floating granules and floating mudstone clasts. Modified from Weimer & Link (1991).	29
Figure 5. Diagram showing three increasing levels of detail in the field description of the unit of interest. Modified from Weimer & Link (1991).	30
Figure 6. A) Major architectural elements composing modern turbidite systems. B) Generic distribution of the architectural elements in the physiographic domains, from the continental shelf to the deep basin. Modified from Normark <i>et al.</i> (1983).	31
Figure 7. Specialized well-logging topics. Modified from Worthington <i>et al.</i> , (2007).....	35
Figure 8. Basic log set interpretation. Modified from Varhaug (2016).....	36
Figure 9. Marine seismic acquisition – pulses of sound energy penetrate the subsurface and are reflected back towards the hydrophones from rock interfaces. Modified from http://www.open.edu/openlearncreate/mod/page/view.php?id=41010	40
Figure 10. Basics of seismic and sequence stratigraphy of siliciclastic sequences. Modified from Abreu <i>et al.</i> , (2010).	41
Figure 11. Definition of porosity. Modified from Schön, (2015).....	42

Figure 12. Tendency of decreasing porosity related to a series of rocks. Modified from Schön (2015).	43
Figure 13. Calculated neutron-density crossplot: x-axis gives the neutron porosity for a limestone-calibrated tool; y-axis gives the bulk density. Lines are plotted for sandstone/quartz; limestone; dolomite. Modified from Schön (2015).	44
Figure 14. Left side: experimental variogram. Right side: model variogram fitted to the experimental variogram. Modified from Petrel E&P software platform of Schlumberger.....	48
Figure 15. Experimental and model variogram key parameters Modified from Petrel E&P software platform of Schlumberger.	49
Figure 16. Model built using the kriging algorithm (Deterministic). Modified from Petrel E&P software platform of Schlumberger.....	51
Figure 17. Model using the Sequential Gaussian algorithm (stochastic). Modified from Petrel E&P software platform of Schlumberger.....	52
Figure 18. 3D grid cells. Modified from Petrel E&P software platform of Schlumberger.	52
Figure 19. Measures of central tendency. Modified from Petrel E&P software platform of Schlumberger.	56
Figure 20. Percentiles. Modified from Petrel E&P software platform of Schlumberger.	56
Figure 21. Location map showing the available seismic and well log information provided by the ANP in the study area. A) Location map of the Campos Basin in the SE offshore of Brazil showing the localization of the Eastern Marlim oilfield. B) Location map of the Eastern Marlim oilfield showing the available seismic lines (2D and 3D) and well logs information utilized in the current research. ...	57
Figure 22. Mistie processing developed in the 2D and 3D seismic lines used in the current research project.....	59
Figure 23. Example of well-seismic tie processing developed in the well-12 located in the 3D seismic cube in the Eastern Marlim oilfield based on time-depth tables and check shots merged with density and sonic logs.	60
Figure 24. Example of a well section of the wel-7 showing the basic profile data set (GR, DT, NPHI, Resistivity-Deep, Permeability and porosity) used in the current research.....	61
Figure 25. Seismic and sequence stratigraphy analysis sequential methodology used in the current case study.	64
Figure 26. Geological modeling basis. Taken from Overeem (2008), University of Colorado at Boulder.....	65
Figure 27. Forward modeling (static model) methodology used in the current case study.....	66

Figure 28. Typical high seismic amplitude response (poststack time-migrated seismic lines/zero-phase American polarity/Black-Gray-white color scale) of the “Marlim sandstones” and Blue Marker in the study area. A) Interpretation of the 2D Seismic line 5 in W-E direction. B) Interpretation of the 2D Seismic line 6 in N-S direction.	68
Figure 29. Location map of the developed chronostratigraphic correlations based on the selected type wells that describes the principal characteristics of the Oligocene-Miocene reservoirs in the study area.	72
Figure 30. W-E oriented stratigraphic correlations (1 and 2) showing the type wells that describe the major zones (US: Upper Sandstone, MS: Middle Sandstone, LS: lower Sandstone) of the Oligocene-Miocene reservoirs in the Eastern Marlim oilfield.	73
Figure 31. W-E oriented stratigraphic correlations (3 and 4) showing the type wells that describe the major zones (US: Upper Sandstone, MS: Middle Sandstone, LS: lower Sandstone) of the Oligocene-Miocene reservoirs in the Eastern Marlim oilfield.	74
Figure 32. N-S oriented stratigraphic correlations (5, 6 and 7) showing the type wells that describe the major zones (US: Upper Sandstone, MS: Middle Sandstone, LS: lower Sandstone) of the Oligocene-Miocene reservoirs in the Eastern Marlim oilfield.	75
Figure 33. Seismic images displaying typical seismic amplitude response (poststack time-migrated seismic lines/zero-phase American polarity/seismic (default) color scale) of the US, MS and LS zones in the Eastern Marlim oilfield in: A) normal visualization, and, B) regular wiggle-trace imagery of seismic amplitude. 1) 2D seismic line 8 in S-N direction located in the northern portion of the study area displaying a suitable well-seismic tie. The three recognized major zones (US, MS and LS) of the Oligocene-Miocene section can be observed, as well as the Blue Marker (MFS) below them. 2) 2D seismic line 5 in W-E direction located in the middle portion of the Eastern Marlim oilfield displaying a suitable well-seismic tie. The MS and LS zones (absent of the US zone) of the Oligocene-Miocene section can be observed, as well as the Blue Marker (MFS) and top of the Eocene sandstones below them.	76
Figure 34. Sand proportion map of the Carapebus Formation (Oligocene-Miocene) in the Eastern Marlim oilfield. An increase of sand content (90-240m approximately) can be observed in the northern and middle portion of the study area.	79
Figure 35. A) Distribution map of the Lower Sandstone (LS) of the Carapebus Formation (Oligocene-Miocene) showing its extensive distribution in the Eastern Marlim oilfield. B) Presence of lobe features observed in the study area.	81
Figure 36. A) Distribution map of the Middle Sandstone (MS) of the Carapebus Formation (Oligocene-Miocene) displaying an increase in its thickness towards to the north and middle portion of the Eastern Marlim oilfield. B) Presence of channelized and lobe features observed in the study area.	82
Figure 37. A) Distribution map of the Upper Sandstone (US) of the Carapebus Formation (Oligocene-Miocene) displaying an increase in its thickness towards to the north portion of the Eastern Marlim oilfield. B) Pinch-out towards to the eastern and middle portion of the study area.	83

Figure 38. Example of petrophysical analysis based on lithotypes defined by the response of the Density-Neutron pair (RHOB - NPHI) and Gamma Ray (GR) log in the Well-6 of the Eastern Marlim oilfield. A) Crossplot of RHOB vs NPHI displaying a ternary diagram (dashed red triangle) with sandstones, shales, and limestones zones (red circles zones). B) Crossplot of RHOB vs NPHI vs GR showing the five petrophysical lithotypes identified in the Oligocene-Miocene interval of the Carapebus Formation (Clean Sandstones (Ss1), Muddy Sandstones (Ss2), Calcareous Sandstones (Ss-Lm), Calcareous (Lm), and finally Shaly (Sh) lithotypes). 85

Figure 39. Result obtained for the Shale Volume calculation (VSH) exemplified in the interpreted petrophysical lithotypes in the Well-6 of the Eastern Marlim oilfield. A) Histogram of the calculated VSH for the Carapebus Formation (Oligocene-Miocene). B) Table showing the identified lithotypes and the minimum and maximum values of VSH. C) Well-track of the Well-6 presenting the identified lithotypes and calculated VSH values (GR: gamma ray log (gAPI), VSH log (v/v)). 86

Figure 40. Effective porosity estimation (PHIE) for the interpreted petrophysical lithotypes in the Well-6 of the Eastern Marlim oilfield. A) Crossplot of PHIE calculated from the Sonic (PHIE_S) and the Density-Neutron pair (PHIE_ND) well logs. The Ss2 petrophysical lithotype displayed a marked difference between the calculated porosities. This difference was explained by the mineralogical composition of this lithotype that is associated with a calcareous-feldspathic composition. B) Well-track of the Well-6 presenting the identified lithotypes into the Gamma Ray track, a track of Sonic (DT), Neutron (NPHI), and Density (RHOB) logs, a track of effective porosity estimations (PHIE), and a track of effective porosity index (IPHIE). 87

Figure 41. Example of the final distribution of PHIE in the interpreted petrophysical lithotypes in the Well-6 of the Eastern Marlim oilfield. 88

Figure 42. RWe analysis for the formation of interest in the Well-6 of the Eastern Marlim oilfield... 89

Figure 43. Oil-water contact (OWC) seen at 2773m depth in the Well-6 in the Eastern Marlim oilfield. 89

Figure 44. Final model displaying: A) Elevation map, B) Sand proportion trends, C) Major zones, D) Sequence stratigraphic interpretation, and E) depositional/stratigraphic framework for the Oligocene-Miocene interval of the Carapebus Formation in the Eastern Marlim oilfield..... 92

Figure 45. Visualization, use and interpretation of different seismic attributes available in the library of the Petrel E&P software platform 2013 of Schlumberger (academic license), and generated from an available seismic line (seismic line 1) at normal phase (Seismic Default) in the Eastern Marlim oilfield. 94

Figure 46. Principal seismic facies representing the set of major seismic reflections patterns in the Eastern Marlim oilfield. 95

Figure 47. Seismic interpretation of the seismic line1 (normal phase/Black-Gray-white color scale) in the Eastern Marlim oilfield. A) Seismic Line in blank, B) Interpreted seismic horizons and faults, C) Interpreted tectonostratigraphic units, faults and depositional surfaces..... 98

Figure 48. Seismic interpretation of the seismic line2 (normal phase/Black-Gray-white color scale) in the Eastern Marlim oilfield. A) Seismic Line in blank, B) Interpreted seismic horizons and faults, C) Interpreted tectonostratigraphic units, faults and depositional surfaces..... 99

Figure 49. Seismic interpretation of the seismic line3 (normal phase/Black-Gray-white color scale) in the Eastern Marlim oilfield. A) Seismic Line in blank, B) Interpreted seismic horizons and faults, C) Interpreted tectonostratigraphic units, faults and depositional surfaces.....	100
Figure 50. Seismic interpretation of the seismic line 4 (normal phase/Black-Gray-white color scale) in the Eastern Marlim oilfield. A) Seismic Line in blank, B) Interpreted seismic horizons and faults, C) Interpreted tectonostratigraphic units, faults and depositional surfaces.....	101
Figure 51. Seismic interpretation of the seismic line 5 (normal phase/Black-Gray-white color scale) in the Eastern Marlim oilfield. A) Seismic Line in blank, B) Interpreted seismic horizons and faults, C) Interpreted tectonostratigraphic units, faults and depositional surfaces.....	102
Figure 52. Seismic interpretation of the seismic line 6 (normal phase/Black-Gray-white color scale) in the Eastern Marlim oilfield. A) Seismic Line in blank, B) Interpreted seismic horizons and faults, C) Interpreted tectonostratigraphic units, faults and depositional surfaces.....	103
Figure 53. Seismic interpretation of the seismic line 7 (normal phase/Black-Gray-white color scale) in the Eastern Marlim oilfield. A) Seismic Line in blank, B) Interpreted seismic horizons and faults, C) Interpreted tectonostratigraphic units, faults and depositional surfaces.....	104
Figure 54. Seismic interpretation of the seismic line 8 (normal phase/Black-Gray-white color scale) in the Eastern Marlim oilfield. A) Seismic Line in blank, B) Interpreted seismic horizons and faults, C) Interpreted tectonostratigraphic units, faults and depositional surfaces.....	105
Figure 55. Semi-regional seismic line (Line 1) showing A) the prograding clinoforms successions found at multiple stratigraphic levels in the study area, and B) the moment of change from predominantly carbonate to clastic deposition in the entire Campos Basin (shift between the TSU3 to TSU4).....	106
Figure 56. Location map of the developed structural correlations based on the 3D seismic cube that displays the better quality and describes the principal characteristics of the Oligocene-Miocene reservoirs at seismic scale in the study area.	107
Figure 57. Schematic structural correlation 1 developed in the Eastern Marlim oilfield.	108
Figure 58. Schematic structural correlation 2 developed in the Eastern Marlim oilfield.	109
Figure 59. Schematic structural correlation 3 developed in the Eastern Marlim oilfield.	109
Figure 60. Principal faults affecting the geometry of the 3D seismic cube in the study area. A) Time slice of the seismic cube without fault interpretation. B) Time slice of the seismic cube with fault interpretation. C) Cross-line and Strike-line seismic cube visualization without fault interpretation. D) Cross-line and Strike-line seismic cube visualization with fault interpretation. E) Structural and fault schematic model of the Eastern Marlim oilfield displaying a normal and listric normal fault system associated with a distensive regime affected by salt tectonics.	110
Figure 61. 3D static model workflow developed in the current case study.	111
Figure 62. Time-Depth conversion (average velocities vs interval velocities).	112

Figure 63. Time-Depth conversion of the Oligocene Miocene interval of the Carapebus Formation in the Eastern Marlim oilfield.	112
Figure 64. Time-Depth conversion match between the geological surfaces generated in time and transformed into depth units, versus the geological tops in depth of the formation of interest in the study area.	113
Figure 65. Example of the well scale up processing in the Well-6 in the study area.	114
Figure 66. Data analysis of the lithological facies in the distribution of the 3D model. A) Curve of vertical proportion. B) Variogram in principal direction. C) Variogram in minor direction. D) Variogram in vertical direction.	114
Figure 67. 3D facies modeling using the sequential indicator simulation (Gslib) method for the Oligocene-Miocene interval of the Carapebus Formation in the Eastern Marlim oilfield.	115
Figure 68. Facies codification and data analysis of the lithological facies observed in the interval of study in the current research. A) Facies codes of all interpreted facies. B) Variograms of the analyzed facies in the Oligocene-Miocene interval of the Carapebus Formation.	116
Figure 69. Distribution maps for the major lithological facies observed in the research area. A) Marl, B) Shale, C) Sandstone (clean), and D) Sandstone (muddy).	117
Figure 70. Fence diagram displaying a 3D view of the original facies distribution obtained using the Truncated Gaussian simulation method, following the trend of the four-chronostratigraphic sections in W-E direction and three sections in N-S direction.	118
Figure 71. 3D models of the petrophysical properties. A) Porosity. B) Water saturation.	119
Figure 72. Net to gross process developed in the generated volume (static model).	120
Figure 73. OOIP calculation (deterministic model) for the Eastern Marlim oilfield.	121
Figure 74. Probabilistic modeling for the Eastern Marlim oilfield.	121

TABLE OF CONTENTS

1. INTRODUCTION	19
2. OBJECTIVES	21
2.1 GENERAL OBJECTIVE	21
2.2 SPECIFIC OBJECTIVES	21
3. JUSTIFICATION	22
4. THEORETICAL FRAMEWORK.....	23
4.1 STATE OF THE ART	23
4.2 REGIONAL SETTING	25
4.3 TURBIDITE SYSTEMS	28
4.3.1 Elements of Turbidite Systems.....	32
4.4 WELL LOG INTEPRETATION	35
4.4.1 Spontaneous Potential	36
4.4.2 Resistivity Logs.....	37
4.4.3 Porosity Logs.....	37
4.4.4 Gamma Ray Log.....	38
4.5 SEISMIC INTERPRETATION	40
4.6 SEISMIC-SEQUENCE STRATIGRAPHY	41
4.7 RESERVOIR CHARACTERIZATION.....	42
4.7.1 Porosity	42
4.7.2 Fluids in the pore space – Saturation and Bulk Volume fluid	44
4.7.3 Permeability	45
4.8 GEOSTATISTICS.....	46
4.8.1 Rock Property Modeling.....	46
4.8.2 Property Modeling	46
4.9 MODELING PROCESS	50
4.9.1 Geometrical modeling.....	50

4.9.2	Petrophysical modeling.....	50
4.9.3	Facies modeling.....	50
4.9.4	Deterministic algorithm.....	51
4.9.5	Stochastic algorithm.....	51
4.9.6	Upscaling of well log properties	52
4.9.7	Fault analysis.....	53
4.10	HYDROCARBON VOLUME CALCULATION.....	54
4.10.1	Estimation methods	54
5	MATERIALS AND METHODS	57
5.1.	SEISMIC AND WELL DATA	58
5.2.	MISTIE CORRECTION	58
5.3.	SEISMIC-WELL TIE	60
5.4.	SEISMIC INTERPRETATION	60
5.5.	WELL LOG INTEPRETATION	61
5.6.	LITHOFACIES CHARACTERIZATION, STRATIGRAPHICS CORRELATIONS, DISTRUBUTION AND SAND PROPORTION MAPS	62
5.7.	PETROPHYSICAL ANALYSIS BASED ON LITHOTYPES	62
5.8.	SEISMIC AND SEQUENCE STRATIGRAPHY ANALYSIS.....	63
5.9.	3D GEOLOGICAL MODELING - RESERVOIR CHARACTERIZATION	65
5.10.	HYDROCARBON VOLUME CALCULATION.....	67
6.	RESULTS.....	68
6.1.	LITHOFACIES DESCRIPTIONS AND INTERPRETATION	68
6.1.1	Reservoir facies.....	69
6.1.2	Non-reservoir facies.....	70
6.2	STRATIGRAPHIC FRAMEWORK	72
6.2.1	Stratigraphic correlations	72
6.2.2	Lower sandstone (LS).....	77
6.2.3	Middle sandstone (MS).....	77

6.2.4	Upper sandstone (US).....	78
6.3	DISTRIBUTION AND SAND PROPORTION MAPS.....	78
6.4	PETROPHYSICAL ANALYSIS BASED ON LITHOTYPES	84
6.4.1	Petrophysical lithotypes interpretation.....	84
6.4.2	Petrophysical properties estimation.....	85
6.5	DEPOSITIONAL AND STRATIGRAPHIC MODEL.....	90
6.6	SEISMIC INTERPRETATION	93
6.6.1	Seismic attributes.....	93
6.6.2	Seismic stratigraphy analysis.....	95
6.6.3	Tectonostratigraphic units.....	96
6.7	STRUCTURAL AND FAULT MODELING	107
6.7.1	Structural Correlations:	108
6.8	3D GEOLOGICAL MODELING (STATIC MODEL)	111
7.	FORWARD MODELING LIMITATIONS	122
7.1	STRATIGRAPHIC FRAMEWORK.....	122
7.2	PETROPHYSICAL MODELING.....	122
7.3	SEISMIC INTEGRATION	122
7.4	3D GEOLOGICAL MODELING	122
8.	DISCUSSION	123
8.1	STRATIGRAPHIC AND DEPOSITIONAL MODEL.....	123
8.2	PETROPHYSICAL MODELING.....	123
8.3	STRUCTURAL MODELING.....	124
8.4	3D GEOLOGICAL MODELING (STATIC MODEL)	125
9.	CONCLUSIONS	127
10.	REFERENCES.....	130

1. INTRODUCTION

Geological modeling is the most common tool from exploration and production geologists to represent through computerized representations portions of subsurface Earth's crust based on geophysical and geological observations. These models are highly regarded as one of the most important geological methods for reservoir simulations in hydrocarbon development. The application of this technique embrace an integrated approach based on different disciplines such as stratigraphy, sedimentology, structural geology, biostratigraphy, geophysics, petrophysics, geostatistics, and so on (Yarus & Chambers 1994, Casar-González, R. et al., 2012). All the mentioned disciplines collaborate in a common workspace aiming to establish tridimensional geological simulations.

According to Overeem (2008), a static reservoir modeling has a strict relationship between data-driven modeling and process modeling data. As stated by the same author, different mathematical and geostatistical approaches are used in reservoir modeling, but they need to be mixed with a geological background, because mathematics and geostatistics are very powerful geological modeling tools, but only when they are firmly supported by geological knowledge achieve a realistic approach. Thus, a geological model should include information from several sources taking into account that more information provides a better description and understanding of the reservoir. There are some investigations related to this kind of research trying to simulate and quantify the geometry and spatial distribution of hydrocarbon reservoirs and the continuity of flow units using geological and geostatistical approaches (Baldissera, 1992; Cosentino, 2001, Ravenne et al., 2002, Ravenne, 2002a, Ravenne, 2002b, Posamentier & Kolla, 2003, Bessa F., 2004, Mata-Lima, 2005, Doligez et al., 2007, Qi et al. 2007, Lee et al., 2007, Remacre et al., 2008, Azevedo, 2009, Azevedo et al. 2010, Caetano 2012, Correia, 2014, Casar-González, R et al., 2012, Correia, 2015). The methodology used in this study is similar to the one used in the mentioned investigations, but focused and sustained by a robust geological approach point toward to achieve a more realistic tridimensional reservoir model.

The current research aims at establishing the 3D geological modeling of the Oligocene-Miocene turbidite system in the Eastern Marlim oilfield located in the Marlim Complex in the Campos Basin, southeastern offshore of Brazil (Fig. 1). The scope of this investigation is to develop a representative “static model” merging geological and geostatistical simulation methods, providing a realistic approach based on the application of seismic interpretation, well log analysis, sedimentology, stratigraphy, petrophysics, and

geostatistics, combined in a three-dimensional model honoring the geological features observed in the research area. The conclusions obtained by this study explain the geological configuration of the Eastern Marlim oilfield contributing to the understanding of the petroleum geology of Brazil and identifying heterogeneities of depositional systems of turbidite reservoirs.

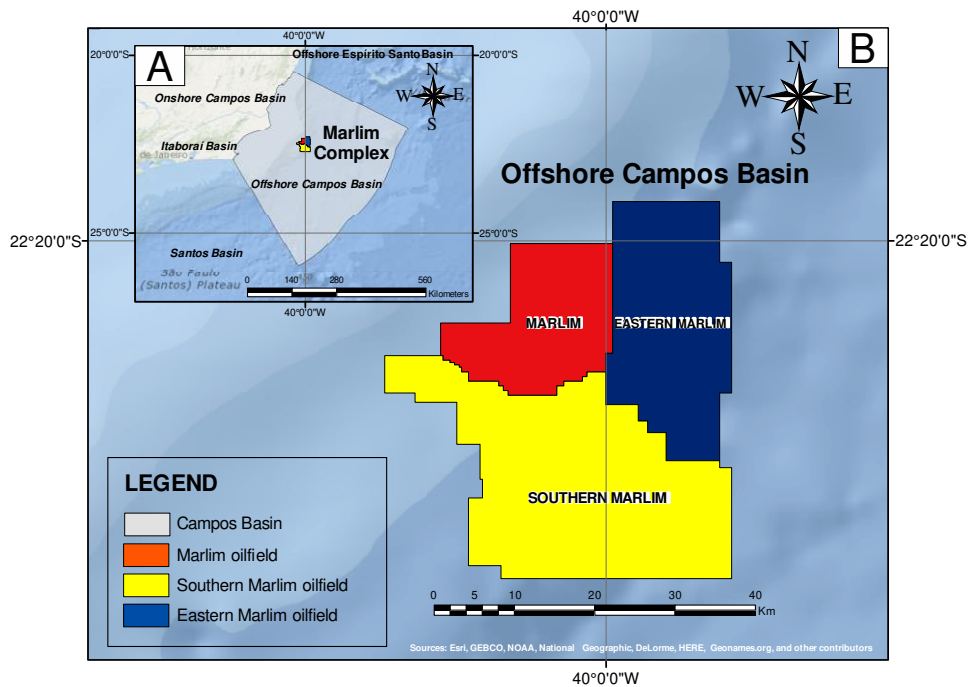


Figure 1. Location map of the Marlim Complex in the Campos Basin, offshore, Brazil. Modified from Delgado (2017). A) Location map of the Campos Basin in the SE offshore Brazil displaying the localization of the Marlim Complex. B) Location map showing the three giant oilfields that compose the Marlim Complex (Marlim, Southern Marlim and Eastern Marlim, respectively).

Finally, the results obtained in the current research are going to be published in specialized index journals (e.g. Marine and Petroleum Geology, Journal of Petroleum Geology, Petroleum Geoscience, etc.) as two research articles entitled:

- 1- *“Stratigraphic framework and petrophysical analysis of Oligocene-Miocene turbidites systems in SE Brazil. Case study: Eastern Marlim oilfield, Campos Basin, Brazil”*.
- 2- *“3D geological modeling and calculation of reserves of the Oligocene-Miocene turbidite system in the Eastern Marlim oilfield, Campos Basin, Brazil”*.

2. OBJECTIVES

2.1 GENERAL OBJECTIVE

- Develop a 3D geological model of the Eastern Marlim oilfield located in the Marlim Complex in the Campos Basin, southeastern offshore of Brazil.

2.2 SPECIFIC OBJECTIVES

- Generate lithofacies profiles incorporating cuttings and core descriptions, and accompanying well logging interpretation.
- Analyze facies and rock properties relationships to determine major lithofacies controlling the behavior and reservoir quality of the studied section.
- Establish the stratigraphic and structural framework of the Eastern Marlim oilfield based on stratigraphic, sedimentological, seismic and well log information.
- Determine reservoir quality from cuttings and core analysis reports and the relationships between rock properties from core measurements.
- Perform petrophysical analysis based on lithotypes determining porous-permeable and net pay intervals within the Oligocene-Miocene reservoirs of the Carapebus Formation.
- Approximate the geological framework of the research area through gridded reservoir static models.
- Develop multiple static models based on reasonable geological and petrophysical interpretations.
- Integrate petrophysical characteristics and conceptual geological models in the study area looking forward to support hydrocarbon volume calculations.

3. JUSTIFICATION

Limited data, private information and/or unpublished studies related with geological modeling in the Campos Basin located in the southeastern offshore of Brazil, restrict the knowledge, importance and understanding of this kind of research. In this manner, it is required to encourage the development of this type of investigations to enhance the quantity and quality of information of reservoir simulation data in the petroleum geology field. Thus, knowing the geological framework and the heterogeneities of depositional systems of turbidite reservoirs, and addressing a coherent static model in the Eastern Marlim oilfield, the current research contributes to the construction of a representative geological model that can be used as an analog in other research areas of interest in the Campos Basin, Brazil.

4. THEORETICAL FRAMEWORK

4.1 STATE OF THE ART

According to De Jager (2012), the first geological model can be said to have been created implicitly by Darcy (1856). Although his experiments described flow in a homogeneous layer, he produced cross sections of an aquifer tapped by an artesian well, therefore implicitly differentiating between an aquifer and an impervious layer (De Jager, 2012). Consistent with the same author, other early work was done by Dupuit (1857), who extended Darcy's law to homogeneous natural aquifers. Subsequent, as cited by Terry & Rogers (2014), Fancher et al. (1933) made one of the earliest petrophysical studies of reservoir rocks, and Wycoff et al. (1934) developed a method for measuring the permeability of reservoir rock samples based on the fluid flow equation discovered by Darcy (1856). Later, Theis (1935) used well data to obtain average rock properties (De Jager, 2012). As well, Wycoff & Botset in 1936 made a significant advance in their studies of the simultaneous flow of oil/water, and gas/water in unconsolidated sands (Terry & Roger, 2014). According to the same authors, this work was later extended to consolidated sands and other rocks, and Leverett & Lewis (1941) reported research on the three-phase flow of oil, gas, and water (Terry & Rogers (2014).

During the 1960s, the terms reservoir simulation and reservoir mathematical modeling became popular (Terry & Rogers, 2014). According to the same authors, these terms are synonymous and refer to the ability to use mathematical formulae to predict the performance of an oil or gas reservoir. Reservoir simulation was aided by the development of large-scale, high-speed digital computers, and sophisticated numerical methods were also developed to allow the solution of a large number of equations by finite-difference or finite-element techniques (Terry & Rogers, 2014). Then, geostatistical methods such as two-point stochastic modeling techniques were used to interpolate data between two or more measurement points. In this way, Kriging was earliest technique, developed by Matheron (1963) based on the work of Krige in 1951 (De Jager, 2012). In the 70's, geological modeling mainly consisted of automatic 2D cartographic techniques such as contouring, implemented routines communicating directly with plotting hardware (Mallet et al, 1989). As cited by De Jager (2012), after the success of the first object-based models by Haldorsen & Chang (1986), pixel-based techniques were developed which also allowed discontinuous facies to be modeled. As a first technique, Disjunctive Kriging was introduced as early as the 1970s

(Matheron, 1973), but it was not until the 1980s that discontinuous facies modeling was popularized with the Indicator Kriging method (Journel, 1983). In the same year, Matheron proposed the Gaussian Threshold model (Matheron et al. 1983), where a facies is assigned based on where the value of a site falls within user-defined threshold values. For many types of reservoir, these Gaussian methods are very well suited, for instance where heterogeneities are defined by differences in cementation or ore abundance. However, more complex facies relationships cannot be modeled as well as complex geometries such as curvilinear structures, such as found in fluvial and submarine channel systems (De Jager, 2012). The arrival of workstations with 3D graphics capabilities during the 80's gave birth to a new generation of geological modeling software with graphical user interface, which became mature during the 90's. Since its inception, geological modeling has been mainly motivated and supported by oil and gas industry. In this way, Sequential Gaussian Simulation and Truncated Gaussian Simulation are used as the most common techniques in reservoir modeling (Deutsch 2002).

Currently, the role of the geological model in the oil and gas industry is essential and seems to continue from coming years. Realistic geological models are required as an input to reservoir simulator programs. A reservoir could be developed and produced if a coherent geological model or “static model” was developed. Using geological models and reservoir simulations, reservoir engineers can identify which recovery options offer the safest, economic, efficient and effective development plan for a particular reservoir, process known as “dynamic model”. In this way, the challenges that face the geologists and reservoir engineers are to provide more seamless interaction between static and dynamic models (Robinson et al, 2007). A comprehensive geological modeling uses all available information and embrace different process that controls the storage and production capacity of oil and gas reservoirs. The adequate description of reservoir properties includes from geological descriptions at basin scale, rock types and facies distribution, environmental deposition and processes, geometry of the bodies that make up the reservoir, to its petrophysical properties at reservoir scale, such as porosity, permeability, water saturation, etc. These data come from various sources of information, such as regional geological studies, exploration wells, seismic surveys, well log and seismic interpretation, core samples, drill cuttings, production data, etc. Different geostatistical and petrophysical-based models are created through numerical and statistical models trying to simulate and represent the results of all the mentioned information. Therefore, these models try to be consistent with the conceptual idea of the geological setting and honor all the available information.

4.2 REGIONAL SETTING

The Campos Basin is located on the north coast of the State of Rio de Janeiro and on the southern portion of the State of Espírito Santo, bounded to the north by the Arc of Vitória and to the south by the Arc of Cabo Frio, with an approximate area of 100,000 km². Its completion is based on the gneisses of the Proterozoic Province of Ribeira, and is divided into three tectonic phases, called as Rift Super-Sequence, Post-Rift Super-Sequence and Drift-Super Sequence (Winter et al., 2007), or according to Cainelli & Mohriak (1999) known as continental, transitional and marine depositional mega-sequences respectively (Fig. 2).

Different seismic surveys and exploratory wells collected during almost thirty years of petroleum exploration in Brazil have contributed to the recognition of four tectono-stratigraphic units in the Eastern Marlim oilfield (Fig. 3). The lowest sequence consists of Neocomian clastics sediments deposited on basalts dated at 120-130 Ma (Mohriak et al., 1990), which was generated in the beginning of the rift tectonic evolution of the basin.

Consecutively, the Barremian-Aptian sequence marks the continental rift and transitional stages, characterized by organic-rich carbonate mudstones deposited in lacustrine environments, and evaporitic deposits.

Successively, a passive margin tectonic evolution begins with an open-marine environment in the Albian-Cenomanian period, represented by a thick sequence of post rift carbonates represented by organic rich calcareous rocks, locally with clastic input, which grades upwards and basin wards into deep-water marls and shales.

Finally, a marine Upper Cretaceous to Recent clastic section was deposited, recording a phase characterized by thermal subsidence with some residual halokinetic activity that increases in intensity towards deeper waters.

The principal reservoirs of the Eastern Marlim oilfield are related to a deep-water turbidite system generated in the Cretaceous-Recent tectono-sequence (marine regression) corresponding to the Carapebus Formation (Campos Group) (Fig. 3). Schaller (1973) defined first as Carapebus Member, and later Rangel et al. (1994) designate as Carapebus Formation constituted by fine grained to conglomerate sandstones interbedded with pelitic deposits of the Ubatuba Formation.

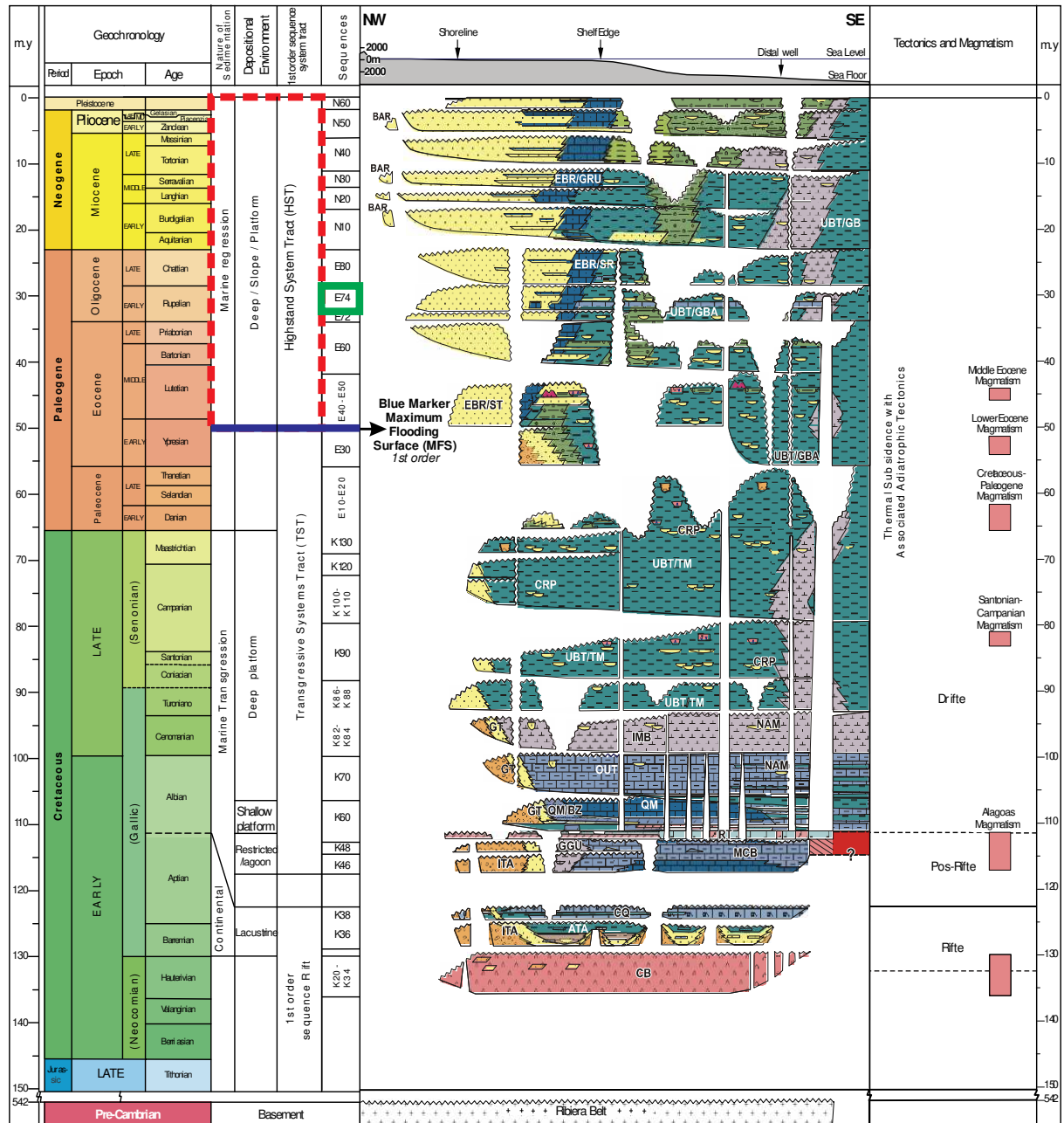


Figura 2. Stratigraphic chart showing the three supersequences proposed by Winter et al. (2007) that compose the sedimentary fill of the Campos Basin.. In this work, the studied section contains amalgamated sandstones deposits overlying the Blue marker (Blue line in the chart) considered as a maximum flooding surface (MFS) in the entire Campos basin (Winter et al, 2007). As well, the studied interval is part of the first-order Highstand system tract (HST) (dashed red square) of the Campos Basin (Winter et al., 2007). The reservoirs studied in this article are of Early Oligocene to Early Miocene age, covering the entire time span of the E64 sequence (green square) proposed by winter et al. (2007) including the Ubatuba (Geribá Member), Carapebus, and Emborê (São Tomé and Grussaí Members) formations respectively. Modified from Winter et al., (2007).

4.3 TURBIDITE SYSTEMS

According to Weimer & Link (1991), turbidites are deposits accumulated by turbidity currents into deep-waters. The main agent of deposition is the gravitational energy that provides sediment transport in behalf of the continental shelf, slope and abyssal plain. In submarine basins can cover many km² and can be deposited at least 100km or more of the margin of the platform. They are characterized by the presence of allochthonous shallow wildlife interbedded with silt, clay and deepwater sediments reworked by the background current deposits. Submarine fans and turbidite systems are the major petroleum reservoirs in many sedimentary basins worldwide (Weimer & Link, 1991). More than 80 sedimentary basins contain major petroleum-producing submarine fan deposits; and these reservoirs produce from a variety of structural, stratigraphic, and combined traps. Reservoir properties in turbidite systems are variable and ultimately controlled by grain size, sorting, diagenesis, and areal distribution. The best turbidite reservoirs are medium-to coarse-grained, moderate to well sorted, with little cementation and diagenetic effects.

A turbidite system is defined as a body of genetically related mass flow and turbidity current facies and facies associations that were formed in virtual stratigraphic continuity (Mutti & Normark, 1987). This definition includes reservoirs that are associated with submarine canyons, deep-water carbonate-related deposits, slope-related turbidite systems, prodelta turbidites, and lacustrine turbidite deposits (Weimer & Link, 1991). The terminology of depositional environments and units within submarine fan and turbidite systems has been probably the single most debated topic when discussing deep-water systems (e.g. Nelson *et al.*, 1977; Nilsen, 1980; Normark, 1980; Walker, 1980; Mutti and Normark, 1987). During the 1960s and 1970s, facies-related terms such as "upper, middle, lower vs. inner, middle, outer fan;" "distal vs. proximal turbidite;" "flysch vs. turbidite" were hotly debated; most of these differences in terminology are now resolved. Terms under debate generally fall into three categories: (1) specific features, their positions and relations with other fan segments, such as depositional lobe vs. fan lobe; (2) depositional processes, such as levee/overbank vs. contourite/bottom-reworked processes; and (3) appropriate models or concepts, such as basin-floor fans vs. type I turbidite system (Mutti, 1985; Posamentier et al).

Kuenen & Migliorini (1950), and Kuenen (1957) introduced the concept of normal grading for turbidites deposited by a single waning turbidity current. In a waning flow, velocity (u) decreases with time (t). As a result, a waning flow would deposit coarse-grained material first followed by fine-grained material, causing a normal grading (Fig. 4). The term "normal grading" has lost its original process-sedimentological meaning for a single

depositional event. In other words, one can manufacture normal grading in a depositional package, composed of multiple depositional events, by selectively designating a coarse bottom unit and a fine top unit in arriving at a desired outcome. Such a “normal grading” is sedimentologically meaningless (Weimer & Link, 1991).

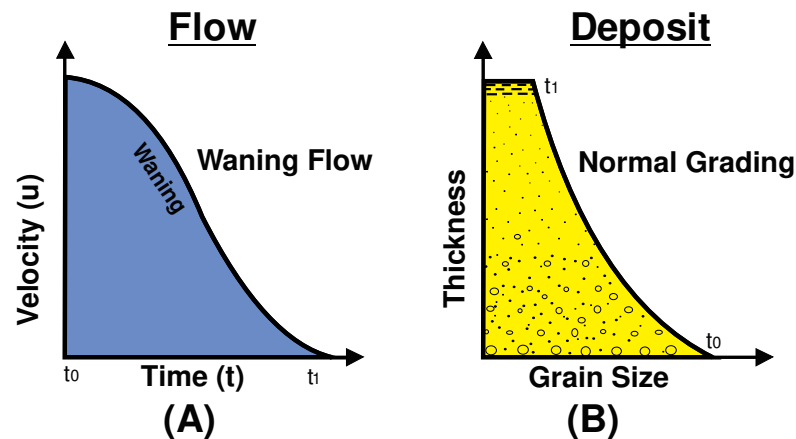


Figure 4. (A) Waning flow in which velocity (u) decreases with time (t). (B) Normal grading is the product of a waning flow from which deposition of coarse-grained material is followed by fine-grained material. Normal grading is the product of a single depositional event. Normal grading does not contain complex features, such as sudden vertical increase in grain size or floating granules and floating mudstone clasts. Modified from Weimer & Link (1991).

Bouma (1962), created a model known as the “Bouma Sequence” describing a turbidite sequence composed by sedimentary structures occurring in sedimentary rocks deposited in areas of deep-water sedimentation. In theory, a complete Bouma sequence comprises sediments that fine upwards, consisting of a lowermost layer of coarse-grained, chaotic clastic sediments deposited under conditions of high depositional energy overlain by successively finer grained and better stratified sediments like sands and muds deposited under calmer conditions. In practice, however, the chaotic, high-energy nature of turbidite deposition can alter or remove underlying sediments so that incomplete sequences of sediments typically remain preserved.

According to Weimer & Link (1991), other discussion exist in the turbidite systems. For example, the same unit could be described and interpreted differently by different workers, and is dependent for the degree of detail observed in the field. Figure 5, show different scenarios with variations in the degree of detail.

The Level 1 exhibits the least amount of detailed (Fig. 5, Level 1). This section of interest can be described as a simple “normally graded” bed, but with the most amount of

detail the same unit can also be described as “amalgamated” (Fig. 5, Level 3,). The significance of these differences in detail is that the level 1 description would ignore pockets of gravels and inverse grading, whereas the level 3 descriptions would include pockets of gravels and inverse grading. On the other hand, Level 2 represents an intermediate degree of detail (Fig. 5, Level 2). As a result, the Level 1 description would result in an interpretation of the unit as deposit of a single waning turbidity current, whereas the Level 3 description would result in an interpretation of the unit as deposits of multiple depositional events by sandy debris flows and bottom currents.

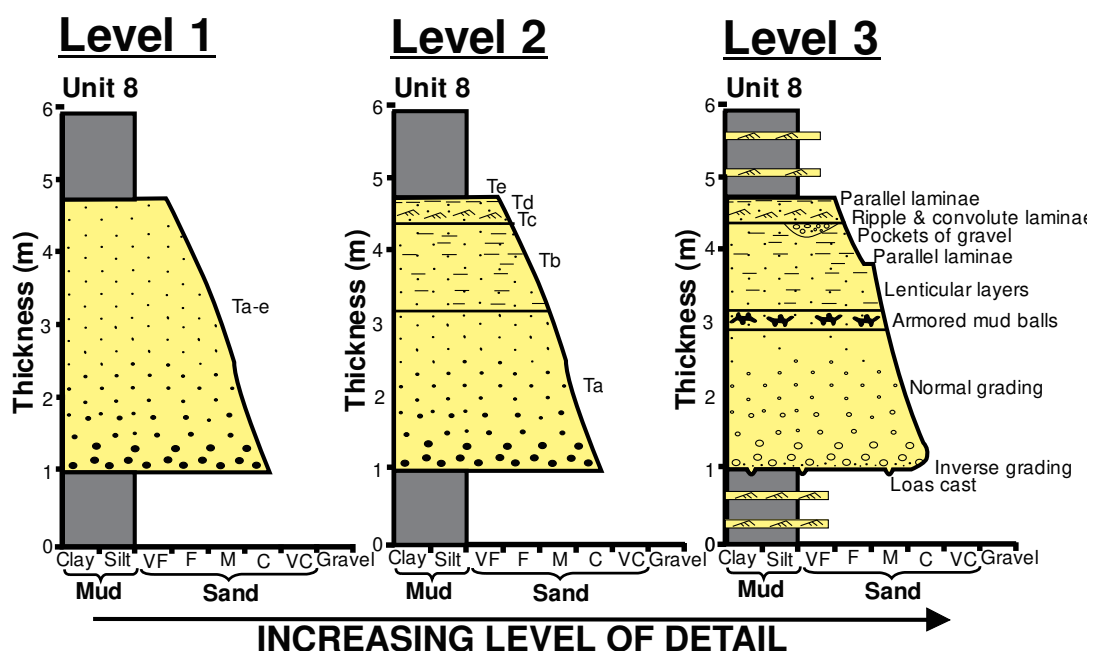


Figure 5. Diagram showing three increasing levels of detail in the field description of the unit of interest. Modified from Weimer & Link (1991).

Turbidite systems can occur in any tectonic setting. Concerning the current research, the tectonic setting related is a salt-influenced passive margin. Salt associated with passive margins was deposited during rifting events. Salt has considerable variability in its deformational styles, which reflects the nature and evolution of the passive margin, and the salt response to regional stresses (Jackson & Talbot, 1986).

In the Brazilian Atlantic margin, turbidite deposits occur above or adjacent to salt pillows. The Upper Cretaceous/Eocene Namorado Field formed in the Campos Basin is associated with the movement of a salt pillow (Bacoccolli et al., 1980; Peres and Arso, 1986).

On the other hand, the Oligocene turbidite reservoirs of the giant Marlim Complex (which contains the Eastern Marlim oilfield, the target of this study) and Albacora

fields, also located in the Campos Basin, were deposited in deep waters and are underlain by salt pillows. The main topographic low area created the accommodation space and deposition of these turbidite reservoirs, where the greatest accumulation of turbidites was deposited. Later salt movement created structural traps, as well as migration paths for oil generated at greater depths in the syn-rift source rocks (Peres & Arso, 1986; Bacoccolli & Toffoli, 1988; Guardado *et al.*, 1990; Carminatti & Scarton). Turbidite systems probably contain the elements that best reflect the occurrence of long distance particle transport by gravity flows. Slumps, turbidity flows and mass flows/debris flows are the most frequent processes that contribute to the construction of the architectural elements (Normark & Piper, 1979; May *et al.*, 1983; Farre *et al.*, 1983; Hagen *et al.*, 1994; Pratson & Coakley, 1996). Flood-generated gravity flows, or hyperpycnal flows, and dense shelf water cascading episodes can occur (Lastras *et al.*, 2007). The most important processes affecting deep clastic systems are summarized in Figure 6.

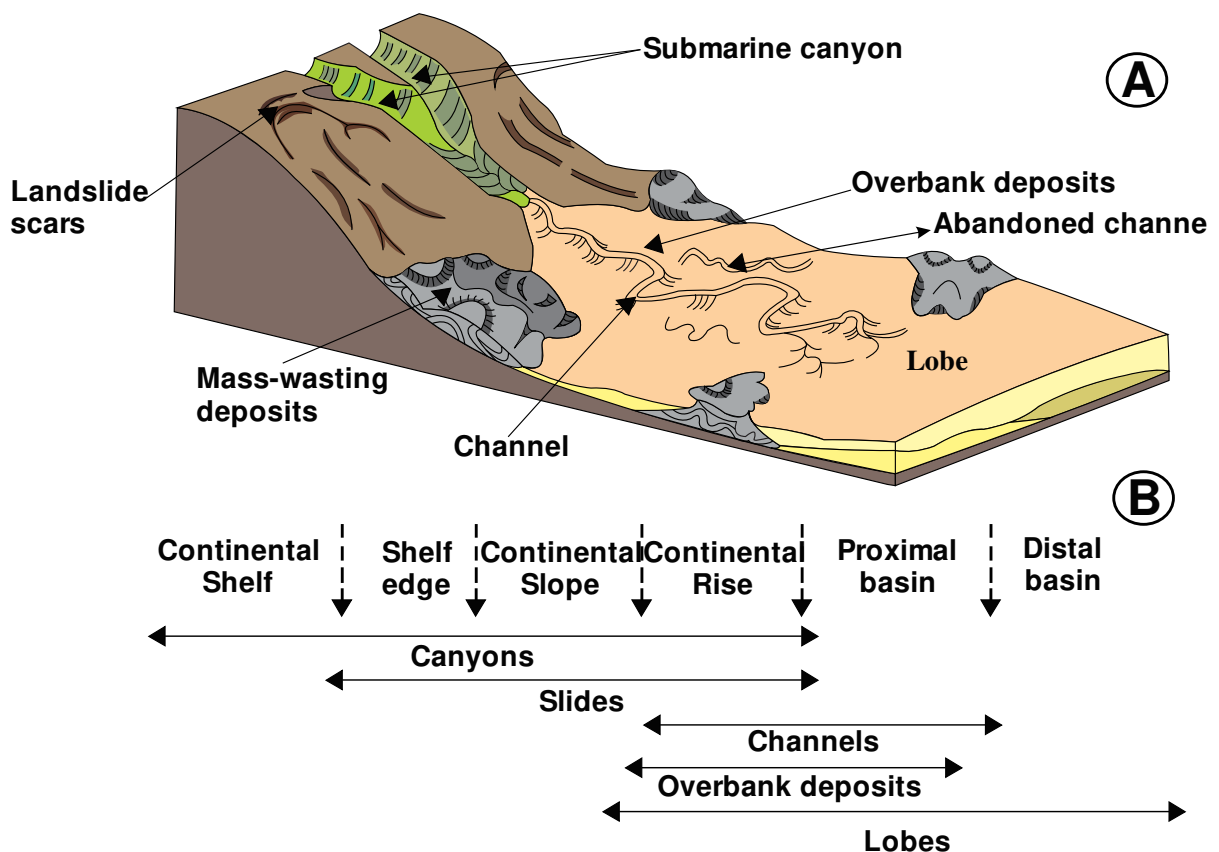


Figure 6. A) Major architectural elements composing modern turbidite systems. B) Generic distribution of the architectural elements in the physiographic domains, from the continental shelf to the deep basin. Modified from Normark *et al.* (1983).

4.3.1 Elements of Turbidite Systems

As stated by Weimer & Link (1991), elements are the basic mappable components of both modern and ancient turbidite systems and stages that can be recognized in marine, outcrop, and subsurface studies. Elements can have depositional and/or erosional characters. Depositional elements are characterized by a distinctive assemblage of similar facies and facies associations that permit differentiation from adjacent strata that bound them both vertically and laterally. Detailed outcrop studies are the best technique to define the characteristics of depositional elements. Erosional elements are particularly well expressed in modern fans and, if sufficiently large, having a distinctive seismic expression in the subsurface. For turbidite systems five primary elements are recognized: (1) major erosional features (excluding channels), (2) channels, (3) overbank deposits, (4) depositional lobes, and (5) channel-lobe transition deposits and related morphologic features.

4.3.1.1 Major erosional features

This element includes a number of large-scale erosional features that are particularly well expressed in modern fan systems as well as in the seismic expression of some ancient systems. These features include (1) shelf-edge failures, (2) slope failures, (3) failures within the basin turbidites, and (4) canyons. The fill of these large-scale erosional features is highly variable and generally quite complex because they are commonly related to repeated periods of erosion and sedimentation (Mutti, 1985).

4.3.1.2 Channels

Channels are elongate negative relief features produced and/or maintained by turbidity-current flow; as such, channels represent major, relatively long-term pathways for sediment transport. Channel shape and position within a turbidite system are controlled either by depositional processes in the case of those associated with large levee/overbank wedges or by erosional downcutting, especially where the channel has been initiated by a slump or levee breach. Features scoured and filled by one or only a few flow events do not constitute channels because they do not represent longterm conduits. Such features, which have been referred to as scours (Mutti & Normark, 1987), are very common in both modern and ancient turbidite deposits and can develop at a wide range of scales.

4.3.1.3 Overbank deposits

Overbank deposits are generally fine-grained, thin-bedded turbidite sediments that can be laterally extensive and are adjacent to the main channels in a turbidite system. Seismic-reflection profiles show that these large complexes aggrade as the system grows such that the relative relief between channel floor and levee crests tends to reach a fixed value as the channel progrades downstream. The levees prograde rapidly down system and laterally, away from the levee crests, thus exhibiting downlap geometry in both directions. Levee crests have a longitudinal slope that is only slightly greater than the adjacent channel-floor slope except in the levee termination zone, where the steepest gradient of depositional slopes on the fan can occur (Normark *et al.*, 1983).

4.3.1.4 Depositional lobes

Lobes on modern fans are defined on the basis of morphology (generally lobate in plan view), a lack of sub bottom penetration with 3.5-kHz systems, and surficial samples confirming the presence of sand. On the other hand, in ancient systems, sandstone lobes are represented by roughly tabular, non-channelized bodies that have individual thicknesses generally of 3- 15 m. The downcurrent extent of sandstone lobe packages depends on the size of the system and on basin size and configuration and is primarily controlled by the volume of the individual turbidity currents (Mutti, 1985). This extent generally varies from a few kilometers to several tens of kilometers. Sandstone lobes can thus be basin-wide features with abrupt onlap terminations against the basin margins (Cazzola *et al.*, 1985; Elliott *et al.*, 1985), as well as roughly tabular bodies that gradually thin and shale-out into peripheral thinner bedded lobe-fringe deposits (Ricci Lucchi and Valmori, 1980). In any given system, the sandstone lobes represent the maximum downcurrent extent of the sand transported to the basin. For this reason, lobe deposits show the internal structures, including vertical grading, indicative of the largest and longest traveled turbidity currents. These sandstone bodies tend to consist of "classical" turbidites, i.e., sandstone beds that can be described in most cases as complete Bouma sequences (Weimer & Link, 1991).

4.3.1.5 Channel-lobe transition deposits and related morphological features

This element is of fundamental importance to understand the depositional setting and facies distribution of turbidite systems and their component stages. It exhibits not only some characters common to both channel-fill and lobe sediments but also a range of both erosional and depositional features that reflect the transformation of turbidity currents

undergoing hydraulic jumps in this region. Although conceptually easy to define as the natural link between channels and lobes, this element is, however, difficult to recognize and map in both modern and ancient systems. Mutti and Normark (1987) relate the characters found in the channel-lobe transition zone to major changes in flow conditions of turbidity currents in this part of a turbidite system. Turbidity currents moving across the transition zone are changing from confined, channelized conditions with higher gradients to unconfined, lateral spreading across more gently sloping lobe (depositional) areas. The depositional features of the transition zone in part reflect the effects of the hydraulic jump or flow deceleration but are dependent on the composition and size of the turbidity currents. For turbidity currents composed of a high proportion of sand and coarser sediment, large scours can be formed but, more important, the dilution of the flow results in rapid deposition of the sediment load (Weimer & Link, 1991).

Robust well log analysis is essential to most geophysical work. Well logs are the only near-field remote sensing of the formation that is available to the geophysicist. Diverse authors described the techniques used in each well log and its applications. In this research, the concepts of Asquith & Krygowski (2004) were used for describing the principal well logs utilized in hydrocarbon exploration and production, as follows:

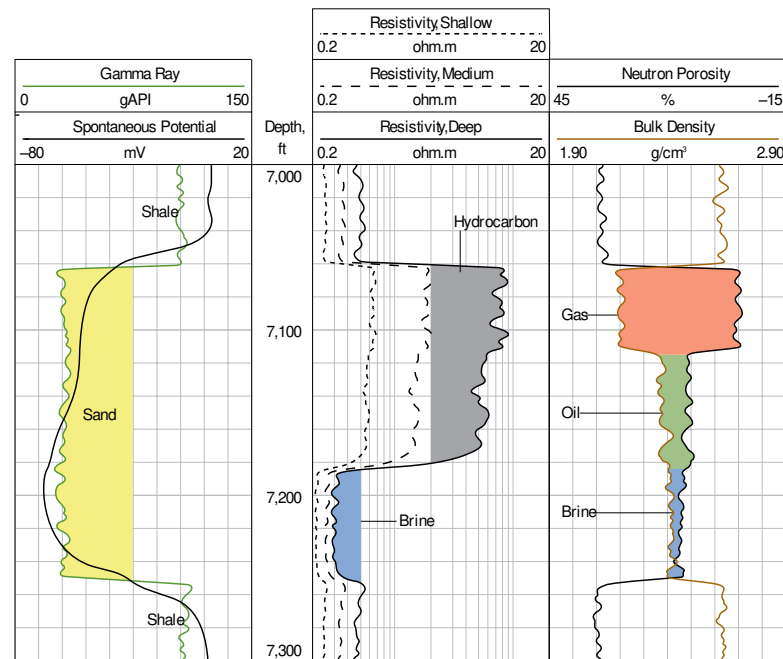


Figure 8. Basic log set interpretation. Modified from Varhaug (2016).

4.4.1 Spontaneous Potential

The spontaneous Potential (SP) log was one of the earliest electric logs used in the petroleum industry, and has continued to play a significant role in well log interpretation. Primarily the spontaneous potential log is used to identify impermeable zones such as shale, and permeable zones such as sand. The SP log is a record of direct current voltage differences between the naturally occurring potential of a moveable electrode in the wellbore, and the potential of a fixed electrode located at the surface (Doll, 1948). It is measured in millivolts. The SP is used to (1) detect permeable beds, (2) detect boundaries of permeable beds, (3) determine formation water resistivity and (4) determine the volume of shale in permeable beds.

4.4.2 Resistivity Logs

The resistivity log is fundamental in formation evaluation because hydrocarbons do not conduct electricity while all formation waters do; it is expressed in ohm-m. The resistivity can take a wide range of values, and, therefore, for convenience it is usually presented on a logarithmic scale. The resistivity logs are used to: determine hydrocarbon versus water-bearing zones; indicate permeable zones; and determine resistivity porosity. The most important use of resistivity logs is the determination of hydrocarbon versus water-bearing zones.

4.4.3 Porosity Logs

4.4.3.1 Sonic Log

The sonic log is the basis for calibration of surface seismic data and in favorable cases for detailed seismic interpretation. The adjustment of the sonic log is important for reliable detailed studies. There are various factors that affected the sonic measurements. The sonic log is a porosity log that measures interval transit time (Δt) of a compressional sound wave traveling through one foot of formation. Interval transit time (Δt) in microsecond per foot is the reciprocal of the velocity of a compressional sound wave in feet per second. Interval transit time (Δt) of a formation is increased due to the presence of hydrocarbons. If the effect of hydrocarbons is not corrected, the sonic derived porosity will be too high.

4.4.3.2 Density Log

The formation density log is a porosity log that measures electron density of a formation. It can assist the geologist to: identify evaporite minerals; detect gas-bearing zones; determine hydrocarbon density; and evaluate shaly sand reservoirs and complex lithologies (Schlumberger, 1972).

4.4.3.3 Neutron Log

Neutron logs are porosity logs that measure the hydrogen ion concentration in a formation. In clean formations (i.e. shale free) where the porosity is filled with water or oil, the neutron log measures liquid-filled porosity. Neutrons are created from a chemical source in the neutron logging tool. The chemical source may be a mixture of americium and beryllium which will continuously emit neutrons. These neutrons collide with the nuclei of the formation material, and result in a neutron losing some of its energy. Because the hydrogen atom is almost equal in mass to the neutron, maximum energy loss occurs when the

neutron collides with a hydrogen atom. Therefore, the maximum amount of energy loss is a function of a formation's hydrogen concentration. Because hydrogen in a porous formation is concentrated in the fluid-filled pores, energy loss can be related to the formation's porosity. Neutron log responses vary, depending on: differences in detector types; spacing between source and detector; lithology.

4.4.4 Gamma Ray Log

Gamma Ray logs measure natural radioactivity in formation and because of this measurement, they can be used for identifying lithologies and for correlating zones. Shale-free sandstones and carbonates have low concentrations of radioactive material, and give low gamma ray readings. As shale content increases, the gamma ray log response increases because of the concentration of radioactive material in shale. A gamma ray log allows a (qualitative) lithological profiling. Clean (sand, carbonates) and shally sections can be separated. In geological applications, the gamma ray is a tool for: (1) sedimentological studies by typical curve shapes for channel, coarsening upward, fining upward and other formations (Rider, 1996) and (2) well-to-well correlation in sedimentary areas and trend derivation. Throughout the GR index, it is possible to determine the log that provides the clayey relationship present in the specific intervals, the content in clays (V_{sh}) in porous reservoirs is obtained and is calculated as follows.

4.4.4.1 Volume of Shale Calculation (V_{sh})

A shale content estimate can be derived from a Gamma Ray measurement based on the correlation between shale content and radioactive isotope content, which originates natural gamma activity. It is assumed that only shale or clay is responsible for the radiation; no other “radioactive minerals” are present. For this application, in many cases an integral measurement is used. In order to eliminate the effect of variability of the uranium content, a spectral measurement of the potassium and thorium contribution is recommended (Schön, 2015). The analysis consists of two steps:

1- Calculation of an IGR or “gamma-ray index”, which is the actual gamma reading normalized by the value for the clean rock (minimum gamma reading) and the shale (maximum gamma reading):

$$IGR = \frac{GR - GR_{cn}}{GR_{sh} - GR_{cn}} \quad (1)$$

Where, GR_{cn} is the log response in a clean zone – no shale, GR_{sh} is the log response in a shale zone, and GR is the log response in the zone of interest.

This normalization of the logs results in IGR=zero, for clean rocks; and IGR=one, for shale (100% shale).

2- Transformation of the gamma-ray index into shale content. For the transformation, empirical equations are recommended for various formations:

$V_{sh} = IGR$	Linear relationship (upper limit)
$V_{sh} = 0.0083 \cdot (2^{3.7 \cdot IGR} - 1)$	Tertiary Clastics (Larionov, 1969)
$V_{sh} = 0.33 \cdot (2^{2.20 \cdot IGR} - 1)$	Mesozoic and older rocks (Larionov, 1969) (2)

4.5 SEISMIC INTERPRETATION

In searching for new reserves of oil and gas, the seismic method is commonly used to obtain seismic reflection profiles usually known as seismic lines, recognized as one of the most common ways used to identify geological structures in the subsurface that acts as oil traps (Fig. 9). Interpreting seismic data requires an understanding of the geological framework of a study area addressing how the geological formations that are located in the subsurface may affect the seismic method. Seismic becomes quite useful in identifying features through some concepts of seismic geomorphology using some key seismic attributes to assist the identification and characterization of seismic reflectors (Brown, 2004). One of the fundamental premises of seismic interpretation is that the reflectors follow chronostratigraphic units and not lithostratigraphic tops (Hardage *et al.*, 2006). However, Tipper (1993) cited Hardage *et al.* (2006) questioning whether the seismic reflections behave in fact an implicit chronostratigraphic meaning.

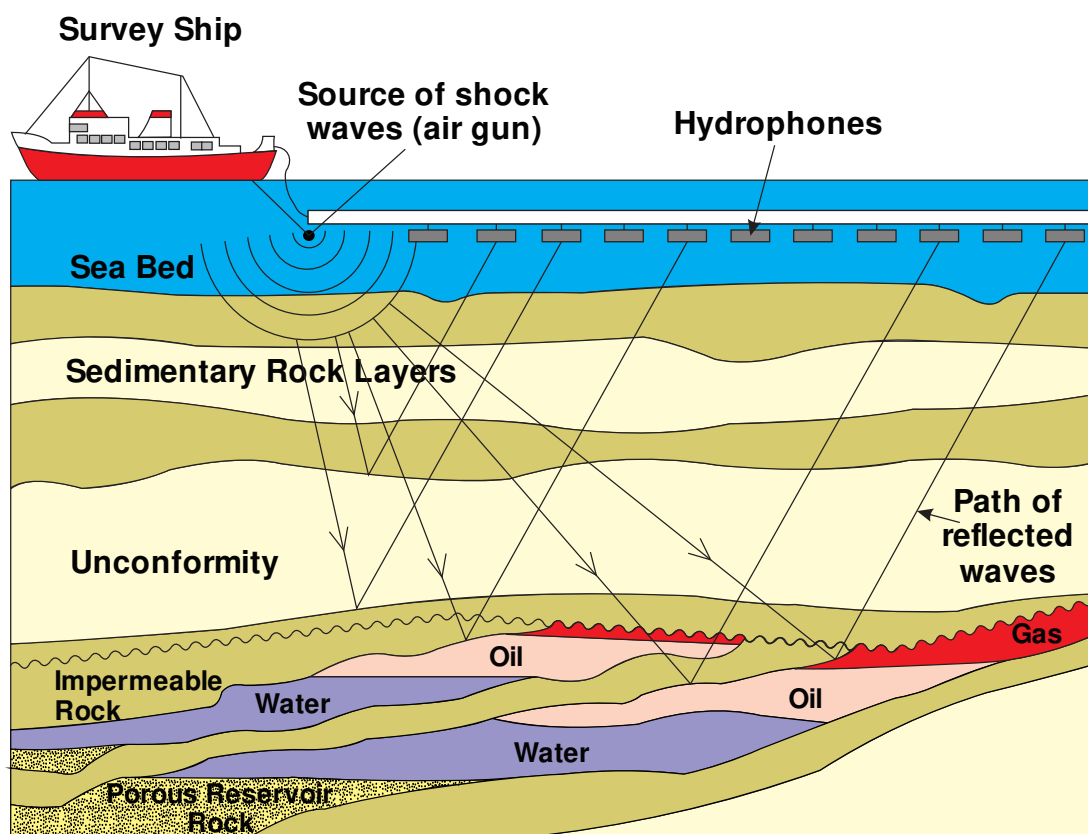
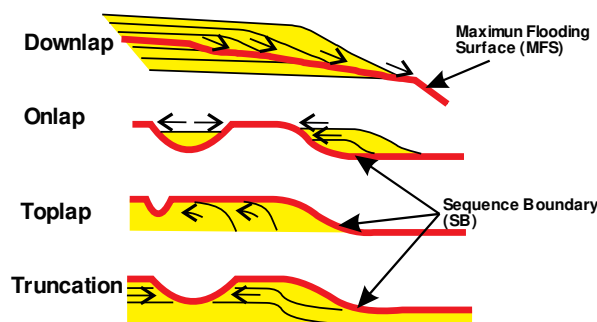


Figure 9. Marine seismic acquisition – pulses of sound energy penetrate the subsurface and are reflected back towards the hydrophones from rock interfaces. Modified from <http://www.open.edu/openlearncreate/mod/page/view.php?id=41010>.

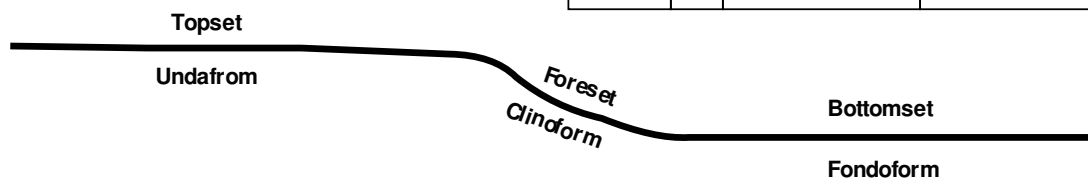
4.6 SEISMIC-SEQUENCE STRATIGRAPHY

The application of sequence and seismic stratigraphy has been used approximately since 40 years ago, as an important geological tool to analyze past climate and oceanographic conditions during deposition of sedimentary sequences. The concept of seismic stratigraphy is associated with the study of stratigraphy and depositional facies as interpreted from seismic data (Mitchum *et al.*, 1977). On the other hand, sequence stratigraphy has been used to integrate interpretation of stratal patterns from seismic, well log information, outcrop, cuttings and core data together with associated depositional environments and lithofacies (Vail & Sangree, 1977). Sequence stratigraphy is an important discipline used to interpret the depositional origin of sedimentary sequences and predict the heterogeneity, extent and character of lithofacies. The use of seismic and sequence stratigraphy combines the framework of major depositional and erosional surfaces bounding these successions of strata, and the geometry that successive contemporaneous strata have followed their accumulation. The key to using seismic and sequence stratigraphy as a tool for interpreting the sedimentary section are the major bounding and subdividing surfaces. These surfaces are commonly generated by the changes in relative sea level that can be observed in seismic lines (Fig. 10).

Termination Types



Depositional Terminology



Chronostratigraphic Surfaces and Systems Tracts

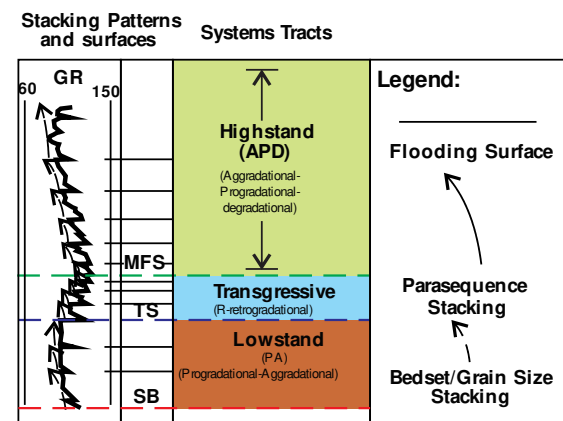


Figure 10. Basics of seismic and sequence stratigraphy of siliciclastic sequences. Modified from Abreu *et al.*, (2010).

4.7 RESERVOIR CHARACTERIZATION

Reservoir characterization is defined as the construction of realistic three-dimensional images of geological and petrophysical properties to be used to predict reservoir performance. The goal of reservoir characterization is to describe the spatial distribution of petrophysical parameters such as geological facies, porosity, permeability, and fluid saturations linked through pore size. Wireline logs, core analyses, production data, pressure buildups and tracer tests provide quantitative measurements of petrophysical parameters near the wellbore, but they generally provide only one-dimensional spatial information. Therefore, wellbore data must be integrated with geologic models to display the petrophysical properties in three-dimensional space (Lucia, 2007).

4.7.1 Porosity

Porosity is a fundamental volumetric rock property that describes the potential storage volume of fluids (water, gas and oil) and influences most physical rock properties (for example elastic wave velocity, electrical resistivity, density, etc.). Porosity can be determined directly by various laboratory techniques and indirectly by logging methods (Schön, 2015). Porosity is defined as the summarized volume of all pores, fractures, cracks, etc., or generalized all fluid (gas, water, hydrocarbons) or “non-solid” containing parts of a sample related to the total volume of the sample:

$$\phi = \frac{V_{\text{pore}}}{V_{\text{bulk}}} = \frac{V_{\text{bulk}} - V_{\text{solid}}}{V_{\text{bulk}}} \quad (3)$$

Where, V_{pore} is the volume of all pores, V_{bulk} is the volume of the sample, and V_{solid} is the volume of the solid mineral components, frequently called “grain volume” (Fig. 11).

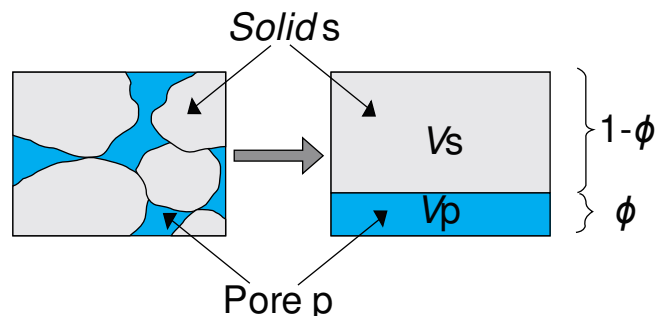


Figure 11. Definition of porosity. Modified from Schön, (2015).

Porosity can be determined by: (1) direct measurements (laboratory) based on determination of bulk and solid volume, gas expansion or displacement techniques and/or (2) indirect measurements (logging and seismic methods) based on correlation between porosity and properties, like density, neutron response, and seismic wave velocity. Porosity can also be derived from nuclear magnetic resonance (NMR) measurements.

4.7.1.1 Porosity of Clastic Rocks

In clastic sediments, pre-diagenetic factors control primary porosity: grain size distribution (sorting), grain packing, and particle shape (Schön, 2015) (Fig. 12).

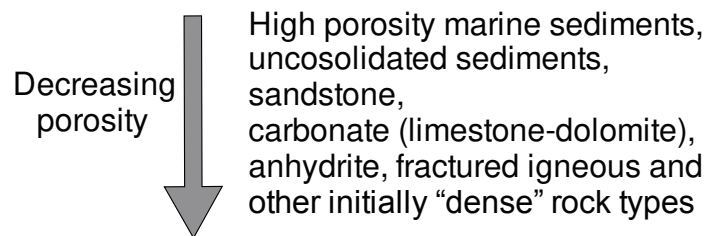


Figure 12. Tendency of decreasing porosity related to a series of rocks. Modified from Schön (2015).

Secondary porosity is the result of mechanical processes (compaction, plastic and brittle deformation, fracturing) and geochemical processes (dissolution, precipitation, volume reductions by mineralogical changes, etc).

4.7.1.2 Determination of Volumetric Rock Composition from Density and Neutron Logs

Porosity is a key parameter for reservoir studies. Porosity can be calculated from density and neutron porosity if the matrix and fluid properties are known. Two techniques – graphic, using crossplots, and numeric, using a mathematical formalism- are presented in order to solve such problems and deliver information about both porosity and mineral composition (Schön, 2015). In the current research project, the crossplot technique was used.

4.7.1.2.1 Crossplots

Crossplots are two-dimensional graphic presentations of the response equations. Crossplots present the variation of any two “porosity-sensitive” properties. All combinations are possible: (1) Neutron-density plot, (2) Density-slowness plot and (3) Slowness-neutron plot.

The most frequently applied plot is the neutron-density crossplot (Fig. 13) shows the principle of a neutron-density crossplot for the three main reservoir rock components: sandstone, limestone and dolomite. Plots start in the lower left corner with the “matrix point” and go up to the right upper corner with the “water-point”. The three lines describe pure limestone, dolomite and sandstone. Lines are scaled in porosity units.

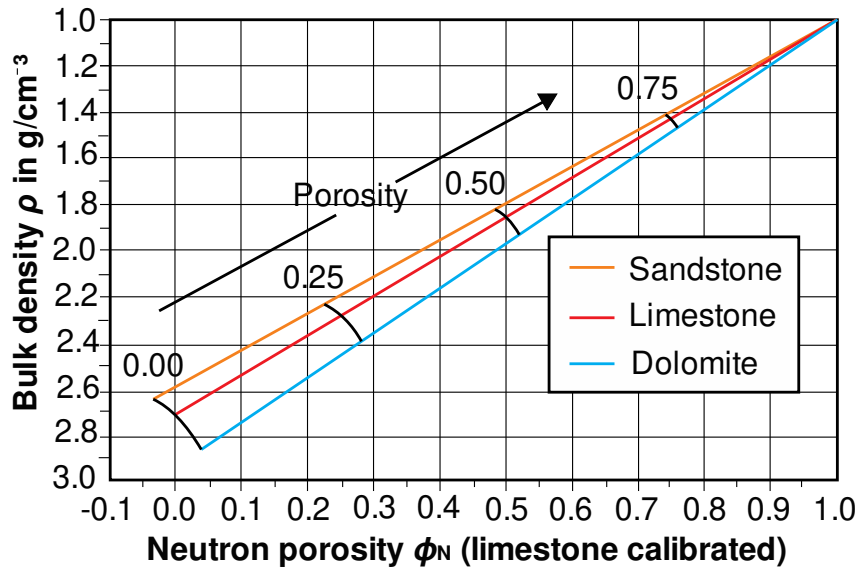


Figure 13. Calculated neutron-density crossplot: x-axis gives the neutron porosity for a limestone-calibrated tool; y-axis gives the bulk density. Lines are plotted for sandstone/quartz; limestone; dolomite. Modified from Schön (2015).

4.7.2 Fluids in the pore space – Saturation and Bulk Volume fluid

The pore space is filled with fluids (normally gas/air, water, oil). If more than one fluid is present, the spatial distribution of the different fluids depends on the physical properties of the rock material, on the fluid properties, and on interactions between the fluids and between fluids and solids (interfacial tension) (Schön, 2015). Fluid saturation can be determined: (1) directly from cores, plugs, or samples (fluid extraction, capillary pressure measurements), (2) indirectly from logs (resistivity, dielectric, neutron measurements, etc.), and (3) by NMR measurements. For the description of the volume fraction of a fluid i in a porous rock, the term saturation S_i is used and defined as follows:

$$S_i = \frac{\text{Volume of fluid } i}{\text{pore volume}} \quad (4)$$

Thus, saturation is the fluid volume, normalized by pore volume. Saturation is given as a fraction or as percentage. A reservoir with the fluid water, oil, and gas is characterized by three saturation terms and their sum must be 1:

$$S_{\text{water}} + S_{\text{oil}} + S_{\text{gas}} = 1 \quad (5)$$

In addition to the parameter “saturation”, the parameter “bulk volume of the fluid - BVW” is also used. Bulk volume of a fluid *i* refers the volume of that fluid to the rock bulk volume. Bulk volume water is, for example,

$$BVW = \frac{\text{Volume of water}}{\text{Rock volume}} = S_w \cdot \phi \quad (6)$$

4.7.3 Permeability

Permeability characterizes the ability of a rock to transmit a fluid; it connects the fluid flow rate with the applied pressure gradient and the fluid viscosity. It is controlled by the connected passages of the pore space and is a tensorial property which exhibits, in many cases, anisotropy (Schön, 2015). In the oil industry, the Darcy (d) or millidarcy (md) are the typical units used. Different methods are implemented to determine permeability such as direct measurements at samples (cores, core plugs,) direct tests (well and drillstem tests), wireline formation testers, pump tests, indirect methods using grain size parameters (particularly for unconsolidated sediments) and indirect methods using wireline logs (NMR, Stoneley waves). Permeability relates the laminar flow (fluid volume/time) of a non-reactive fluid to a macroscopic cross-section of rock, to the viscosity of the fluid, and the fluid pressure gradient. Depending on the fluid composition must be distinguished between absolute permeability, effective permeability and relative permeability. In this way, permeability results as:

$$k = \eta \cdot \frac{u}{\text{grad } p} \quad (7)$$

Where, *k* is permeability, η is the flux, *grad p* is the transmembrane partial pressure, and *u* is the thickness. The permeability has the unit of an area m² (in SI units). This explains permeability as a pore geometrical measure.

4.8 GEOSTATISTICS

Geostatistics has been defined by Matheron (1970) as the application of probabilistic methods to regionalized variables, which designates any function distributed in a real space. From the very start, the aim of this discipline was to develop theoretical and methodological elements to meet the needs of the industrial world. At the beginning, applications concerned exclusively mining industry, but they rapidly expanded to the oil and gas industry, and other fields as meteorology, sea mapping, air, water, etc. In the hydrocarbons industry, geostatistics commonly refers to the regionalization of variables and related techniques used to predict rock variables that were not sampled, using mathematical methods to group, organize and interpret data, making decisions reasonably. As follows, some of the most important concepts of geostatistics in 3D reservoir modeling used in the present study are going to be explained:

4.8.1 Rock Property Modeling

Following a robust well log analysis and construction of physical properties relationships for an area, the next step is to build rock properties models that honor the geological setting and stratigraphic patterns. A typical rock properties modeling exercise will include the construction of multiple models of the subsurface. These models are then compared to the actual seismic responses to assess the quality of the match between the model and actual seismic data.

4.8.2 Property Modeling

The objective of property modeling is to distribute properties between the available wells while preserving the realistic reservoir heterogeneity and matching the well data. It is possible to use the data analysis process to interpret the data, perform quality control, identify key geological features, and prepare the input for facies and petrophysical modeling. Statistics, histograms, and variograms are used to perform a quantitative check of the upscaling in the statistical quality control.

4.8.2.1 Data analysis

Data analysis is the process of exploring and quality controlling the data. The data analysis process enables a detailed analysis of both discrete and continuous properties. Facies proportion, thickness, attribute probability, and variogram modeling are available for discrete

properties. General data analysis uses the histogram to inspect the property distributions and the correlation between properties.

4.8.2.2 Histograms

Histograms provide a convenient way to visualize well related dynamic results such as pressure, volume, and rates. Histogram shows the distribution of values for the selected well logs or for a selected individual property. The histograms are used for checking and comparing input- and model- data.

4.8.2.3 Variogram

A variogram is a method for describing spatial variation of a reservoir property. It is based on the principle that closely spaced samples are likely to have a greater correlation than those located far from one another, and that beyond a certain point a minimum correlation is reached and the distance is no longer important. This spatial correlation may of course be anisotropic and several variograms oriented in different directions may be required to describe the variation in a property. Variogram analysis involves determine the directions of the variogram analysis (usually three directions orthogonal to each other: vertical, major and minor). For each direction, the analysis includes calculating an experimental variogram and create a model variogram fitted to the experimental variogram. It is possible to determine two types of calculated variograms; experimental variogram and variogram model (Fig. 14).

(1) Experimental variogram (also called sample variogram): variogram calculated for a sample data set using a direction and separation distance. It is generated by finding pairs of data with similar separation distances and then calculating the degree of dissimilarity between these pairs.

(2) Variogram model: a continuous mathematical expression used to describe the sample variogram. A variogram model is defined by its type, nugget, sill and ranges.

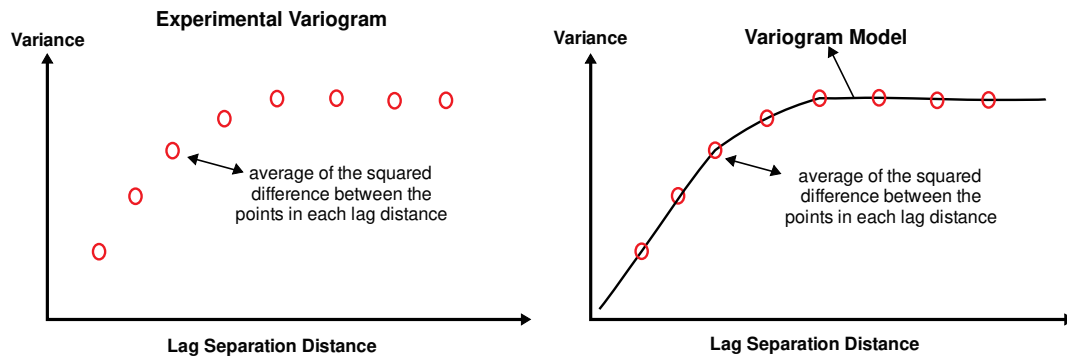


Figure 14. Left side: experimental variogram. Right side: model variogram fitted to the experimental variogram. Modified from Petrel E&P software platform of Schlumberger.

4.8.2.3.1 Variogram directions:

Variograms should be calculated in several different directions, as geological data is usually anisotropic (at least between the vertical and horizontal directions). These are commonly chosen as the major and minor directions in the horizontal plane, and the vertical direction.

- **Major direction:** the major direction defines the direction where the sample points have the strongest correlation. The azimuth angle of this major direction can be changed interactively by editing the direction in the search cone. Azimuth angle is specified as the clockwise angle from the north (in degrees).

- **Minor direction:** this is the minor search direction and is perpendicular to the major direction.

- **Variogram dip:** the dip is specified as the inclination (upward angle) in degrees between the major direction and the horizontal.

The procedure for data sampling in different directions is approximately the same; except that the vertical sample variograms are always calculated isotropically (i.e. orientation is not used). Nugget, sill and variogram type values will be identical in all three directions while ranges will vary.

4.8.2.3.1 Variogram parameters

The variogram displays five parameters: range, sill, nugget, plateau and transition (Fig. 15).

- **Range:** Describes where the variogram model reaches its plateau (i.e. the separation distance where there is no longer any change in the degree of correlation between pairs of data values). The range is specific in each direction for the model variogram.

- **Sill:** The semi-variance where the separation distance is greater than the range (on the plateau). It describes the variation between two unrelated samples. Transformed data should have a value of one (1) and values much higher or lower than this (e.g. ± 0.3) may indicate a spatial trend. The sill of a variogram structure is common for all directions for the model variogram.
- **Nugget:** The semi-variance where the separation distance is zero. It describes the short scale variation in the data. This is often most accurately identified from vertical data where the sampling interval is usually much lower. The nugget of a variogram model is common for all variogram structures and all directions.
- **Plateau:** The part of the variogram model where an increase in separation distance no longer increases the variogram value.
- **Transition:** Variogram models that reach a plateau are referred to as transition models. Different types of variogram models are used to describe the transition, such as Exponential, Spherical and Gaussian variograms.

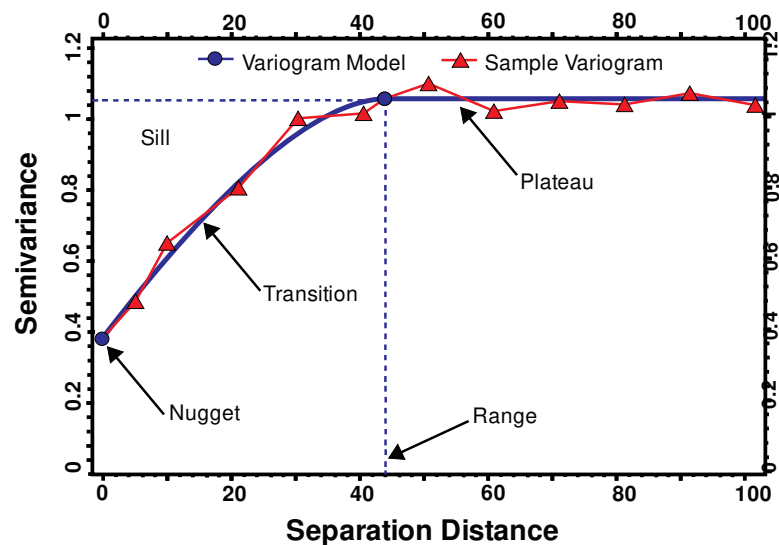


Figure 15. Experimental and model variogram key parameters Modified from Petrel E&P software platform of Schlumberger.

4.9 MODELING PROCESS

Property modeling processes are used for filling the cells of the grid with discrete (facies) or continuous (petrophysical) properties. The modeling process is dependent on the geometry of the existing grid. Property modeling is divided into several separate processes; Geometrical modeling, Facies modeling and Petrophysical modeling.

4.9.1 Geometrical modeling

Geometrical modeling is the process where properties can be generated by using pre-defined system variables, such as cell volume, seismic resampling, zone index, etc. Each cell will get a numerical value corresponding to the selected system variable.

4.9.2 Petrophysical modeling

Petrophysical modeling is the interpolation or simulation of continuous data (for example, porosity or permeability) throughout the model grid. Well data, facies realization, variograms, a secondary variable and/or trend data can be used as input and various user settings are available. Usually, upscaled well logs with continuous properties are the dataset available in the model grid. Filters and settings can be used to model different parts of the grid separately (for example, filter on facies, values, index, zones and segments and local model updated settings).

4.9.3 Facies modeling

Facies modeling is a means of distributing discrete data (e.g. facies) throughout the 3D model. The Facies modeling algorithms run in parallel, in two different ways: first through reuse of the Kriging and Simulation algorithms and second by parallelization by zone or realization. The first method is used to parallelize parts of those algorithms, which are based on Kriging and Simulation algorithms, such as, Adaptive channel. The second method is used for those algorithms which are Sequential by nature, such as, Sequential indicator simulation and Multi-point facies simulation. The Truncated Gaussian algorithms have both types of parallelization. Some exceptions as Fluvial channel and Object models were not parallelized.

Likewise, modeling process could be developed employing deterministic and stochastic methods, which are the main division in the modeling algorithms.

4.9.4 Deterministic algorithm

These always give the same result with the same input data and, in general, have a quick run-time. Deterministic algorithms are very transparent; it is easy to see why a particular cell has been given a particular value. The disadvantage is that models with little input data will automatically be smooth even though evidence and experience may suggest that this is not likely. Getting a good idea of the uncertainty of a model away from the input data points is often difficult in such models (Fig. 16).

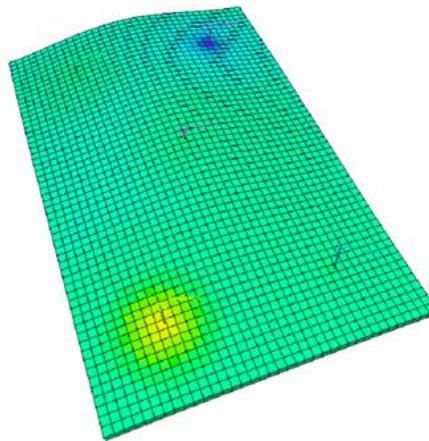


Figure 16. Model built using the kriging algorithm (Deterministic). Modified from Petrel E&P software platform of Schlumberger.

4.9.5 Stochastic algorithm

These use a random seed in addition to the input data. Therefore, while consecutive runs will give similar results with the same input data, the details of the results will be different. Stochastic algorithms such as Sequential Gaussian Simulation are complex and take much longer to run than deterministic algorithms. According to Bohling (2007), the basic idea of Sequential Gaussian Simulation is very simple. Recall that kriging gives us an estimate of both the mean and standard deviation of the variable at each grid node, meaning we can represent the variable at each grid node as a random variable following a normal (Gaussian) distribution. Rather than choosing the mean as the estimate at each node, Sequential Gaussian Simulation chooses a random deviate from this normal distribution, selected according to a uniform random number representing the probability level (Bohling G., 2007). However, they honor more aspects of the input data, specifically the variability of the input data. This means that local highs and lows will appear in the results that are not steered by the input data and whose location is purely an artifact of the random seed used. The

resulting distribution is more typical of the real case, although the specific variation is unlikely to match. This can be particularly useful when taking the model further to simulation, as the variability of a property is likely to be just as important as its average value. The disadvantage is that some important aspects of the model can be random and it is important to perform a proper uncertainty analysis with several realizations of the same property model with different random seeds (Fig. 17).

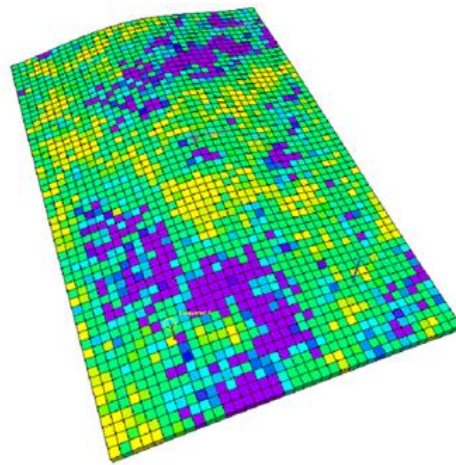


Figure 17. Model using the Sequential Gaussian algorithm (stochastic). Modified from Petrel E&P software platform of Schlumberger.

The main processes to develop the modeling properties include the following steps; scale up well logs, data analysis, and fault analysis.

4.9.6 Upscaling of well log properties

When upscaling well logs, we will first find the 3D grid cells which the wells penetrate (Fig. 18). For each grid cell, all of the log values that fall within the cell will be averaged according to the selected algorithm to produce one log value for that cell.

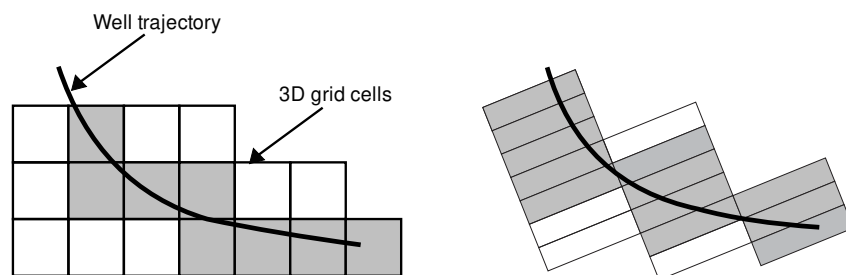


Figure 18. 3D grid cells. Modified from Petrel E&P software platform of Schlumberger.

For discrete well logs (for example, facies or zone logs), the average method Most of is recommended. The upscaled value will then correspond to the value that is most represented in the log for that particular cell. The layout and the resolution of the 3D grid will control how many and which cells each well penetrates. A dipping layering scheme, compared to a horizontal scheme, can dramatically alter the results from the scale up of well logs process and the subsequent property modeling.

The result of the scale up well logs process is placed as a property model icon in the properties folder for the 3D grid. It only holds values for the 3D grid cells, which the wells have penetrated. All other cells have an undefined value. Property modeling (Facies modeling/Petrophysical modeling) is then used to assign values to all the other grid cells, based on the upscaled well logs and optional trend data. In summary, the scale up well logs process assigns log values to the cells in the 3D grid that are penetrated by the well. It is the first step towards distributing petrophysical properties values in all cells of the model.

4.9.7 Fault analysis

Fault analysis allows generating fault transmissibility multipliers, either directly or by modeling fault properties based on grid permeability. These are then used as input to the simulation or simply as a visual assessment of the sealing potential of faults.

4.10 HYDROCARBON VOLUME CALCULATION

Volumetric analysis is a technique that employs geological observations and information to estimate original fluids-in-place. It is often referred to as a "static method" as it primarily sources its data from core samples, wireline logs, and geological maps. Volumetric calculations are typically used prior to production to estimate reserves, and after considerable production to determine the efficiency of recovery, the areal extent of the reservoir, and as a basis for advanced studies such as reservoir simulations.

A comprehensive geologic study of the prospect is necessary to increase the confidence and reliability of determined reservoir properties such as volume, porosity, and fluid saturations. In calculating the volume of the reservoir, accurate determinations of the areal extent and thickness must be made with respect to the geological structure and depositional environment. The use of isopach maps in combination with planimetry is a commonly used method in the determination of reservoir volume. Conclusions drawn concerning lithofacies and depositional settings are used to provide an assessment of porosity, while wireline log and core data provide the analyst with measurements of fluid saturations.

4.10.1 Estimation methods

The process of estimating oil and gas reserves for a producing field continues throughout the life of the field. There is always uncertainty in making such estimates. The level of uncertainty is affected by the following factors:

1. Reservoir type.
2. Source of reservoir energy.
3. Quantity and quality of the geological, engineering, and geophysical data.
4. Assumptions adopted when making the estimate.
5. Available technology.
6. Experience and knowledge of the evaluator.

The magnitude of uncertainty, however, decreases with time until the economic limit is reached and the ultimate recovery is realized. The oil and gas reserves estimation methods can be grouped into the following categories:

- **Analogy:** the analogy method is applied by comparing factor for the analogous and current fields or wells. A close-to-abandonment analogous field is taken as an approximate to the current field. This method is most useful when running the economics on

the current field, which is supposed to be an exploratory field. Analogy method is usually used in the early stages of development.

- **Volumetric method:** entails determining the areal extent of the reservoir, the rock pore volume, and the fluid content within the pore volume. This provides an estimate of the amount of hydrocarbons-in-place. The ultimate recovery, then, can be estimated by using an appropriate recovery factor. This method is usually used in the early stages of development.

- **Decline analysis and material balance calculations:** as production and pressure data from a field become available, these methods become the predominant procedures of calculating reserves. These methods greatly reduce the uncertainty in reserves estimates; however, during early depletion, caution should be exercised in using them. Decline curve relationships are empirical, and rely on uniform, lengthy production periods. It is more suited to oil well, which are usually produced against fixed bottom-hole pressures. In gas well, however, wellhead back-pressures usually fluctuate, causing varying production trends and therefore, not as reliable. On the other hand, material balance calculation is an excellent tool for estimating gas reserves. If a reservoir comprises a closed system and contains single-phase gas, the pressure in the reservoir will decline proportionately to the amount of gas produced.

When calculating reserves using any of the above methods, two calculation procedures may be used: deterministic and/or probabilistic.

- **Deterministic method** is by far the most common. The procedure is to select a single value for each parameter to input into an appropriate equation, to obtain a single answer.

- **Probabilistic method** is more rigorous and less commonly used. This method utilizes a distribution curve for each parameter and, through the use of Monte Carlo Simulation; a distribution curve for the answer can be developed.

Assuming good data, a lot of qualifying information can be derived from the resulting statistical calculations, such as the minimum and maximum values, the mean (average value), the median (middle value), the mode (most likely value), the standard deviation and the percentiles (Figs. 19 and 20).

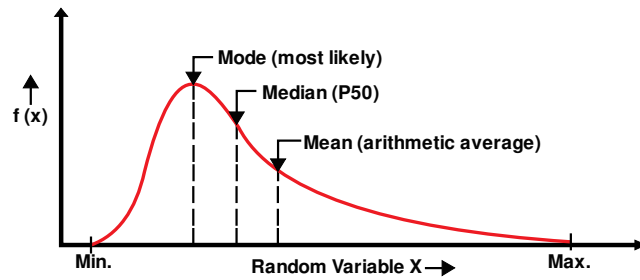


Figure 19. Measures of central tendency. Modified from Petrel E&P software platform of Schlumberger.

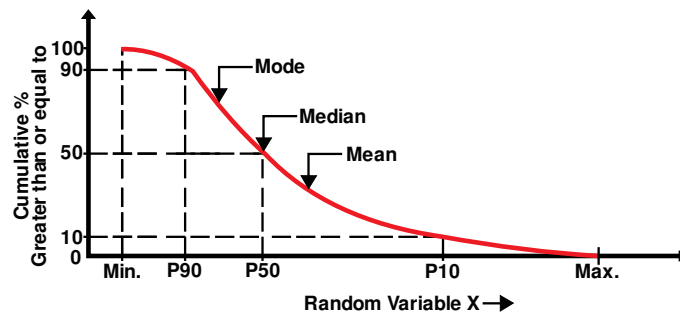


Figure 20. Percentiles. Modified from Petrel E&P software platform of Schlumberger.

The probabilistic methods have several inherent problems. They are affected by all input parameters, including the most likely and maximum values for the parameters. In such methods, one cannot back calculate the input parameters associated with reserves. Only the result is known, but not the exact value of any input parameter. On the other hand, deterministic methods calculate reserve values that are more tangible and explainable. In these methods, all input parameters are exactly known; however, they may sometimes ignore the variability and uncertainty in the input data compared to the probabilistic methods, which allow the incorporation of more variance in the data. A comparison of the deterministic and probabilistic methods, however, can provide quality assurance for estimating hydrocarbon reserves; i.e. reserves are calculated both deterministically and probabilistically and the two values are compared. If the two values agree then confidence on the calculated reserves is increased. If the two values are away different, the assumptions need to be reexamined.

5 MATERIALS AND METHODS

The current research was developed based on eight regional 2D Post-Stack Migrated (PSTM) seismic lines, one 3D Post-Stack Migrated (PSTM) seismic cube, twenty wells and significant amount of cuttings and core descriptions from geological final reports given courtesy of the Brazilian National Agency of Petroleum, Natural Gas and Biofuels (ANP). The research area covered approximately 220 km of seismic interpretation in the Eastern Marlim oil field (Fig. 21). The 2D and 3D seismic surveys, along with the given well dataset, afford fair to appropriate quality and seismic definition for the determination of the stratigraphic and structural configuration of the study area, allowing the characterization and 3D geological modeling of the Eastern Marlim oilfield located in the Campos Basin, Brazil.

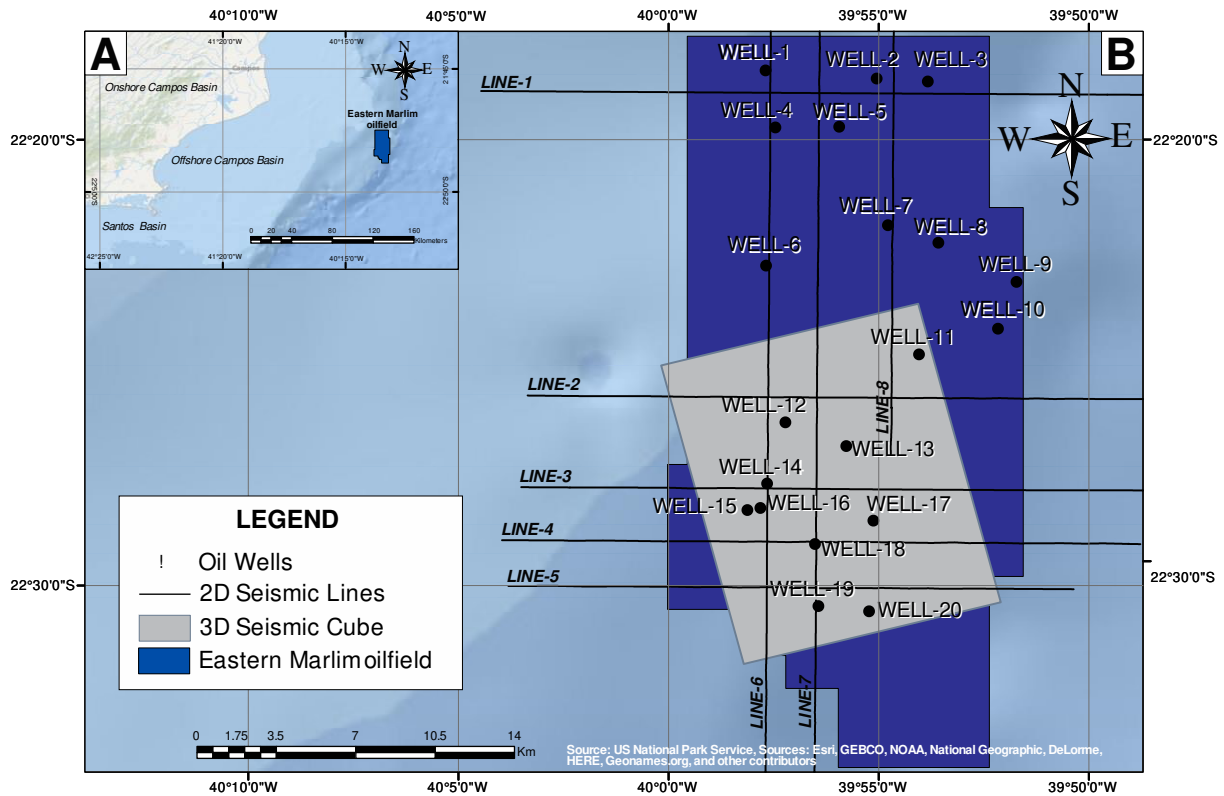


Figure 21. Location map showing the available seismic and well log information provided by the ANP in the study area. A) Location map of the Campos Basin in the SE offshore of Brazil showing the localization of the Eastern Marlim oilfield. B) Location map of the Eastern Marlim oilfield showing the available seismic lines (2D and 3D) and well logs information utilized in the current research.

5.1. SEISMIC AND WELL DATA

The seismic data are of varying quality and there are significant problems with multiples in some areas (multiple reflections from the seafloor and ghost effect). Data quality deteriorates in the pre-salt section, whereas salt tectonics makes challenging the robust seismic interpretation. The 3D seismic volume has crossline and inline intervals of 25 and 23 meters respectively. The 2D seismic data have between 2 and 13 km line spacing.

Regarding the well data, the distance among wells is varying approximately around 2–6 km with good spatial distribution in the study area. Well log interpretation was performed based on a basic dataset including gamma ray (GR), resistivity (RES), density (RHOB), neutron (NPHI), and sonic traveltime (DT) logs, supervised with cuttings and core descriptions. The mentioned dataset allow determining main lithofacies, major zones, petrophysical lithotypes, and stratigraphic/structural framework of the Oligocene-Miocene section at reservoir scale in the Eastern Marlim oilfield.

5.2. MISTIE CORRECTION

Initially, the mistie correction process was performed to correct incoherencies at seismic lines intersections. This process is mandatory in geological modeling because acquisition and seismic processing parameters may differ from one seismic line to another. Commonly, misties are computed by making the difference or shift between seismic lines. Visual inspection is the first analysis level. Anomalies may be distributed randomly or grouped on one or several isolated lines. In the last case, correction is applied easily. In presence of large data sets, statistical tools can be used to detect or to characterize high mistie values.

In the current case study, first, we applied the automatic mistie set in the Petrel E&P software platform of Schlumberger (academic license - UNICAMP). Finally, a manual correction was developed to ensure that all the intersections between 2D and 3D seismic lines were place correctly (Fig. 22).

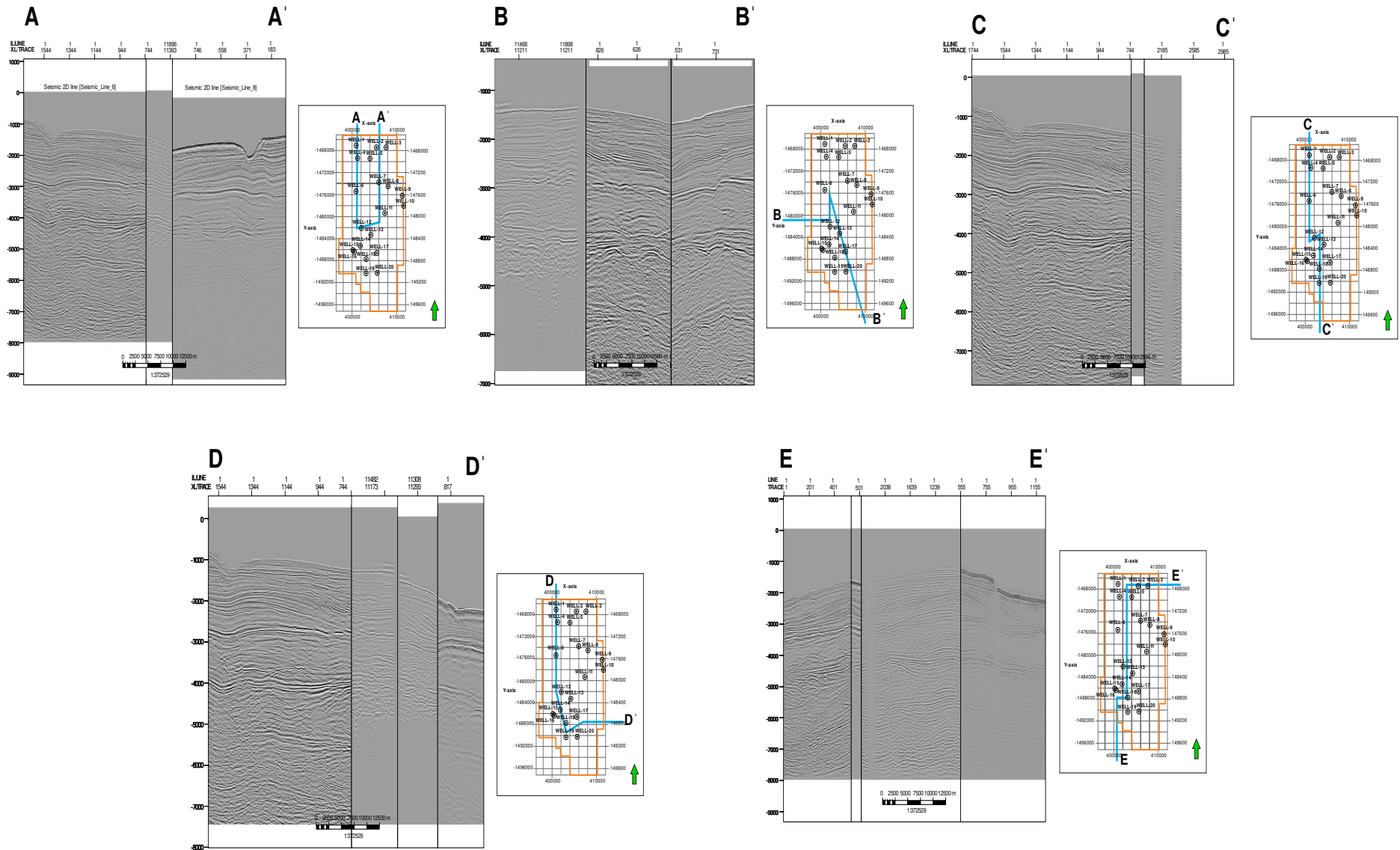


Figure 22. Mistie processing developed in the 2D and 3D seismic lines used in the current research project.

5.3. SEISMIC-WELL TIE

The seismic-well tie processing allows well data, measured in units of depth, to be compared to seismic data, measured in units of time. In the current research, check shots and time-depth tables merged with density and sonic logs were used to developed synthetic seismograms (Fig. 23). The synthetic traces were compared to the real 2D and 3D PSTM seismic data near the well sections. The seismic-well tie processing was developed in the software Hampson Russell of CGGVeritas (academic license - UNICAMP).

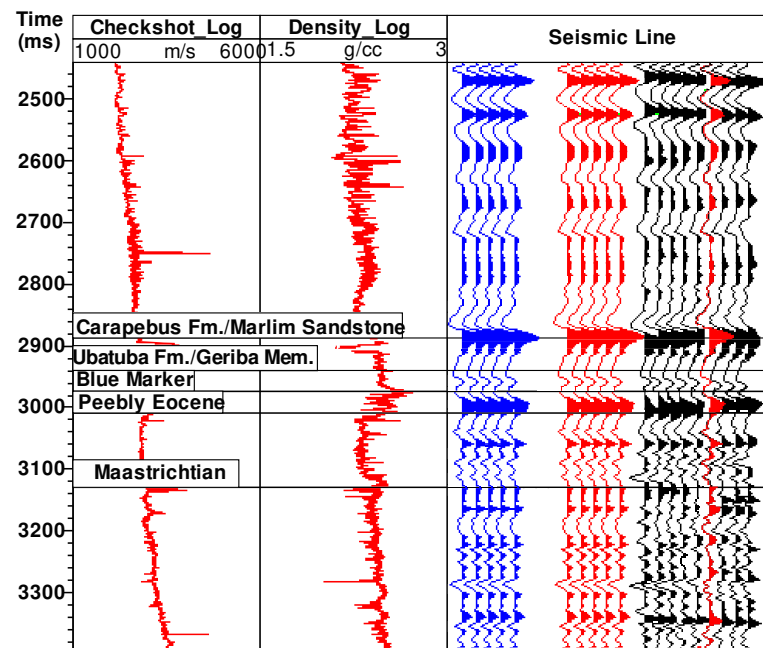


Figure 23. Example of well-seismic tie processing developed in the well-12 located in the 3D seismic cube in the Eastern Marlim oilfield based on time-depth tables and check shots merged with density and sonic logs.

5.4. SEISMIC INTERPRETATION

In-related 2D and 3D seismic lines were established the mapping and interpretation of seismic reflectors identifying key surfaces and principal structures. The main surfaces were defined by terminations of seismic reflectors aiming to recognize seismostratigraphic units related to a specific control (tectonics) and additionally using variations in the relative sea level. The depositional surfaces and tectonostratigraphic units were identified based on various criteria's as follows: (1) the nature of the contact (conformable or discordant), (2) the nature of depositional systems that are in contact with the entire surface, (3) types of terminations associated with seismic reflectors to the surface, and (4) the depositional trends identified below and above the surface contact (Catuneanu, 2006).

As well, pointing to improve the visualization of the available seismic data and the interpretation of the different stratigraphic surfaces and seismic facies in the study area, different seismic attributes were used. The mentioned seismic attributes were applied in different 2D and 3D seismic lines, and then were classified in four different groups called as stratigraphic, structural, signal and complex seismic attributes that are accessible in the seismic attributes library of Petrel E&P software. Successively, we incorporated the recognized seismic facies, seismic attributes; 2D/3D seismic interpretation and well tops correlations allows to identify the principal tectonostratigraphic units in the study area.

5.5. WELL LOG INTEPRETATION

Twenty wells were used to describe the major well-log characteristics of the Oligocene–Miocene reservoirs of the Eastern Marlim oilfield. Each one includes almost without exception Gamma ray (GR), Sonic (DT), Neutron-Porosity (NPHI), Density (RHOB), Resistivity (ILD), Permeability (K) and Porosity (Φ) profiles (Fig. 24). The mentioned well logs play an important role in any exploratory and production phase because they are mandatory to develop lithofacies interpretations, stratigraphic and structural correlations, petrophysical analysis, reservoir characterization and hydrocarbon volume calculations. The mentioned well log information was uploaded and interpreted in the Petrel E&P software pointing to develop the geological modelling of the research area.

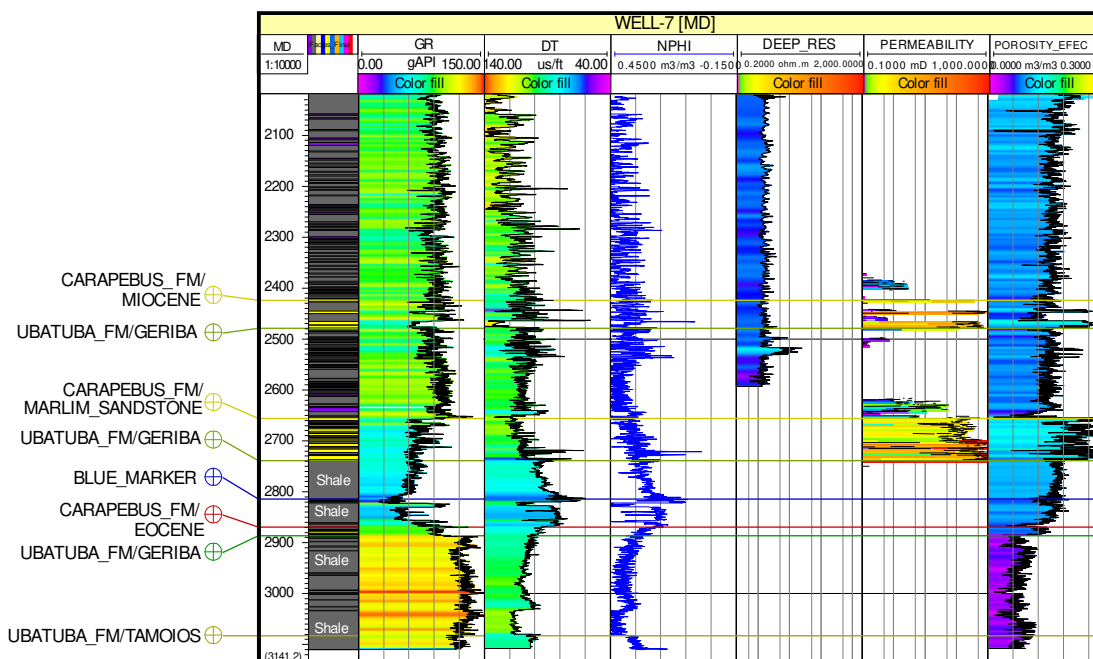


Figure 24. Example of a well section of the wel-7 showing the basic profile data set (GR, DT, NPHI, Resistivity-Deep, Permeability and porosity) used in the current research.

5.6. LITHOFACIES CHARACTERIZATION, STRATIGRAPHIC CORRELATIONS, DISTRUBUTION AND SAND PROPORTION MAPS

Discussion of the Oligocene-Miocene interval in this research is restricted to the subsurface database (Fig. 21). As well, drill cuttings and core descriptions were available for the development of the current investigation. In this way, at least four principal lithofacies were defined primarily based on lithological, compositional, grain size, texture, and sedimentary structure descriptions, following the methodology proposed by Miall (1985, 2010).

Consecutively, the existing type wells and identified lithofacies indicating that is possible to subdivide the Oligocene-Miocene reservoirs into three major zones, identified as Upper Sandstone (US), Middle Sandstone (MS) and Lower Sandstone (LS). Different well logs motifs (electrofacies) were recognized, representing a set of log responses which characterizes a rock type and permits it to be distinguished from the others (Serra, 1986). Interpretative stratigraphic correlations based on the available geological-geophysical database were elaborated covering the entire Oligocene-Miocene interval of study in the research area, form the basis for the development of distribution and sand proportion maps.

5.7. PETROPHYSICAL ANALYSIS BASED ON LITHOTYPES

In the current research a petrophysical analysis based on lithotypes was developed. Methods of multivariate analysis of multi-group dataset or cluster analysis implemented in the Petrel E&P software were used for the processing and interpretation of data on the available wells. Different petrophysical properties estimations were developed such as Shale Volume Calculation (VSH), Effective Porosity estimation (PHIE) and Water Saturation (SW), through different deterministic equations, displaying great correlation between the lithofacies and three major zones recognized in the Oligocene-Miocene reservoirs of the Eastern Marlim oilfield.

Additionally, we merged and supervised the petrophysical characterization with the available lithological information (stratigraphic columns, cuttings and core descriptions, lithofacies characterization and major zones) aiming to validate and complement the results.

5.8. SEISMIC AND SEQUENCE STRATIGRAPHY ANALYSIS

A sequence workflow for the seismic and sequence stratigraphy interpretation was used (Fig. 25). The workflow implemented in the current research started with mapping of depositional surfaces to identify seismostratigraphy units using the methodology of Mitchum (1977) and Catuneanu (2006).

In this way, the interpretation of seismic reflectors based on stratal terminations (onlap, downlap, toplap, and erosive truncations), that can be observed in surface and subsurface data sets, outcrops and seismic sections (Catuneanu, 2006) was made, considered as the main criteria's for the recognition of seismostratigraphy units (Mitchum et al., 1977).

The application of sequence and seismic stratigraphy in the study area was accomplished through the correlation of lithological profiles, interpretation of seismic lines, seismic attributes and analysis of seismic reflections patterns aiming to individualize the seismofacies that best represent the set of lithologies in the study area.

Finally, an integration of the regional geology of the Eastern Marlim oilfield with the sequence-stratigraphic interpretation of the Oligocene-Miocene turbidite system in the study area was developed, displaying the major tectonostratigraphic sequences in the Eastern Marlim oilfield.

In this work, the timing of system tracts and sequence boundaries for the sequence stratigraphy model was elaborated based on the methodology proposed by Catuneanu (2002). The Hierarchy system based on the duration of stratigraphic cycles was developed based on the work of Catuneanu (2009) (modified from Vail et al., 1991).

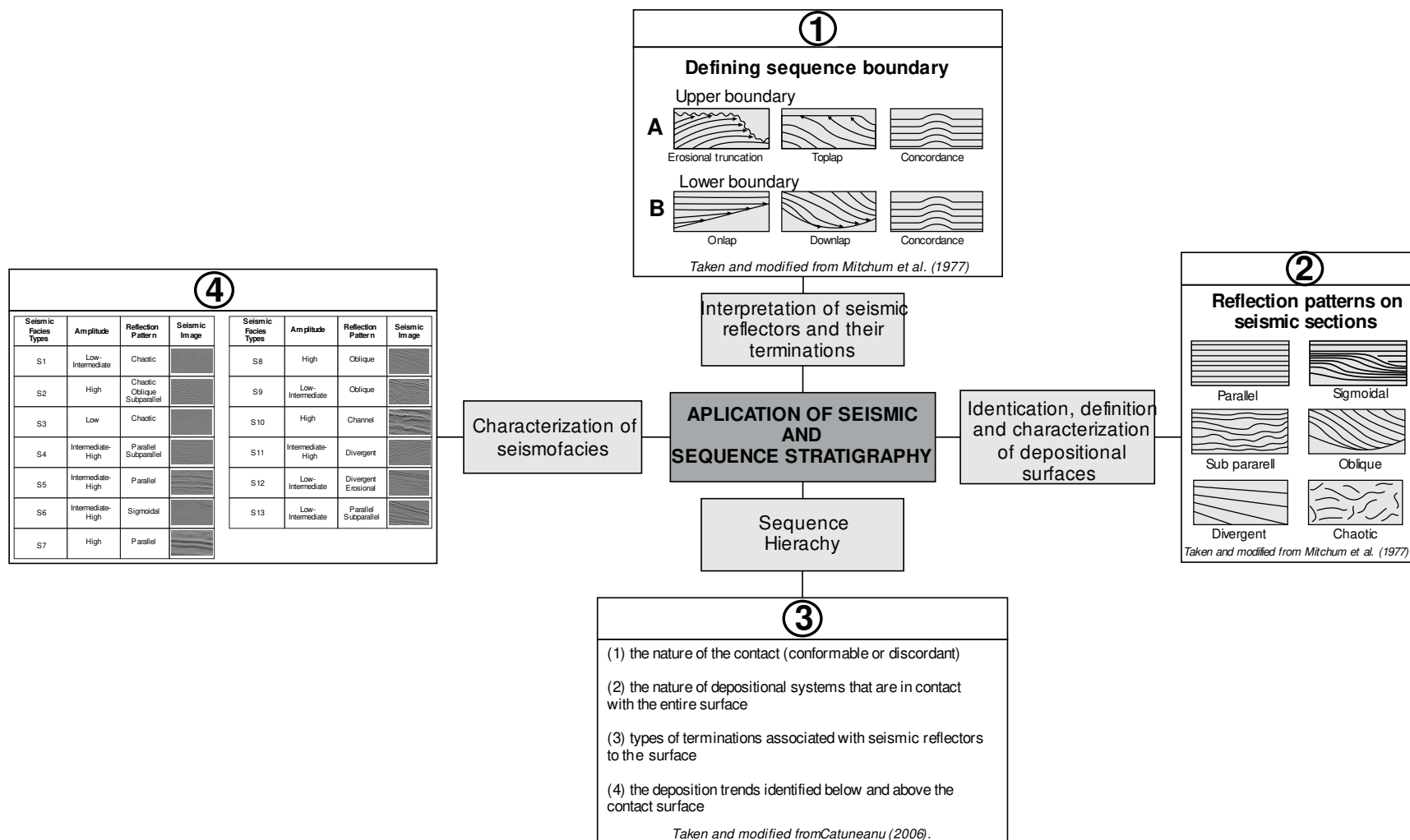


Figure 25. Seismic and sequence stratigraphy analysis sequential methodology used in the current case study.

5.9. 3D GEOLOGICAL MODELING - RESERVOIR CHARACTERIZATION

According to Overeem (2008), a static reservoir modeling has a strict relationship between data-driven modeling (deterministic and stochastic models) and process modeling data (sedimentary process model). The mentioned parts are in turn, controlled by the reservoir data that through upscaling permitting the realization of flow models (Fig. 26). In agreement with Overeem (2008), different mathematical and statistical approaches are used in reservoir modeling, but they need to be mixed with a geological background, because mathematics and statistics are very powerful geological modeling tools. Only when they are firmly supported by geological knowledge achieve a realistic approach.

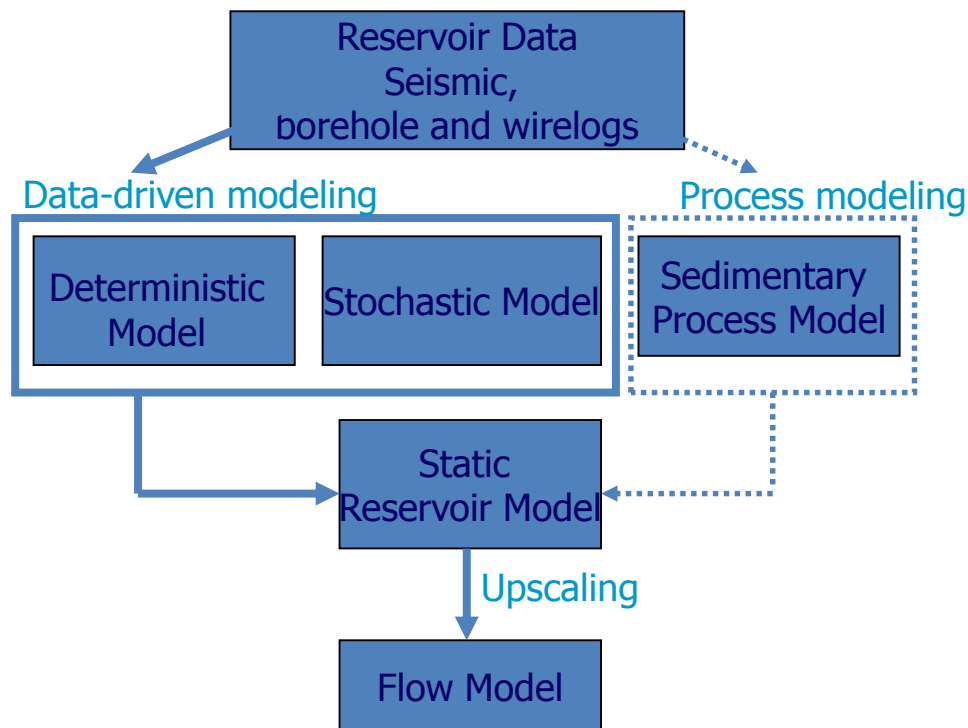


Figure 26. Geological modeling basis. Taken from Overeem (2008), University of Colorado at Boulder.

In the current study, the Petrel E&P software platform of Schlumberger (academic license) was used, and a sequential workflow (Fig. 27) was developed aiming to acquire a 3D static model that honors the 2D and 3D seismic data, well log, cuttings and core information, enhancing the geological interpretation of the study area. Additionally, the mentioned data were analyzed by geostatistical methods prior to populating the geocellular model (static model) with facies and petrophysical properties, using a range of deterministic and stochastic algorithms.

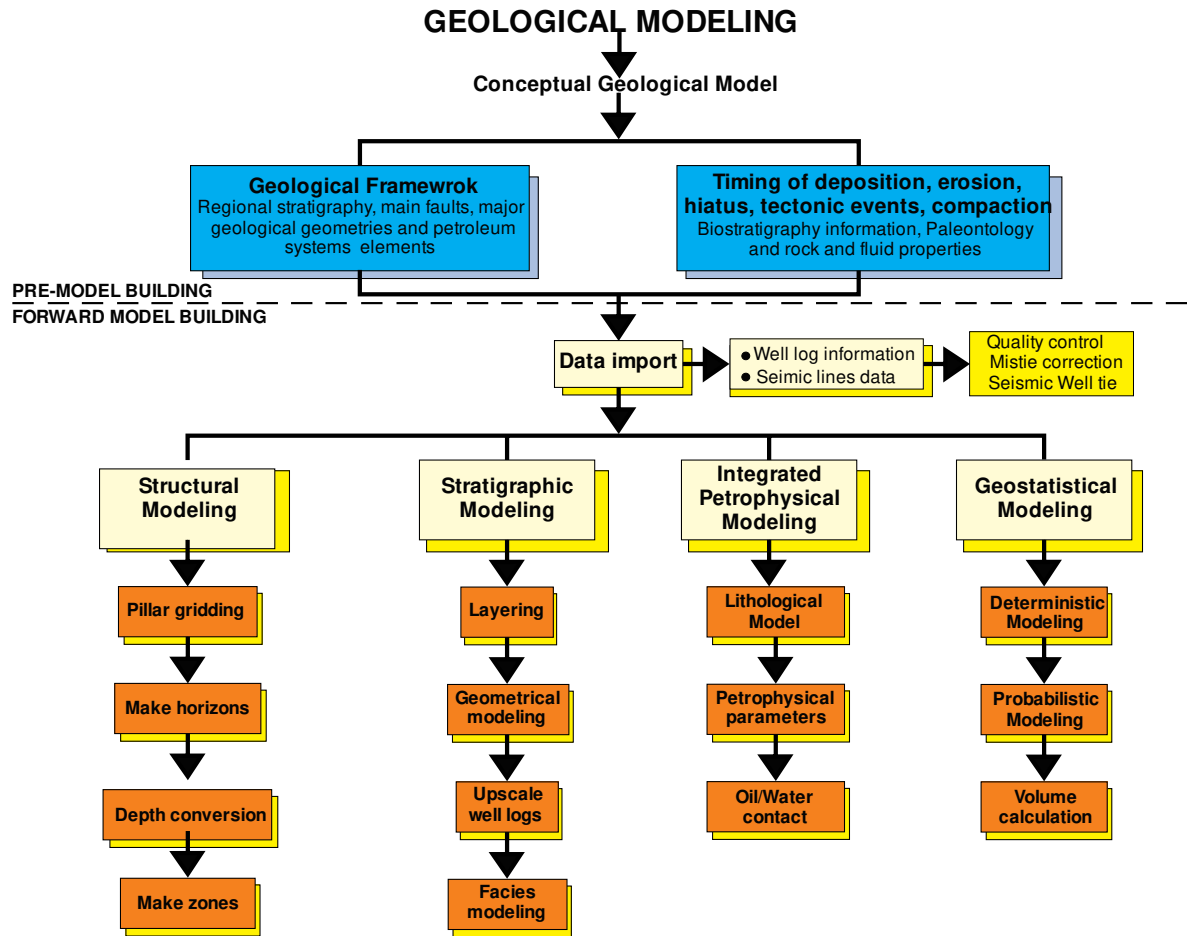


Figure 27. Forward modeling (static model) methodology used in the current case study.

Thus, a 3D static model that accurately represent the stratigraphic and structural framework of the Eastern Marlim oilfield with an unique volume based modeling technique improved the definition and interpretation of porosity, structure, or any other relevant property of the Oligocene-Miocene section at reservoir scale, evaluating uncertainties and volumetrics calculations to complement the results.

5.10. HYDROCARBON VOLUME CALCULATION

Estimating hydrocarbon volumetric calculations is a complex process that involves geological and engineering data. Depending on the quantity and quality of available information, one or more methods may be used to estimate hydrocarbon reserves. In this manner, aiming to accomplish hydrocarbon volume calculations in the Eastern Marlim oilfield, deterministic and probabilistic estimations were developed. In this study, the original oil in place (OOIP) was calculated as a deterministic method having a firm correlation to the total volume of hydrocarbon stored in a reservoir prior to production. Using the following equation, the OOIP of the study area we obtained, displaying good correlation with public and published data related with the Eastern Marlim oilfield:

$$N(t) = \frac{V_b \phi(p(t))(1-S_w(t))}{B_o(p(t))} \quad (8)$$

Where, $N(t)$ =oil in place at time t (STB); $V_b=7758Ah$ =bulk reservoir volume (bbl); 7758 =bbl/acre-ft, A =area (acres); H =thickness (ft); $\phi(p(t))$ =porosity at reservoir pressure p , fraction; $S_w(t)$ =water saturation at time t , fraction; $B_o(p(t))$ =oil formation volume factor at reservoir , pressure p , bbl/STB, and $P(t)$ =reservoir pressure at time t (psia).

In addition, another method used in the present research was the probabilistic estimation. This method utilizes Monte Carlo Simulations pointing to obtain a distribution curve for each parameter; then a distribution curve for the answer was developed, showing the P10, P50 and P90 thresholds, which are the minimum, mean (average value) and maximum value, respectively.

6. RESULTS

6.1. LITHOFACIES DESCRIPTIONS AND INTERPRETATION

The hydrocarbon accumulations in the Marlim complex are associated to a deepwater turbidite system, represented by a series of amalgamated sandstone bodies, known informally as “Marlim Sandstones” (Peres, 1993, Nascimento et al., 2014). The mentioned sandstones are effortlessly to recognize in the seismic data displaying a high seismic amplitude response attributed by Fainstein et al. (2001) to the impedance contrast between the high porosity of the reservoirs (Carapebus Formation) and the relatively low speed of the overlying shale (Blue Marker (MFS), proposed by Winter et al., 2007) (Fig. 28).

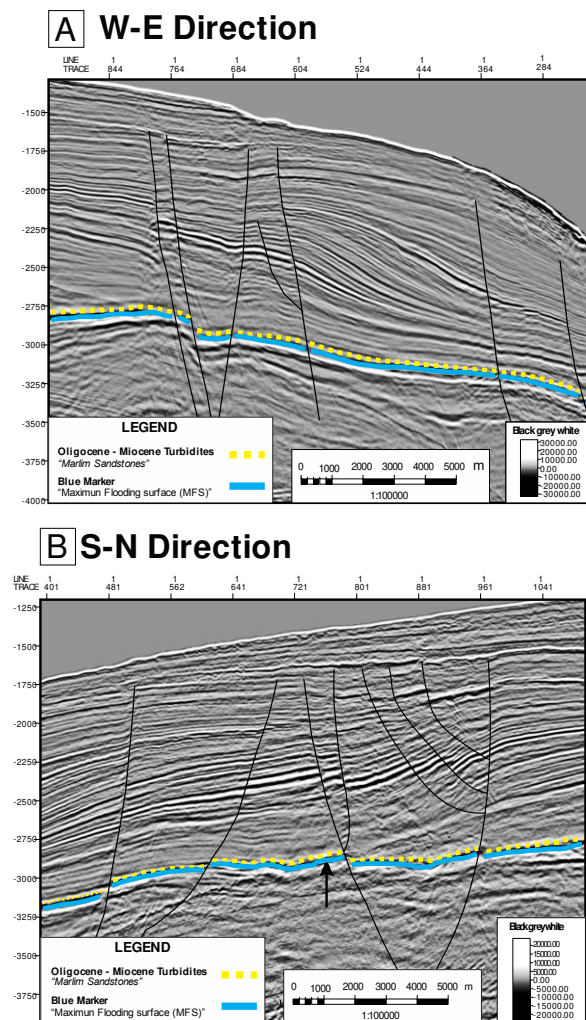


Figure 28. Typical high seismic amplitude response (poststack time-migrated seismic lines/zero-phase American polarity/Black-Gray-white color scale) of the “Marlim sandstones” and Blue Marker in the study area. A) Interpretation of the 2D Seismic line 5 in W-E direction. B) Interpretation of the 2D Seismic line 6 in N-S direction.

Wide-ranging of cuttings descriptions from final geological reports and accompanying core descriptions were used to develop the lithofacies characterization. Based on a descriptive method analysis supported by a combination of different sedimentological properties such as lithology, composition, texture, and sedimentary structure, were identified at least four principal lithofacies as follows: medium to coarse massive feldspathic sand (Sm), medium to coarse massive calcareous-feldspathic sand (Smcf), shales (Sh), and marls (M). The reservoir facies represented by the lithofacies Ss and Smcf are in general unconsolidated to semi-solid, cohesive, whitish sandstones with medium grained average particle size, sub-round rounding, regular sorting, calciferous/feldspathic composition, good apparent porosity and massive structure, with recurrent light brown oil stains presenting total fluorescence and immediate cut. On the other hand, the non-reservoir facies associated with the lithofacies Sh and M are in general shales and marls, displaying local and sporadic stains of dark brown and viscous oil, interbedded with the mentioned reservoir facies (Sm and Smcf) in the entire interval of study.

6.1.1 Reservoir facies

We recognized at least two main reservoir facies associated with sandstones bodies in the study area as follows: medium to coarse massive feldspathic sand (Sm), and medium to coarse massive calcareous-feldspathic sand (Smcf). These facies represent lateral and vertical extent massive unconsolidated amalgamated sandstone bodies with an average thickness of 50m approximately with medium to fine particle size and apparent observable good porosity.

6.1.1.1 (Sm) medium to coarse massive feldspathic sand

This facies is characterized by massive-unconsolidated sandstones, presenting an average thickness of 20m, being able to stack layers of up to 100m approximately. These sandy layers are fine-medium occasional coarse-grained, moderate to regular sorted, displaying null or infrequent calcareous accessory composition. Usually, towards the base, the layers are characterized by a higher concentration of coarse-medium grained sand, with an improvement in the degree of selection to the top. The coarse-grained sands are often rounder than the other grains.

- **Depositional environment interpretation:** massive deepwater sands transported through long distances in the basal layer of a turbulent flow and rapid mass deposition. These sandstones were deposited by high-density turbidity currents in submarine

channels and/or distal lobe settings. This lithofacies are commonly clean and moderate sorted displaying high observable porosity and friable-unconsolidated features representing excellent reservoirs.

6.1.1.2 (Smcf) medium to coarse massive calcareous-feldspathic sand

Considered as massive, semi-solid sandstones with an average thickness of 5m, which may correspond to single layers or amalgamations of smaller layers than approximately 1-2m. These sandstones are weak to poorly cohesive, fine-medium, occasionally coarse-grained sandstones, moderate sorted and presenting calcareous/argillaceous-feldspathic composition. This lithofacies containing coarse grains that occur at the base of layers to fine grains to the upper portion of layers without sedimentary structures.

- **Depositional environment interpretation:** massive sands deposited by turbidity currents and/or submarine channels in a deep marine setting resulting in mass deposition from the residual suspended load of the concentrated turbulent flow. The finer grained more argillaceous and calcareous facies record phases of reduced clastic sedimentation.

6.1.2 Non-reservoir facies

At least, two non-reservoir facies were recognized in the Oligocene-Miocene section of the Eastern Marlim oilfield. The dominant facies are greenish-gray to black micaceous shales (Sh), and light gray micaceous marls (M). The non-reservoir facies are interbedded with the reservoir facies in the entire interval of study researching up to 6m approximately.

6.1.2.1 (Sh) Shales

This facies corresponds to massive, greenish-gray micaceous shales, displaying a thickness distribution varying from 3-5m. This lithofacies presents a calcareous silt-clay matrix, locally pyritic, containing microfossil fragments and variable content of very fine sand. Sometimes, these deposits are slightly carbonaceous with yellowish-brownish fluorescence and immediate radial cut, showing local exudates of dark brown and viscous oil, associated with odor and gas bubbles.

- **Depositional environment interpretation:** shales deposited in low energy conditions suggested by the high silt-clay matrix content and fine texture. Paleontological data suggest an inner to middle neritic environment of deposition, although offshore transport

may have redistributed taxa from shallower waters (Robert, L. & Slater T, 2003). These lithofacies displays thick monotonous sections inferred from core-cuttings descriptions and well log interpretations indicating uniform environmental conditions over long periods, as might be expected in distal shelf or deeper settings. The reservoirs facies (Sm and Smcf lithofacies) were deposited in the axial parts of distal lobes interbedded with the shales lithofacies (Sh) that were deposited on their margins.

■

6.1.2.2 (M) Marls

This lithofacies is mainly constituted by massive light gray micaceous marls, which can reach up to 6m. These marls display limestone-clayey matrix, minor pyrite, containing fragments of undifferentiated microfossils and occasionally intraclasts of limestones, comprising calcareous-siltstones, calcareous-argillites and marls, without sedimentary structures.

■ **Depositional environment interpretation:** these carbonates represent deposition in a low energy, deepwater, possibly distal shelf to basinal setting. The undifferentiated microfossils, texture and mud content of the carbonates are indicative of low energy, relatively deep marine conditions (Robert, L. & Slater T, 2003). The associated massive turbiditic sandstones (Sm lithofacies) would suggest a slope or basinal setting.

6.2 TRATIGRAPHIC FRAMEWORK

6.2.1 Stratigraphic correlations

Besides the lithofacies characterization, the existing information of the wells investigated was integrated with interpretative stratigraphic correlations to complement the results. In this way, aiming to recognize the principal characteristics of the Oligocene-Miocene reservoirs of the Eastern Marlim oilfield seven stratigraphic correlations were developed (Fig. 29).

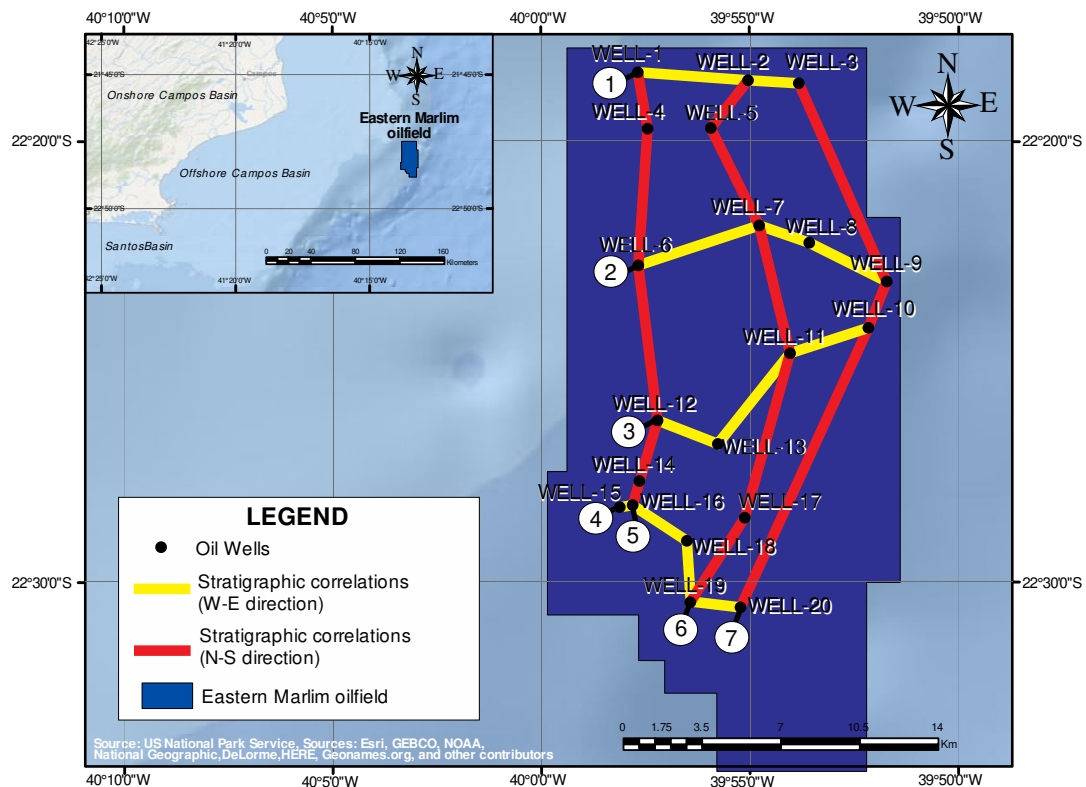


Figure 29. Location map of the developed chronostratigraphic correlations based on the selected type wells that describes the principal characteristics of the Oligocene-Miocene reservoirs in the study area.

As a stratigraphic datum, the top of the Oligocene-Miocene section of the Carapebus Formation was used (Figs. 30, 31 and 32). As a result, the stratigraphic correlations and type wells indicated that it is possible to subdivide the Oligocene-Miocene reservoirs in the study area into three principal reservoir zones, identified as Upper Sandstone (US), Middle Sandstone (MS) and Lower Sandstone (LS). Pelitic and/or calcareous layers characterized by variable log motifs in different wells separate these zones

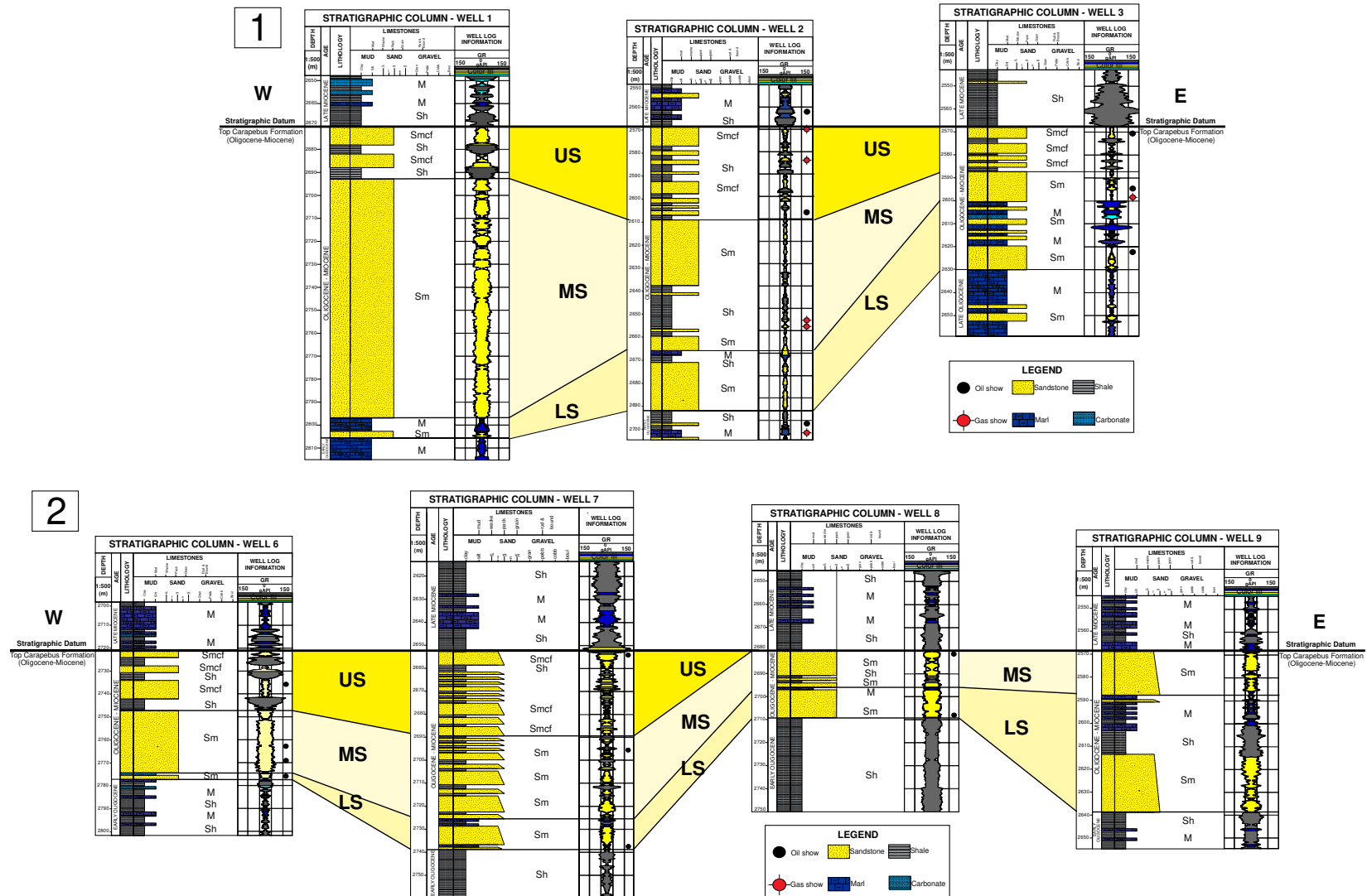


Figure 30. W-E oriented stratigraphic correlations (1 and 2) showing the type wells that describe the major zones (US: Upper Sandstone, MS: Middle Sandstone, LS: lower Sandstone) of the Oligocene-Miocene reservoirs in the Eastern Marlim oilfield.

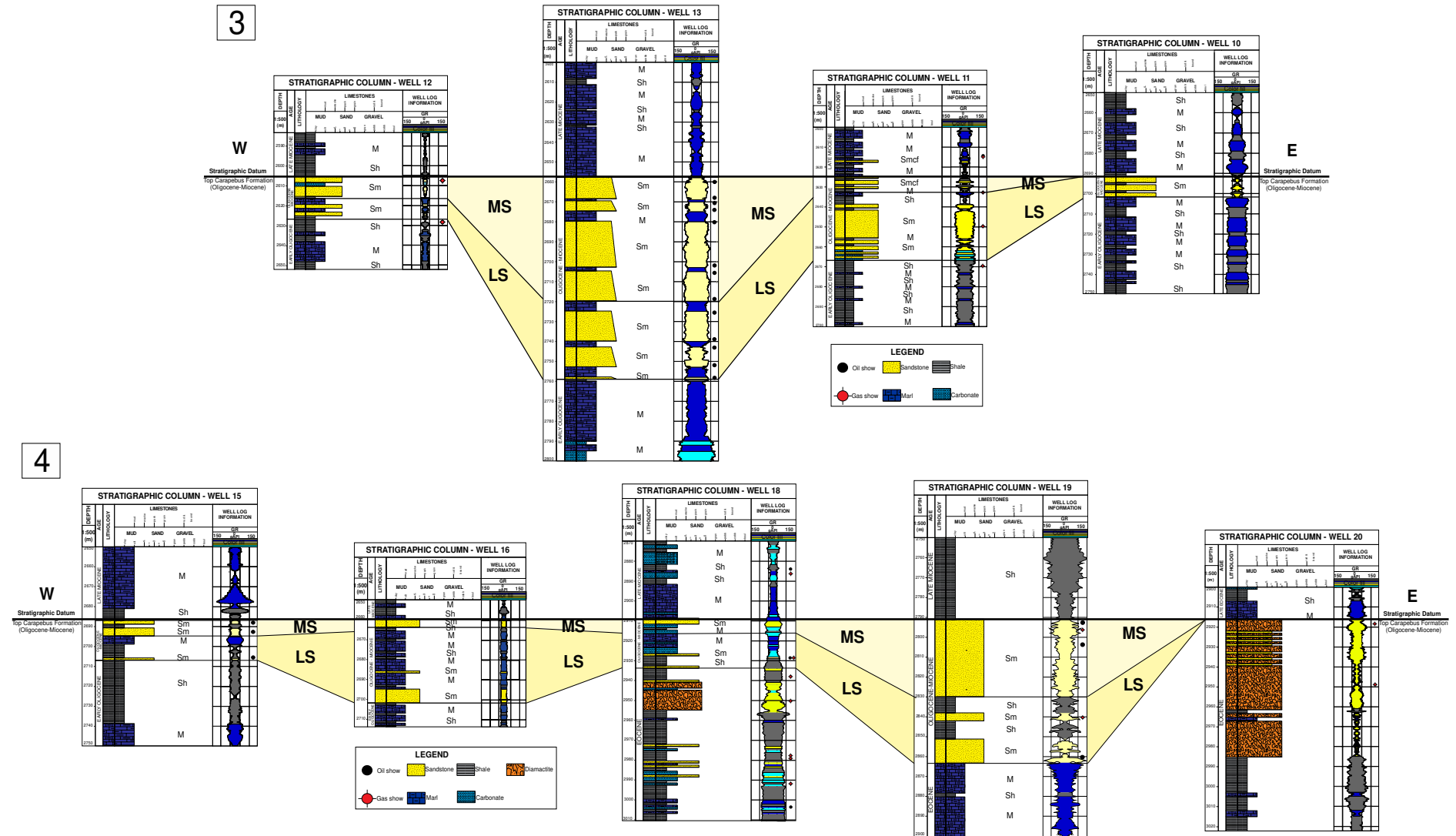


Figure 31. W-E oriented stratigraphic correlations (3 and 4) showing the type wells that describe the major zones (US: Upper Sandstone, MS: Middle Sandstone, LS: lower Sandstone) of the Oligocene-Miocene reservoirs in the Eastern Marlim oilfield.

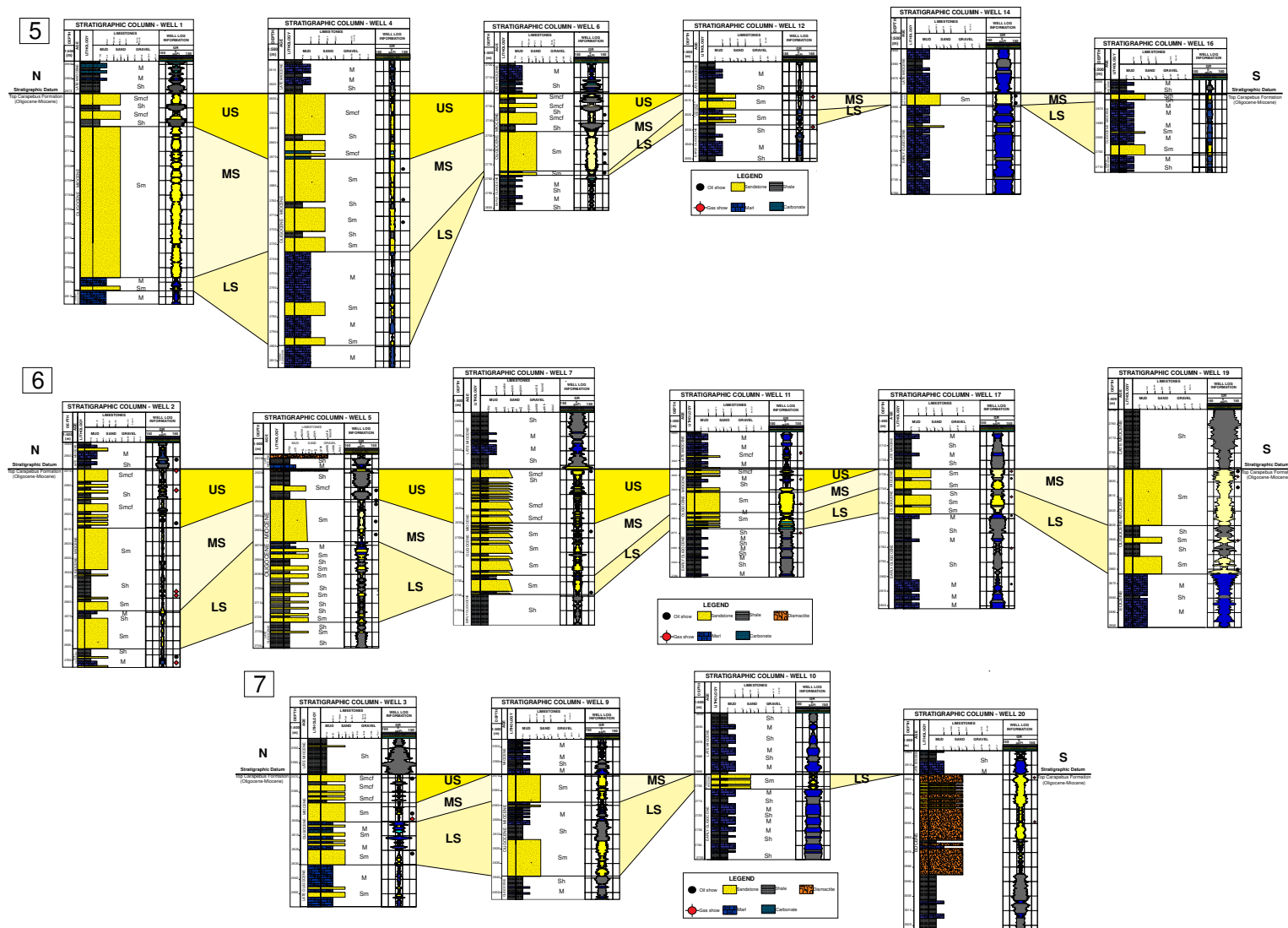


Figure 32. N-S oriented stratigraphic correlations (5, 6 and 7) showing the type wells that describe the major zones (US: Upper Sandstone, MS: Middle Sandstone, LS: lower Sandstone) of the Oligocene-Miocene reservoirs in the Eastern Marlim oilfield.

In the seismic data, the Oligocene-Miocene reservoirs may be hard to distinguish, especially in faulting and pinch out areas, where their thicknesses fall below the seismic resolution. The Figure 33, illustrates synthetic seismograms (wells 7-14), where a suitable well-seismic tie is observed.

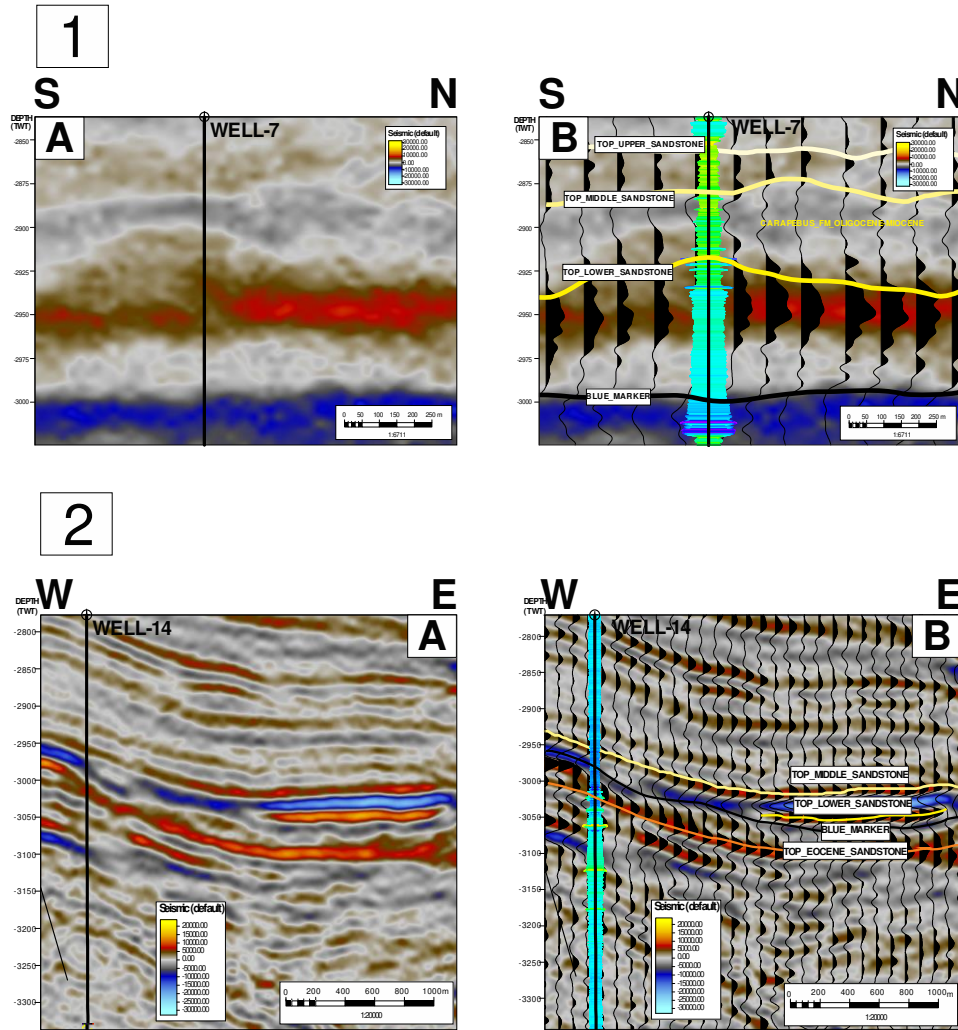


Figure 33. Seismic images displaying typical seismic amplitude response (poststack time-migrated seismic lines/zero-phase American polarity/seismic (default) color scale) of the US, MS and LS zones in the Eastern Marlim oilfield in: A) normal visualization, and, B) regular wiggle-trace imagery of seismic amplitude. 1) 2D seismic line 8 in S-N direction located in the northern portion of the study area displaying a suitable well-seismic tie. The three recognized major zones (US, MS and LS) of the Oligocene-Miocene section can be observed, as well as the Blue Marker (MFS) below them. 2) 2D seismic line 5 in W-E direction located in the middle portion of the Eastern Marlim oilfield displaying a suitable well-seismic tie. The MS and LS zones (absent of the US zone) of the Oligocene-Miocene section can be observed, as well as the Blue Marker (MFS) and top of the Eocene sandstones below them.

The top of the US is represented by a weak positive amplitude, hard to differentiate in some cases, related to the transition between the shales of the Ubatuba Formation and the appearance of the turbiditic sandstones of the Carapebus Formation. In contrast, the top of the MS is also represented by a positive amplitude, but better to recognize than the one that marks the top of the US. The top of the LS is represented by a high positive amplitude, which becomes weaker towards the base. This is explained by the occurrence of shales and marls beds (Bluer Marker-MFS) just below the Oligocene-Miocene reservoirs.

6.2.2 Lower sandstone (LS)

Represented by thin sandstones layers (Sm lithofacies) interbedded with shales and marls (Sh and M lithofacies) beds up to 10m thick, presenting predominant bell retrograding GR log curve shape. These layers may be located at several levels within this stratigraphic interval and they are more continuous laterally than in the US and MS (Figs. 30, 31 and 32). These levels are representative of more than 70% of the LS rock volume. The seismic amplitude response is the most clear in the study area but do not display depositional elements (Fig. 33). The hydrocarbon accumulations and shows are not commonly evident in these levels, and only oil shows were observed at the top of the sandstones packages (Sm lithofacies) positioned near to the MS. As well, this zone is the most extensive and with more variable thickness in relationship with the sandy levels (10-60m), showing the transition of a predominant clastic succession to a calcareous progression (Blue Marker).

6.2.3 Middle sandstone (MS)

This zone displays well-developed blocky GR log curve motifs and is characterized by prominent fine to medium-grained sandstones layers (Sm lithofacies) with at least 30 to 100 meter thick (Figs. 30 , 31 and 32). The MS is the thickest zone in the study area, and more laterally extensive than the US, decreasing its thickness to the east, as well as, to the southern portion of the Eastern Marlim oilfield. These sandstones are the cleanest (well sorted) in the entire area, occasionally interbedded with other non-reservoir lithologies (Sh lithofacies). In addition, oil shows are very common in this zone. The 2D and 3D seismic lines do not reveal features of depositional elements (Fig. 33).

6.2.4 Upper sandstone (US)

The upper sandstone (US) is characterized by fine to medium-grained sandstones (Smcf lithofacies) with predominant bell retrograding GR log curve shape interbedded with grayish dark micaceous shales with predominant cylindrical aggrading GR log curve shape. In addition, it is common to find oil shows in these sandstones. The US is the thinnest and shortest but the most constant thickness zone in the study area, and less laterally extensive than the MS and LS, reaching a maximum thickness of almost 45m (Figs. 30, 31 and 32). The seismic amplitude observed in the different seismic lines images does not reveal features that would allow a clear identification of depositional elements (Fig. 33). This zone interbedded with shale layers (Sh lithofacies) up to 10m thick. These layers may be located at several levels within this stratigraphic interval and they are continuous laterally. The shales facies are decreasing from west to east, and from south to north of the Eastern Marlim Oilfield.

6.3 DISTRIBUTION AND SAND PROPORTION MAPS

In the study area, the Oligocene-Miocene succession consists essentially of siliciclastic facies. The thickness of the siliciclastic facies across the study area ranges from 30-210m approximately. This succession presents thickness variability across the stratigraphic correlations and shows randomly distribution of the sandstones layers laterally. From north to south, and from west to east of the Eastern Marlim oilfield as well, a high diminution of the average thickness of the succession was observed.

In addition, the non-reservoirs facies (Sh and M lithofacies) increase its thickness in the same direction being inversely proportional to the sand content (Sm and Smcf lithofacies) that decreases in the same way. Therefore, more defined clean sandstones (well sorted) are located in the northwestern part and central portion of the Eastern Marlim oilfield, positioned in the same direction of the sediment accumulation of the turbidite system (Fig. 34).

Regarding the major zones observed in the research area, they have a preferential trend with NNW-SSE direction, following the direction of the turbiditic accumulation. Concerning the Lower Sandstone (LS), it is the most laterally extensive zone of the research area, but considered as the weakest reservoir zone in relationship with the decrease in the content of sandy levels (Ss lithofacies) and infrequent oil shows. In addition, it is important to highlight that the LS has a tremendous increase in non-reservoir layers (Sh and M lithofacies) that are laterally continuous and increasing its thickness towards the eastern and southern portions of the study area (Fig. 35).

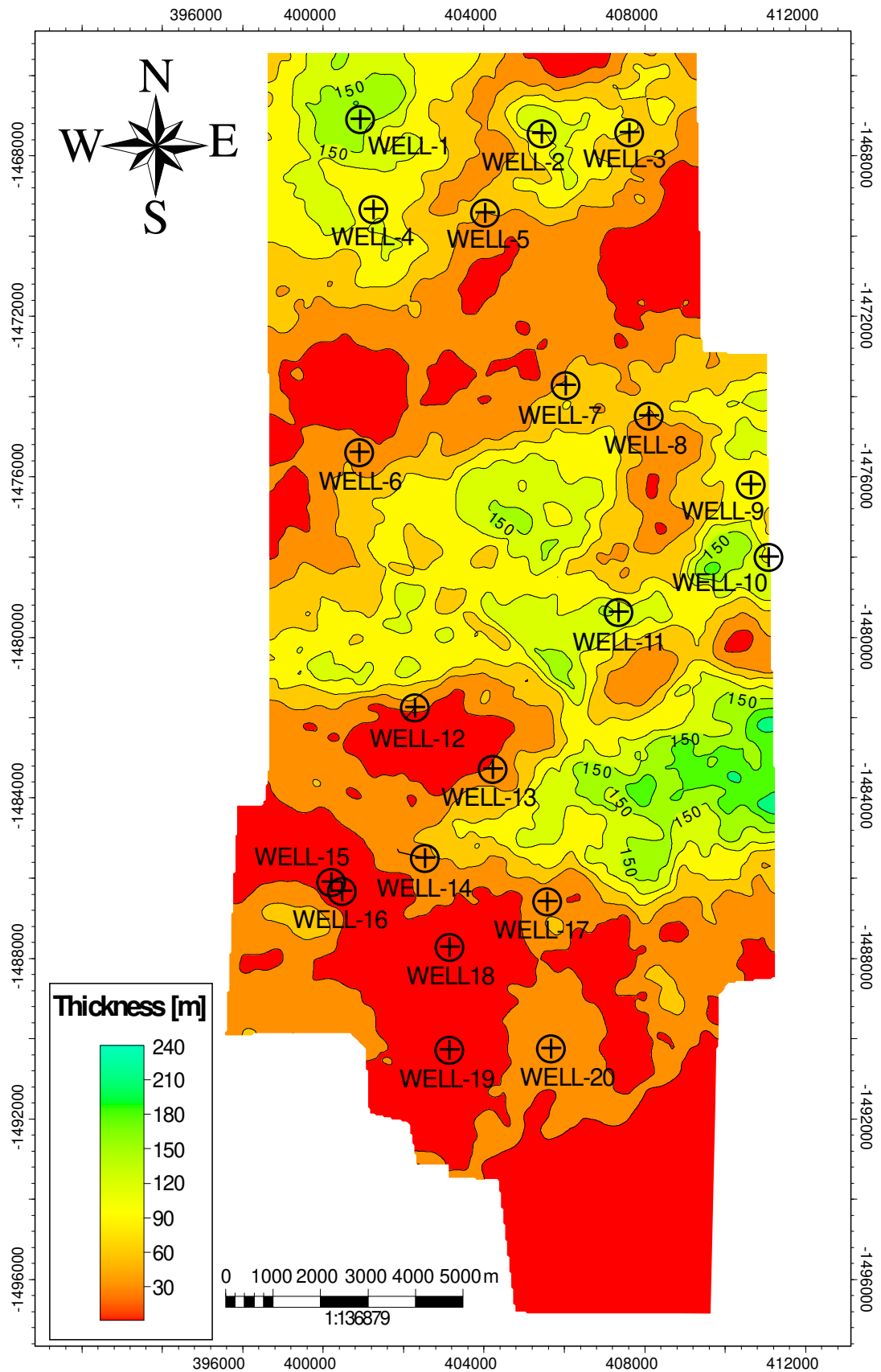


Figure 34. Sand proportion map of the Carapebus Formation (Oligocene-Miocene) in the Eastern Marlim oilfield. An increase of sand content (90-240m approximately) can be observed in the northern and middle portion of the study area.

On the other hand, the Middle Sandstone (MS) is considered as the thickest zone in the Eastern Marlim oilfield, displaying in some regions, abrupt thickness changes (wells 7, 9 and 13), that are observed in W-E direction associated with channelized features (Fig. 36). The largest thickness of the MS coincides with the channels observed in the W-E oriented stratigraphic correlations and with the prevalence of well-developed blocky GR log curve motifs in the well logs (Fig. 31). However, areas of important thickness may also occur laterally to the mentioned channelized features, likewise associated with blocky log motifs. Along the axis of the channels, a thickest sand proportion distribution (Sm lithofacies) was verified; where the blocky GR log curve motifs are more common. Lateral to the channel, where the blocky log motifs are also prevalent, the sand proportion decreases progressively (Figs. 31 and 36).

Finally, the US may reach a maximum thickness of 45m (well-4), and it pinches out to the east (well-8) and middle portion (well-12) of the study area, being the thinnest zone of the studied reservoir interval (Fig. 37).

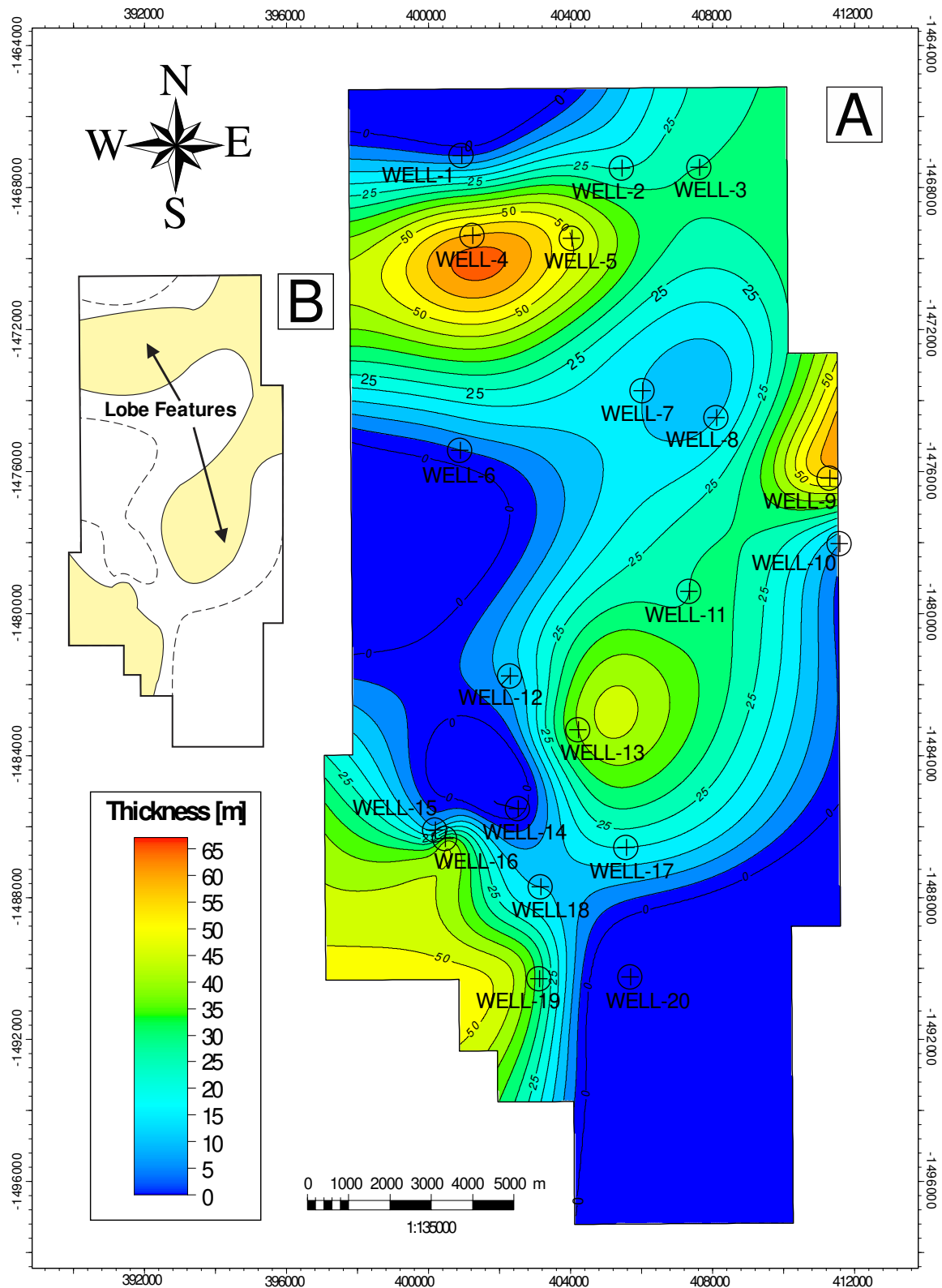


Figure 35. A) Distribution map of the Lower Sandstone (LS) of the Carapebus Formation (Oligocene-Miocene) showing its extensive distribution in the Eastern Marlim oilfield. B) Presence of lobe features observed in the study area.

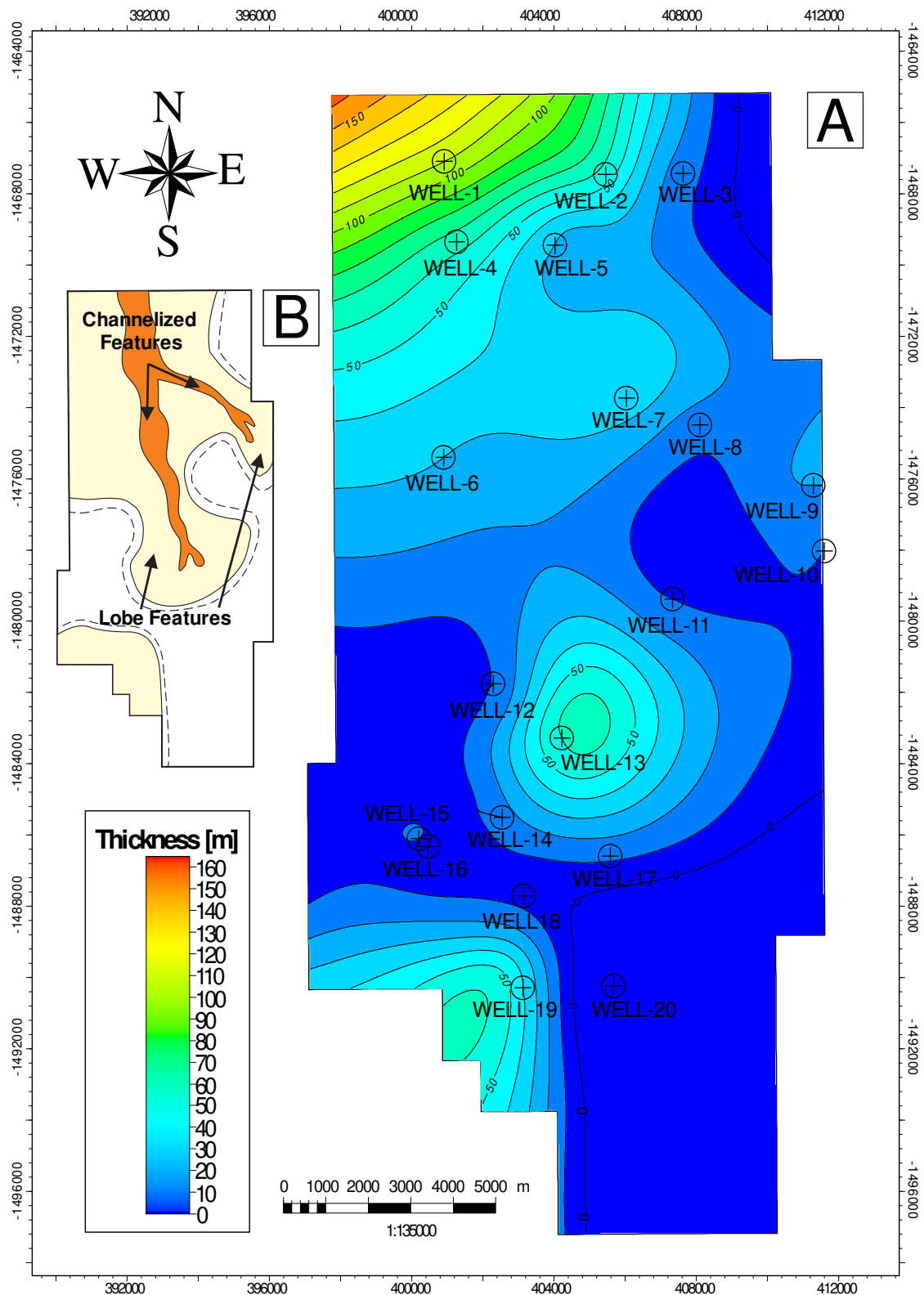


Figure 36. A) Distribution map of the Middle Sandstone (MS) of the Carapebus Formation (Oligocene-Miocene) displaying an increase in its thickness towards to the north and middle portion of the Eastern Marlim oilfield. B) Presence of channelized and lobe features observed in the study area.

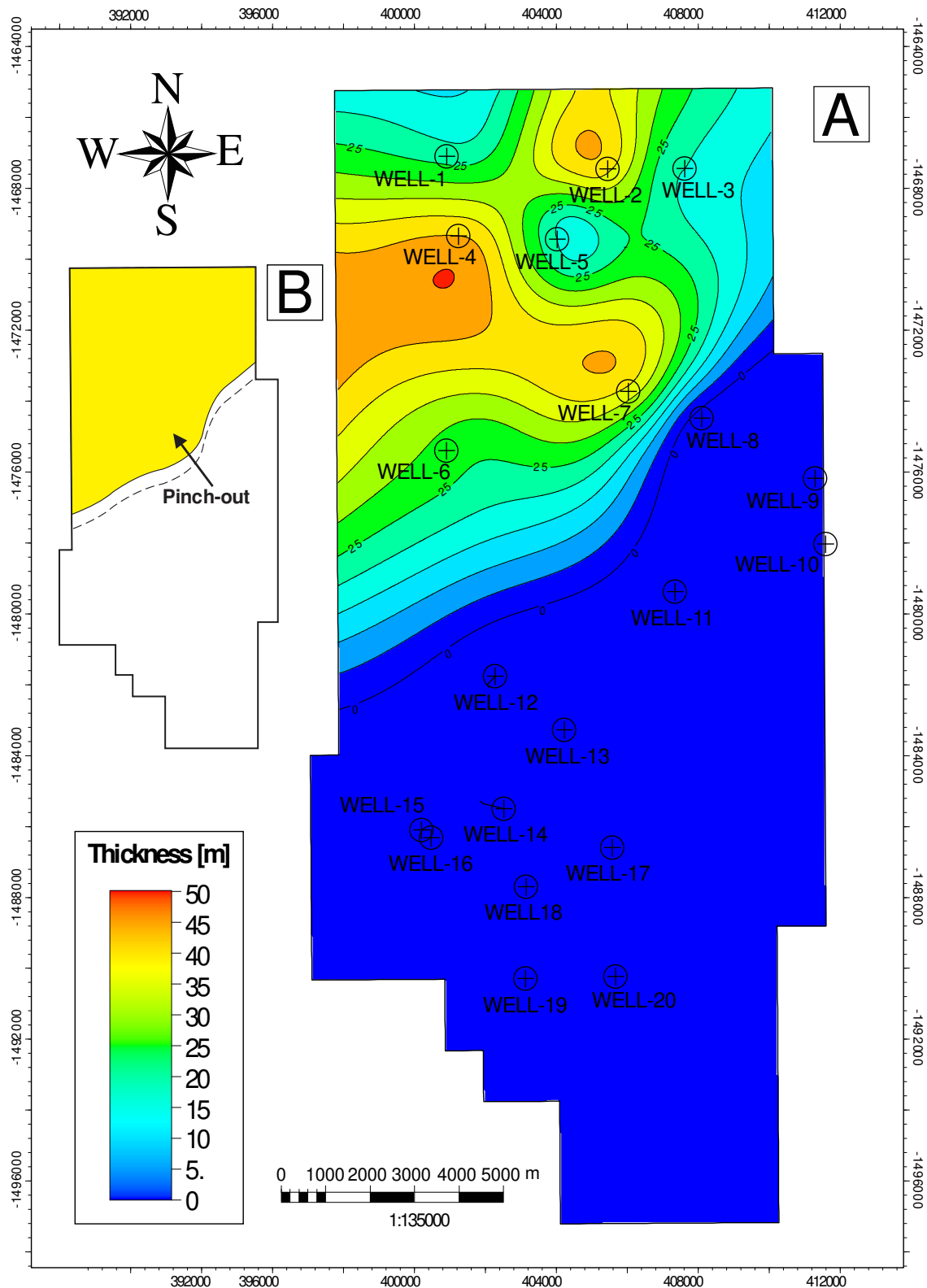


Figure 37. A) Distribution map of the Upper Sandstone (US) of the Carapebus Formation (Oligocene-Miocene) displaying an increase in its thickness towards to the north portion of the Eastern Marlim oilfield. B) Pinch-out towards to the eastern and middle portion of the study area.

6.4 PETROPHYSICAL ANALYSIS BASED ON LITHOTYPES

6.4.1 Petrophysical lithotypes interpretation

Based on the analysis of the different responses and associations of the available well logs with techniques of multivariate analysis of multi-group dataset or clusters, adjusted by geological descriptions realized during drilling presented in the Formation Evaluation Log (FEL), the petrophysical interpretation based on lithotypes it was made. The multivariate analysis is focused on the spatial association of log curves such as Density (RHOB), Neutron (NPHI), Gamma Ray (GR), and Sonic (DT) from two to n-dimensions with the objective of defining groups with common characteristics in the readings of the well logs. As follows, the common characteristics of the well logs were correlated with the lithologies described in the wells and were demarcated particular behaviors (value and distribution) in the petrophysical properties. In this way, a combination of the mentioned characteristics was used to define a petrophysical lithotype. At least, five petrophysical lithotypes were defined in the Oligocene-Miocene interval of the Carapebus Formation as follows: (1) Clean Sandstones (Ss1), (2) Muddy Sandstones (Ss2), (3) Calcareous Sandstones (Ss-Lm), (4) Calcareous (Lm), and finally (5) Shaly (Sh) lithotypes (Fig. 38). Likewise, each lithotype was defined by particular distributions of petrophysical properties that allow classifying them as reservoir (Ss1 and Ss2), retardant (Ss-Lm) or seal-cemented rocks (Lm and Sh).

As a result, the petrophysical lithotypes identified in the Oligocene-Miocene section displays a very good correlation with the main lithofacies recognized in the study area. In this way, the Clean Sandstones petrophysical lithotype (Ss1) have a great correlation with the Sm lithofacies showing the best features as reservoir rocks in the entire oilfield. As well, the Muddy Sandstones and Calcareous Sandstones petrophysical lithotypes (Ss2 and Ss-Lm) have a good correlation with the Smcf lithofacies, being the main second order reservoirs in the Eastern Marlim oilfield. Finally, the calcareous and shaly petrophysical lithotypes (Lm and Sh) have and excellent correlation with the Sh and M lithofacies respectively, linked as the non-reservoir facies in the entire interval of interest. In conclusion, the developed technique allows the improvement and quality of the lithofacies previously identified in the current research with the standard logging suite conducted in the present oilfield displaying an outstanding correlation between the both mentioned methods.

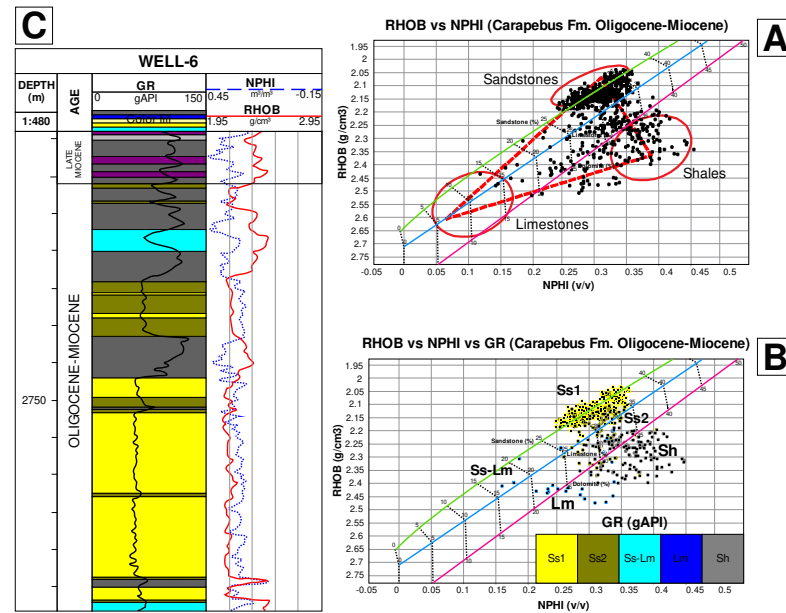


Figure 38. Example of petrophysical analysis based on lithotypes defined by the response of the Density-Neutron pair (RHOB - NPHI) and Gamma Ray (GR) log in the Well-6 of the Eastern Marlim oilfield. A) Crossplot of RHOB vs NPHI displaying a ternary diagram (dashed red triangle) with sandstones, shales, and limestones zones (red circles zones). B) Crossplot of RHOB vs NPHI vs GR showing the five petrophysical lithotypes identified in the Oligocene-Miocene interval of the Carapebus Formation (Clean Sandstones (Ss1), Muddy Sandstones (Ss2), Calcareous Sandstones (Ss-Lm), Calcareous (Lm), and finally Shaly (Sh) lithotypes). C) Well-track of the Well-6 presenting the identified lithotypes into the gamma ray track (GR: Gamma Ray log (gAPI), Density-Neutron pair log (NPHI (m^3/m^3), RHOB (g/cm^3)).

6.4.2 Petrophysical properties estimation

The high friability condition of the reservoirs facies causes a very low recovery of core samples in the oilfield (Marlim Complex), making difficult to measure the petrophysical conditions at reservoir scale. At the same time, the friable nature of the rocks provide the production of solids along with the oil, making necessary special sand containment measures in the producing wells (Milani & Araújo, 2003). In this way, we used the available well log basic dataset aiming to understand and calculate the petrophysical properties of the studied section through deterministic equations and petrophysical methods as follows:

6.4.2.1 Shale Volume Calculation (VSH)

Shale is usually more radioactive than sand or carbonate lithologies. Thus, the gamma ray log (GR) can be use aiming to calculate the shale volume in siliciclastic

reservoirs. The shale volume is represented as a decimal fraction or percentage known as “VSH”. The calculation of the gamma ray index is the first step needed to determine the VSH from the gamma ray log. In the current research, the mentioned parameter was calculated from the deterministic model based on the gamma ray log given by the following equation developed by Larionov (1969):

$$\text{VSHGR} = \frac{\text{GRC} - \text{GRmatrix}}{\text{Grshale} - \text{GRmatrix}} \quad (9)$$

Where, GR_Matrix (40 api), and GR_Shale (100 api), respectively, that were used to determine the content of shale in the current Oligocene-Miocene siliciclastic section.

The figure 39 represents the result of the VSH calculation interpreted in the different petrophysical lithotypes with their respective observed distribution. In this way, we found, as expected, that the reservoir facies (Ss1 and Ss2) had minor content of VSH in contrast with the retardant (Ss-Lm), seal and/or cemented (Lm and Sh) petrophysical lithotypes, displaying a very good correlation with the sedimentological characteristics observed in the main lithotypes already found in the study area.

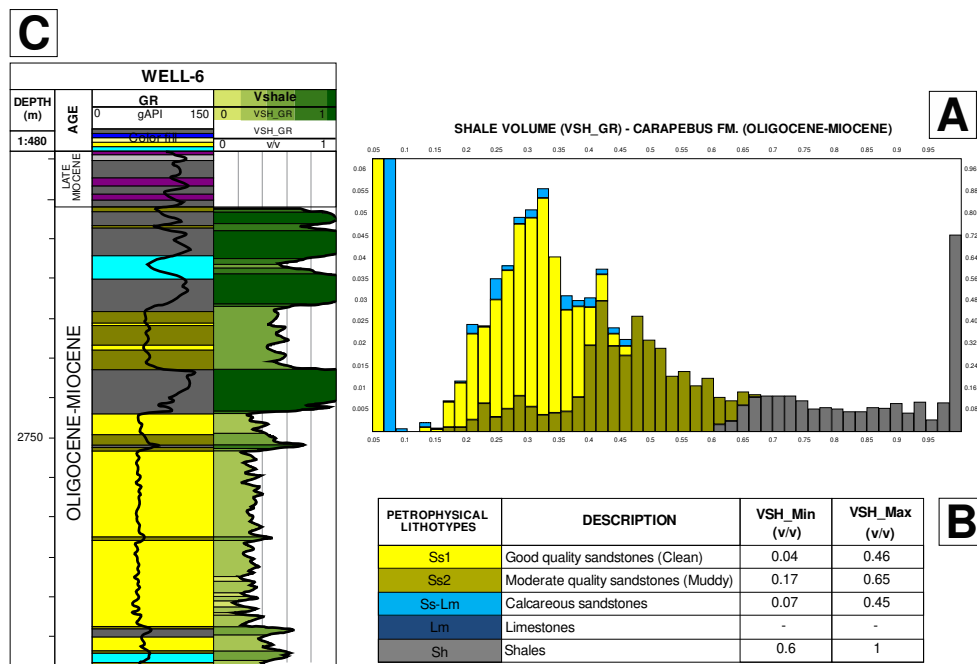


Figure 39. Result obtained for the Shale Volume calculation (VSH) exemplified in the interpreted petrophysical lithotypes in the Well-6 of the Eastern Marlim oilfield. A) Histogram of the calculated VSH for the Carapebus Formation (Oligocene-Miocene). B) Table showing the identified lithotypes and the minimum and maximum values of VSH. C) Well-track of the Well-6 presenting the identified lithotypes and calculated VSH values (GR: gamma ray log (gAPI)), VSH log (v/v)).

6.4.2.2 Effective Porosity estimation (PHIE)

Five available wells had information related with porosity measurements at reservoir scale in the Oligocene-Miocene interval of the Carapebus Formation in the Eastern Marlim oilfield (wells 4-7-13-15-19). Thus, the existing data provide porosity values ranging between 23.4-33% with an average porosity of 30% approximately. Additionally, we developed porosity models based on deterministic equations given by the Density, Neutron-Density pair and Sonic logs for the twenty available wells. For the Muddy Sandstones (Ss2 petrophysical lithotype) a marked difference between the porosity calculated from the Sonic and the Density-Neutron pair log were evidenced (Fig. 40). The mentioned random pattern may be due to the mineralogical composition of this type of rock, which is associated with a calcareous-feldspathic composition observed in the lithofacies characterization, and associated with the Smcf lithofacies.

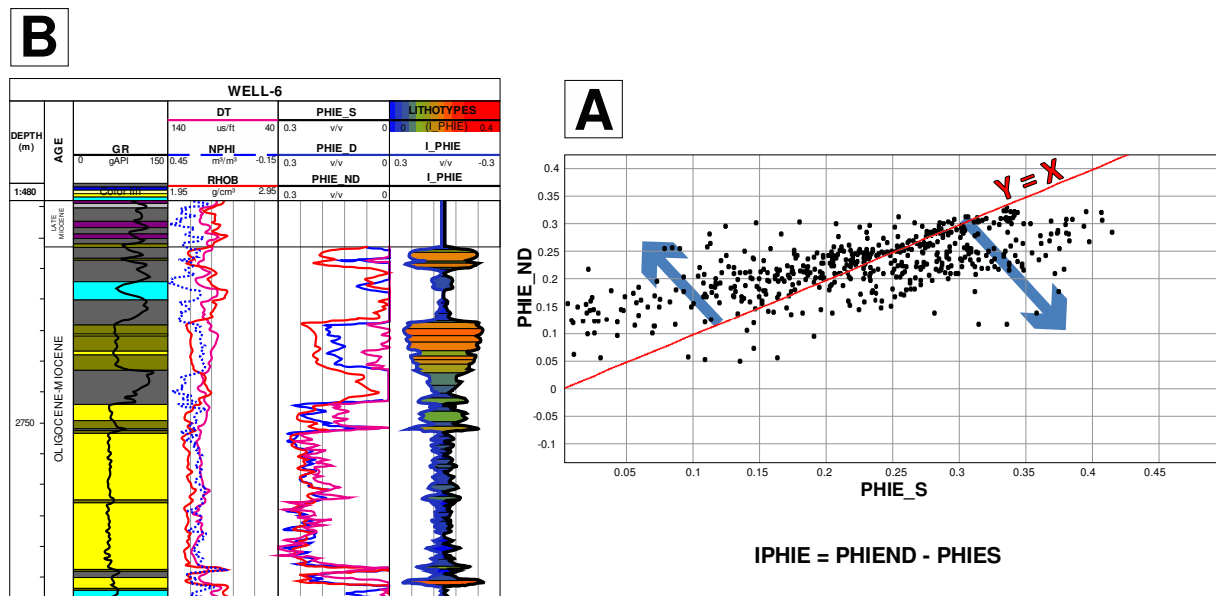


Figure 40. Effective porosity estimation (PHIE) for the interpreted petrophysical lithotypes in the Well-6 of the Eastern Marlim oilfield. A) Crossplot of PHIE calculated from the Sonic (PHIE_S) and the Density-Neutron pair (PHIE_ND) well logs. The Ss2 petrophysical lithotype displayed a marked difference between the calculated porosities. This difference was explained by the mineralogical composition of this lithotype that is associated with a calcareous-feldspathic composition. B) Well-track of the Well-6 presenting the identified lithotypes into the Gamma Ray track, a track of Sonic (DT), Neutron (NPHI), and Density (RHOB) logs, a track of effective porosity estimations (PHIE), and a track of effective porosity index (IPHIE). (GR: gamma ray log (gAPI), DT (us/ft), NPHI (m³/m³), RHOB (g/cm³), PHIE_S (v/v), PHIE_D (v/v), PHIE_ND (v/v), IPHIE (v/v)).

The deterministic model used as the final model for the effective porosity was calculated from the density-neutron pair, since it was a conservative model for the Muddy Sandstones (Ss2 petrophysical lithotype) (Fig. 41). As a result, regarding the reservoir facies, which are the scope of the current study, for the Clean Sandstones (Ss1 petrophysical lithotype), we calculated porosity values around 15-35%, with an average of 25%, displaying excellent characteristics as reservoir rocks.

Concerning the Muddy Sandstones (Ss2 petrophysical lithotype), we observed a considerable diminution in the porosity values ranging between 5-25% approximately, with an average value of 15%, associated with their mineralogical composition, demonstrating that the mentioned facies have fair to good characteristic as reservoir rocks. As a conclusion, the porosity values calculated with the available well logs had a very respectable correlation with the existing measured porosity values in the Eastern Marlim oilfield demonstrating the already proved reservoir potential of the studied section.

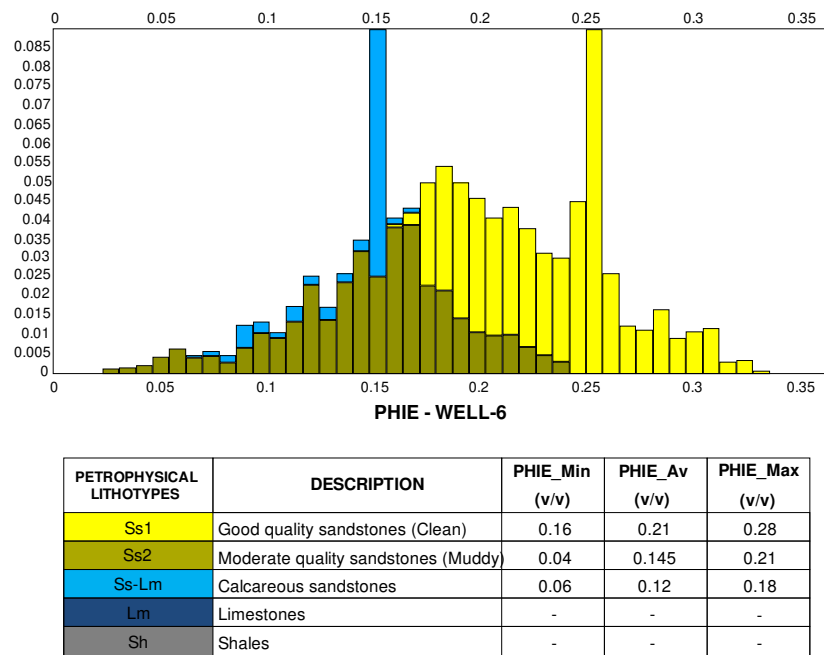


Figure 41. Example of the final distribution of PHIE in the interpreted petrophysical lithotypes in the Well-6 of the Eastern Marlim oilfield.

6.4.2.3 Water Saturation (SW)

Using the Archie's equation, the water saturation was calculated. In this equation, the main critical variable is the formation water resistivity (R_{we}), so we made an analysis to the mentioned variable taking into account production tests and the pickett-plot as shown in figure 42. We used the average value for the calculation of SW.

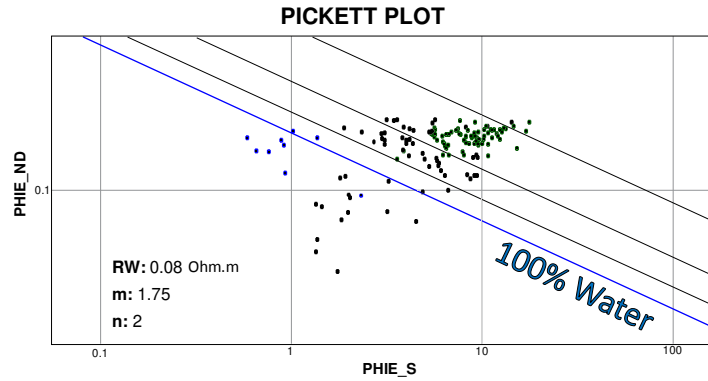


Figure 42. RWe analysis for the formation of interest in the Well-6 of the Eastern Marlim oilfield.

Taking into account the result of the petrophysical evaluation and well log analysis, an oil-water contact was found at 2773m approximately, which can be observed in the well-6 of the Eastern Marlim oilfield (Fig. 43). In this way, we evidenced oil accumulations in the Clean and Muddy sandstones (Ss1 and Ss2 petrophysical lithotypes) respectively. Therefore, the first petrophysical lithotype has better conditions for hydrocarbon production than the second one taking into account the favorable compositional and petrophysical properties of the Clean Sandstones (Ss1 petrophysical lithotypes). Finally, regarding the Muddy Sandstones (Ss2 petrophysical lithotype), we verified fair to good petrophysical features being affected by their calcareous-feldspathic composition, which disturb the behavior for the production of hydrocarbons in the mentioned petrophysical lithotype.

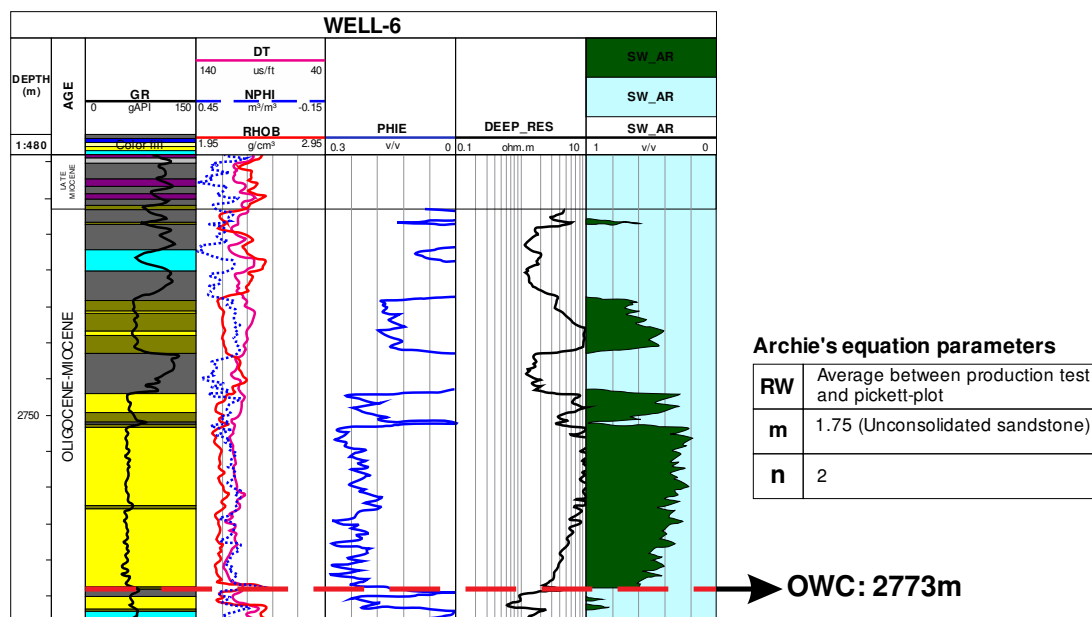


Figure 43. Oil-water contact (OWC) seen at 2773m depth in the Well-6 in the Eastern Marlim oilfield.

6.5 DEPOSITIONAL AND STRATIGRAPHIC MODEL

The lithofacies characterization and petrophysical analysis based on lithotypes gave very good insights about the stratigraphic and sedimentological framework of the Oligocene-Miocene section at reservoir scale in the Eastern Marlim oilfield. Consequently, a deep-water turbidite sequence that includes three major zones composing the elements of a submarine lobe complex associated with sandy facies representing different stages of deposition of bipartite turbidite flows were observed. The mentioned zones express very good lateral and vertical continuity of massive unconsolidated amalgamated sandstones bodies with very good porosity representing excellent reservoirs.

The interval of study represents a second-order, exploration-scale depositional sequence that includes an entire system tract. The deposition of the mentioned sandstones bodies suggest accumulation during a Highstand Systems Tract (HST), associated with regressive deposits that were form when sediment accumulation rates exceed the rate of relative sea-level rise and an increase in accommodation constituted the upper systems tracts in either a type 1 or type 2 sequence (Kendall and Alnaji, 2002).

In this way, the Lower Sandstone (LS) marks the early stages of the HST, where thinner layers of clean sandstones (Sm lithofacies/Ss1 petrophysical lithotype) interbedded with thickest beds of shales and marls (Sh and M lithofacies/Lm-Sh petrophysical lithotypes), were accumulated after the deposition of the maximum flooding surface (MFS) associated with the regional Blue Marker (Fig. 44). The mentioned surface typically marks the time of maximum flooding or transgression of the shelf and separates the transgressive and HST. Seismically, the MFS is often expressed as a downlap surface were marine shelf and basinal sediments associated with this surface are the result of slow rates of deposition by pelagic-hemipelagic sediments that are usually thin and fine-grained. These fine sediments make up a condensed section that corresponds to the time of lowest sediment supply to the deepwater part of the basin (Mitchum, 1977). Like this, following the end of the transgression, the renewed progradation during the HST may mark the return of turbidites into the deep basin (De Gasperi and Catuneanu, 2014).

Successively, the MS display coarsest sediments that become finer towards the top of the studied section (Sm lithofacies/Ss1 petrophysical lithotype) and consist of laterally and vertically amalgamated channel features deposits attributed to high-density turbidity flows.

These renewed progradation of coarser clastics sediments and discrete channelized features marks the principal stages of the HST. In addition, the sandstone bodies

of the MS represent the thickest zone of the research area representing the best reservoirs in the entire Eastern Marlim oilfield (Fig. 44).

Finally, the US is represented by medium to fine-grained sandstones, presenting a regular to moderate fining-upward trend (Smcf lithofacies/Ss2 petrophysical lithotype) interpreted as laterally amalgamated sandstones bodies, which pinches out toward the middle and eastern portion of the Eastern Marlim oilfield marking the sequence boundary of the HST and the final renewed progradation of clastics deposits (Fig. 44).

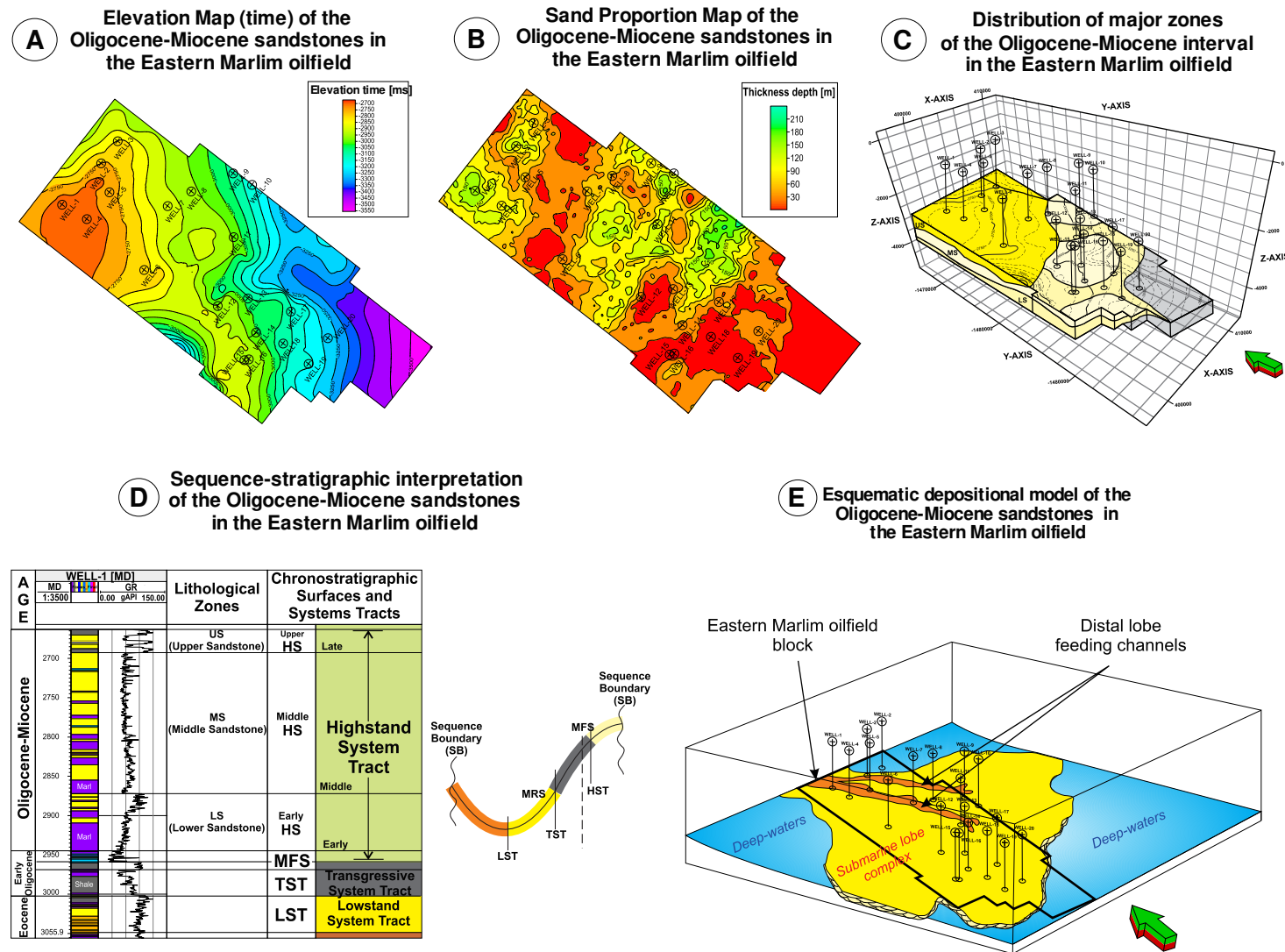


Figure 44. Final model displaying: A) Elevation map, B) Sand proportion trends, C) Major zones, D) Sequence stratigraphic interpretation, and E) depositional/stratigraphic framework for the Oligocene-Miocene interval of the Carapebus Formation in the Eastern Marlim oilfield

6.6 SEISMIC INTERPRETATION

Point toward to understand the geological framework of the Eastern Marlim oilfield a subsurface database were utilized including eight-2D seismic lines and one-3D seismic cube (Fig. 21). In all the mentioned seismic surveys was carried a quality control (Mistie correction) and the seismic-well tie processing pointing for a more accurate geological interpretation. Data quality deteriorates in the pre-salt section and surrounding areas, whereas halokinesis activity or salt tectonics difficulty the seismic interpretation. In this way, different seismic attributes were used (structural, stratigraphic, signal processing and complex seismic attributes), supporting the robust seismic interpretation and enhancing the seismic visualization in areas with low seismic quality. After the mentioned steps, pointing to identify different tectonostratigraphic units, different seismic facies enhancing the geological interpretation of the research area were identified. All the mentioned information was processed and incorporated into a multidisciplinary framework (stratigraphy, sedimentology and structural contexts) to enable mapping and distribution of the different tectonostratigraphic units in geological and geographic terms within the Eastern Marlim oilfield.

6.4.1 Seismic attributes

Aiming to improve the visualization of the available seismic data, as well as the interpretation of the different stratigraphic surfaces and seismic facies in the study area, different seismic attributes were used. Successively, diverse seismic attributes were applied in the available seismic surveys and then classified into four groups as follows: stratigraphic, structural, signal and complex (Fig. 45).

Consequently, as stratigraphic seismic attributes the Chaos and Relative Acoustic Impedance seismic attributes were used providing very good insights in the continuity of seismic reflectors and faulting trends. In addition, the mentioned seismic attributes improved the seismic facies interpretation mainly in carbonates and evaporites facies pointing to mapping the base and top of salt structures.

Moreover, as a structural method, the Amplitude Contrast seismic attribute was performed offering great viewing in the continuity of reflections patterns and very good visualization of faults. As well, the mentioned seismic attribute establishes boundaries between seismic patterns.

Additionally, as a signal-processing attribute, the RMS Amplitude seismic attribute was implemented improving the seismic facies interpretation mainly in carbonates

and evaporites facies. Moreover, this attribute offers insights to mapping the base and top of salt structures.

Finally, as complex methods, the Cosine of Phase and Sweetness seismic attributes were applied improving the visualization of high amplitude responses, providing great visualization in the continuity of seismic reflectors and faulting trends, establishing boundaries of rifting seismic patterns.

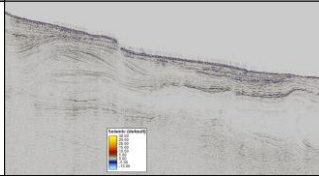
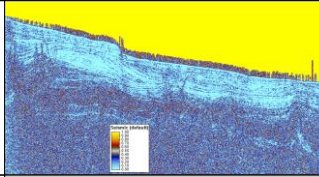
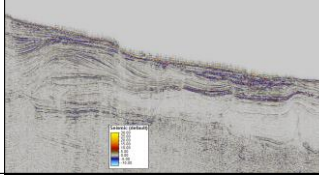
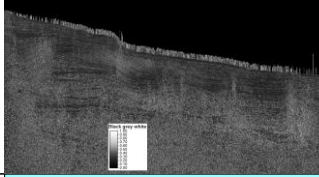
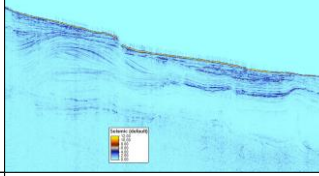
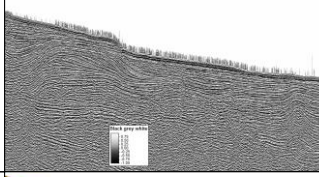
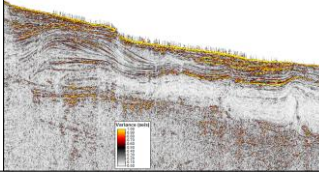
Seismic Attribute	Seismic Reflection Patterns (Visualization)	Usage in Seismic Interpretation
Seismic Default		Seismic Default Method: <ul style="list-style-type: none"> - Default seismic reflection expression that provides very good insights in different geological analysis. - Offers great viewing for structural and stratigraphic analysis, seismic inversion, seismofacies analysis, seismic attributes analysis, etc.
Chaos		Stratigraphic Method: <ul style="list-style-type: none"> - This seismic attribute computes the local chaos, meaning the lack of organization in the structural estimate. - Provides very good insights in the continuity of seismic reflectors and faulting trends.
Relative Acoustic Impedance		Stratigraphic Method: <ul style="list-style-type: none"> - Estimated relative acoustic impedance is calculated by integrating the trace, then passing the result through a high-pass Butterworth filter. No parameters required. - Improved seismic facies interpretation. Great to identify the base and top of salt structures.
Amplitude Contrast		Structural Method: <ul style="list-style-type: none"> - Runs a 3D contrast filter with dip guiding options. - Offers great viewing in the continuity of reflection patterns in the seismic lines and very good visualization of faults. In addition, establishes boundaries between seismic patterns.
RMS Amplitude		Signal Processing Method: <ul style="list-style-type: none"> - RMS Amplitude computes RMS on instantaneous trace sample over a specified window (default 9 samples). - Improved seismic facies interpretation, mainly in carbonates and evaporites. Very good to mapping the base and top of salt structures.
Cosine of Phase		Complex Method: <ul style="list-style-type: none"> - Cosine of instantaneous phase: $\cos(\text{phase})$. Also known as: Normalized amplitude. - Offers great viewing in the continuity of reflection patterns in seismic lines and very good visualization of faults. In addition, establishes boundaries between seismic patterns.
Sweetness		Complex Method: <ul style="list-style-type: none"> - Defined as $\text{Envelope}/\sqrt{\text{instantaneous frequency}}$. For numerical reasons a lower threshold of frequency is set at 1 Hz. - Improved the visualization of high amplitude seismic reflectors, providing very good insights in their continuity and faulting trend. Establishes boundaries of rifting seismic patterns.

Figure 45. Visualization, use and interpretation of different seismic attributes available in the library of the Petrel E&P software platform 2013 of Schlumberger (academic license), and generated from an available seismic line (seismic line 1) at normal phase (Seismic Default) in the Eastern Marlim oilfield.

6.4.2 Seismic stratigraphy analysis

Seismic stratigraphy was used in mapping and creating a framework that honors the 2D and 3D seismic data, well log, cuttings and core information aiming to enhance the geological interpretation of the Eastern Marlim oilfield. Using the sequential methodology proposed in the current case study (Fig. 25), different stratigraphic surfaces were identified based on stratal terminations and regional extent of unconformities. The stratigraphic surfaces were extensive in nature and it was possible to map and tie regional depositional surfaces across the entire study area. The stratal terminations and seismic motifs were taken into account to understand the nature of the different seismic facies looking forward to interpret depositional environments and lithofacies distribution. Different seismic patterns including amplitude, continuity, frequency, geometry and their relationships between seismic facies were also taken into consideration. Through the interpretation of seismic reflectors and their terminations, the principal seismic facies were established. This seismic facies exemplify the set of seismic reflection patterns in the Eastern Marlim oilfield identifying thirteen seismic facies in the entire study area (Fig. 46).


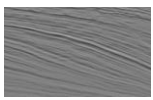
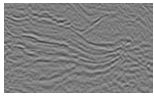
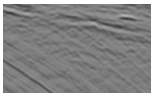

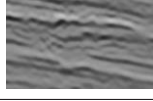
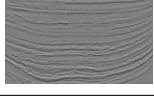
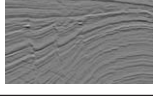

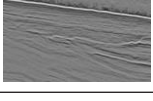

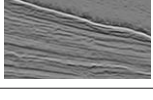

Seismic Facies Types	Amplitude	Reflection Pattern	Seismic Image	Seismic Facies Types	Amplitude	Reflection Pattern	Seismic Image
S1	Low-Intermediate	Chaotic		S8	High	Oblique	
S2	High	Chaotic Oblique Subparallel		S9	Low-Intermediate	Oblique	
S3	Low	Chaotic		S10	High	Channel	
S4	Intermediate-High	Parallel Subparallel		S11	Intermediate-High	Divergent	
S5	Intermediate-High	Parallel		S12	Low-Intermediate	Divergent Erosional	
S6	Intermediate-High	Sigmoidal		S13	Low-Intermediate	Parallel Subparallel	
S7	High	Parallel					

Figure 46. Principal seismic facies representing the set of major seismic reflections patterns in the Eastern Marlim oilfield.

6.6.3 Tectonostratigraphic units

Successively, the different seismic attributes and recognized seismic facies were incorporated aiming to enhancing the 2D/3D seismic interpretation and well tops correlations, allowing to identified the principal tectonostratigraphic units in the study area as follows:

6.6.3.1 Tectonostratigraphic unit 1 (TSU1):

Has a strict relationship with basement structural highs controlling the hydrocarbon accumulations in carbonate and siliciclastic reservoirs in the entire Campos Basin (Figs. 47, 48, 49, 50, 51, 52, 53 and 54). The TSU1 is characterized by chaotic and divergent seismic patterns associated with the depositional surface H0 and seismic facies S1 (Fig. 46) in strict relationship with its nature as basement rocks. The basement structural highs are associated as well with faulting increasing the structuration of the study area an affecting directly the tectonostratigraphic unit 2 (TSU2). As well, the salt structures are, almost without exception, related to basement faults. Unfortunately, salt tectonics makes seismic imaging very difficult, so the basement highs were interpreted the best way as possible taking into account the quality of the available information.

6.6.3.2 Tectonostratigraphic unit 2 (TSU2):

Displaying chaotic, oblique and sub-parallel seismic reflections patterns and representing the transition between the continental rift and transitional stages in the entire basin. The TSU2 is associated with the depositional surface H1 and seismic facies S2 (Fig. 46), characterized by limestones, marls and organic rich shales, deposited in lacustrine environments. Additionally, evaporitic rocks represented by a thick layer of salt undergone intense diapiric activity in deep-waters that were identified by the depositional surface H2 and seismic facies S3 (Figs. 47, 48, 49, 50, 51, 52, 53 and 54). As well, salt tectonics make difficult the seismic interpretation of this pre salt section, thus the different seismic attributes that we applied in the current research improved the seismic visualization and interpretation honoring the geological features observed in the study area.

6.6.3.3 Tectonostratigraphic unit 3 (TSU3):

Characterized by parallel and sub-parallel seismic reflections patterns represented by the depositional surface H3 and the seismic facies S4 and S5 (Fig. 46). This tectonostratigraphic unit is represented by a succession of organic rich calcareous rocks, locally with clastic input, which grades upwards and basin wards into deep-water marls and

shales deposited in an open-marine environment in the Albian-Cenomanian period representing a passive margin tectonic evolution in the entire basin (Figs. 47, 48, 49, 50, 51, 52, 53 and 54). The base of the TSU3 is controlled by the top of the salt layer representing the transition between transitional stages to a passive margin period. In this way, the top of the TSU3 marks the change from predominantly carbonate to clastic deposition in the entire Campos Basin.

6.6.3.4. Tectonostratigraphic Unit 4 (TSU4):

Corresponds to the marine clastic sequence developed from the Upper Cretaceous to Recent and characterized by thermal subsidence with some residual halokinetic activity that increases towards deeper waters (Figs. 47, 48, 49, 50, 51, 52, 53 and 54). Different seismic reflections patterns such as parallel, sub parallel and divergent were identified in the entire research area. Therefore, different depositional surfaces were recognized (H4-H6), as well as seismic facies S6-S13 (Fig. 46) characterized by a succession of a clastic lithofacies represented by a succession of shales, diamictites and sandstones, locally with calcareous input. As a result, the TSU4 is characterized by well-defined, prograding clinoforms successions found at multiple stratigraphic levels in the Eastern Marlim oilfield.

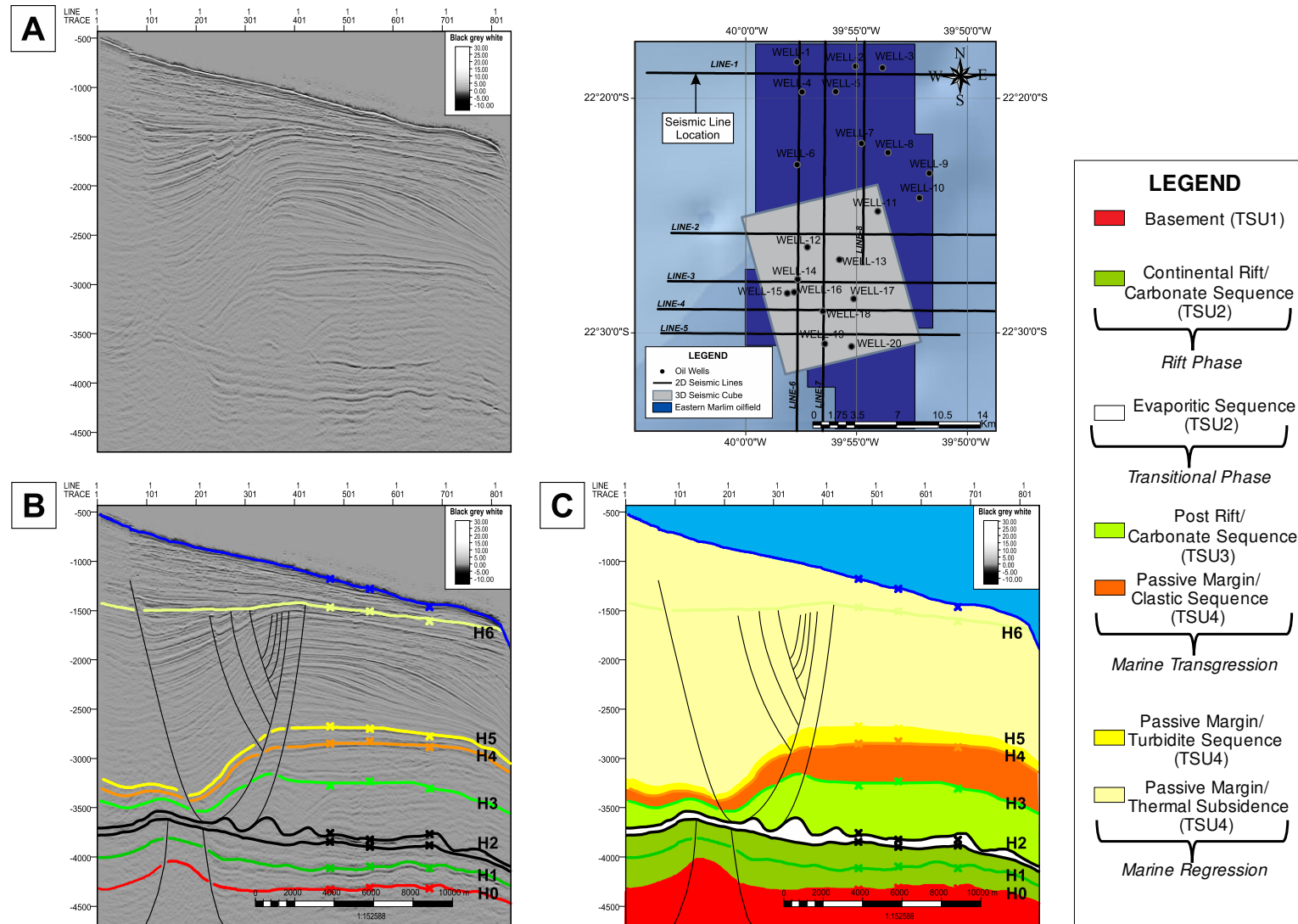


Figure 47. Seismic interpretation of the seismic line1 (normal phase/Black-Gray-white color scale) in the Eastern Marlim oilfield. A) Seismic Line in blank, B) Interpreted seismic horizons and faults, C) Interpreted tectonostratigraphic units, faults and depositional surfaces.

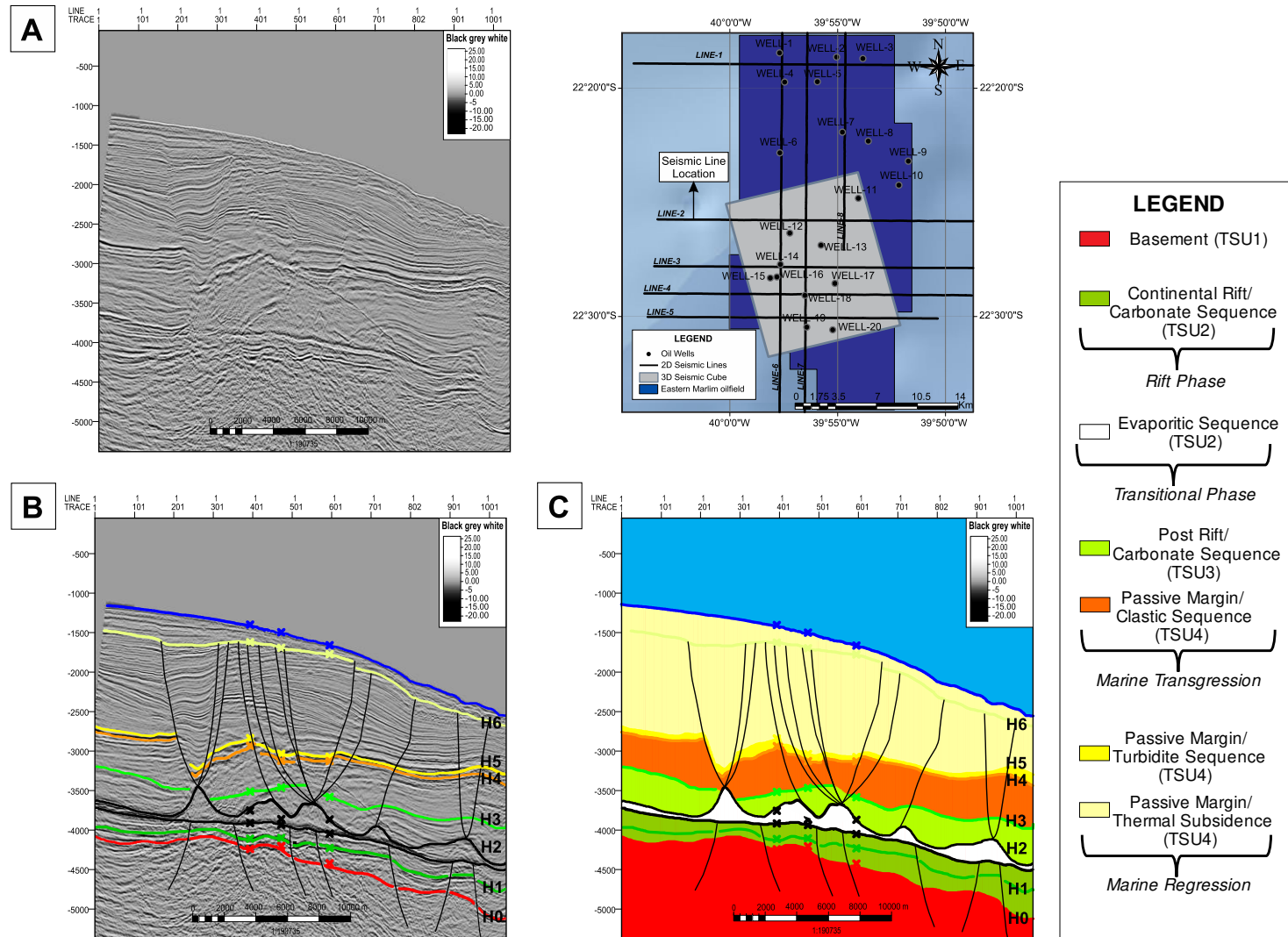


Figure 48. Seismic interpretation of the seismic line2 (normal phase/Black-Gray-white color scale) in the Eastern Marlim oilfield. A) Seismic Line in blank, B) Interpreted seismic horizons and faults, C) Interpreted tectonostratigraphic units, faults and depositional surfaces.

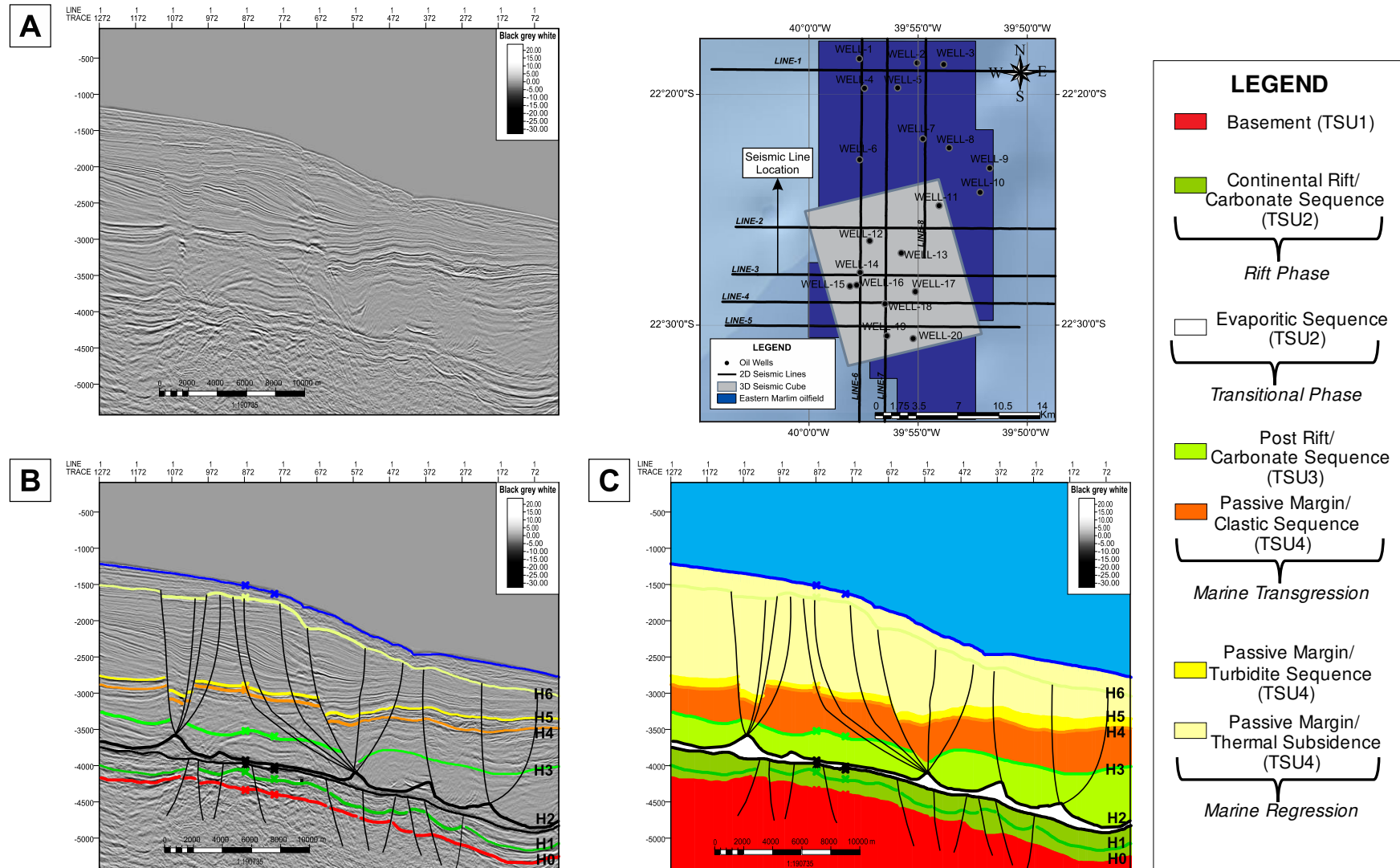


Figure 49. Seismic interpretation of the seismic line3 (normal phase/Black-Gray-white color scale) in the Eastern Marlim oilfield. A) Seismic Line in blank, B) Interpreted seismic horizons and faults, C) Interpreted tectonostratigraphic units, faults and depositional surfaces.

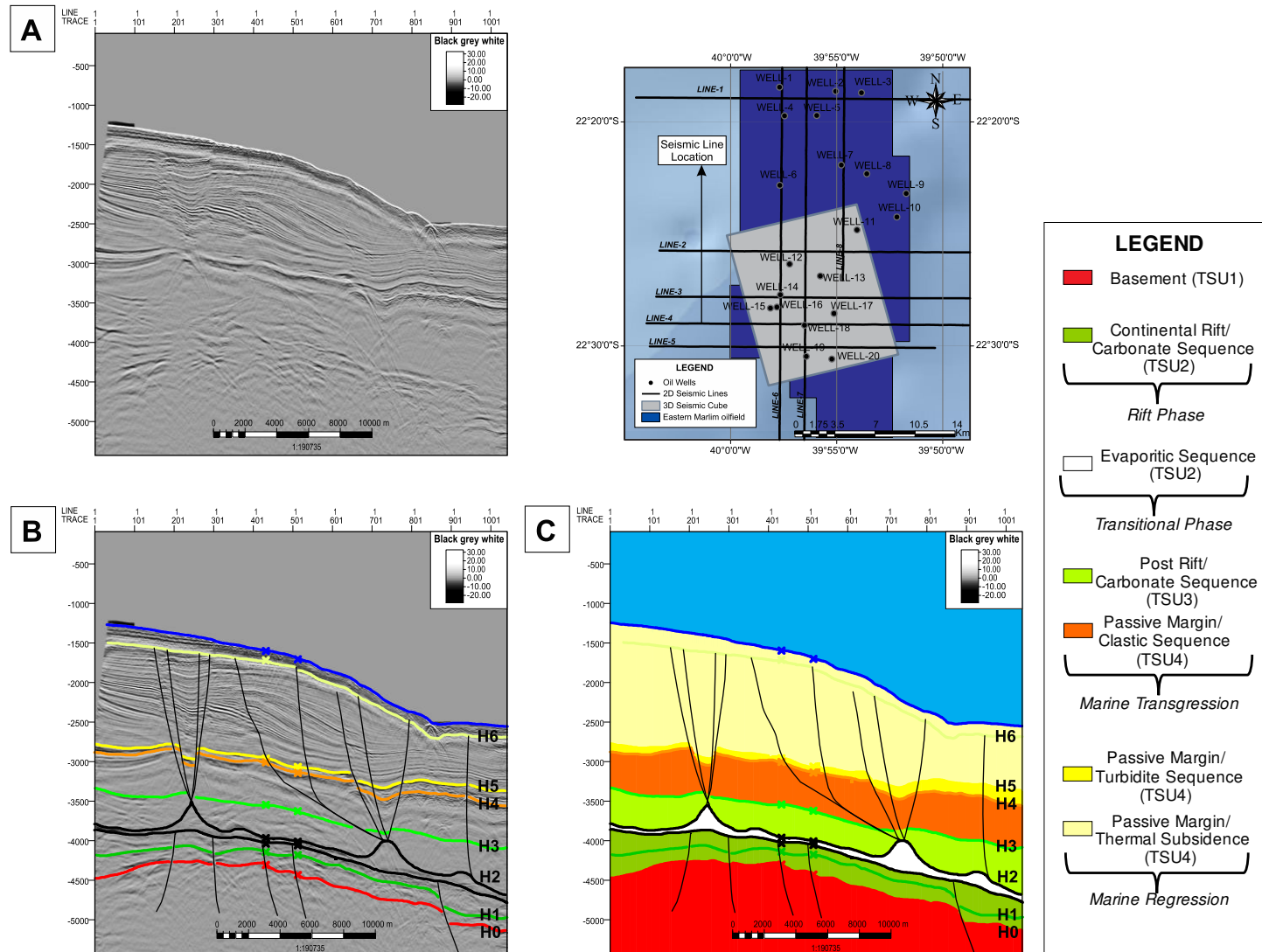


Figure 50. Seismic interpretation of the seismic line 4 (normal phase/Black-Gray-white color scale) in the Eastern Marlim oilfield. A) Seismic Line in blank, B) Interpreted seismic horizons and faults, C) Interpreted tectonostratigraphic units, faults and depositional surfaces.

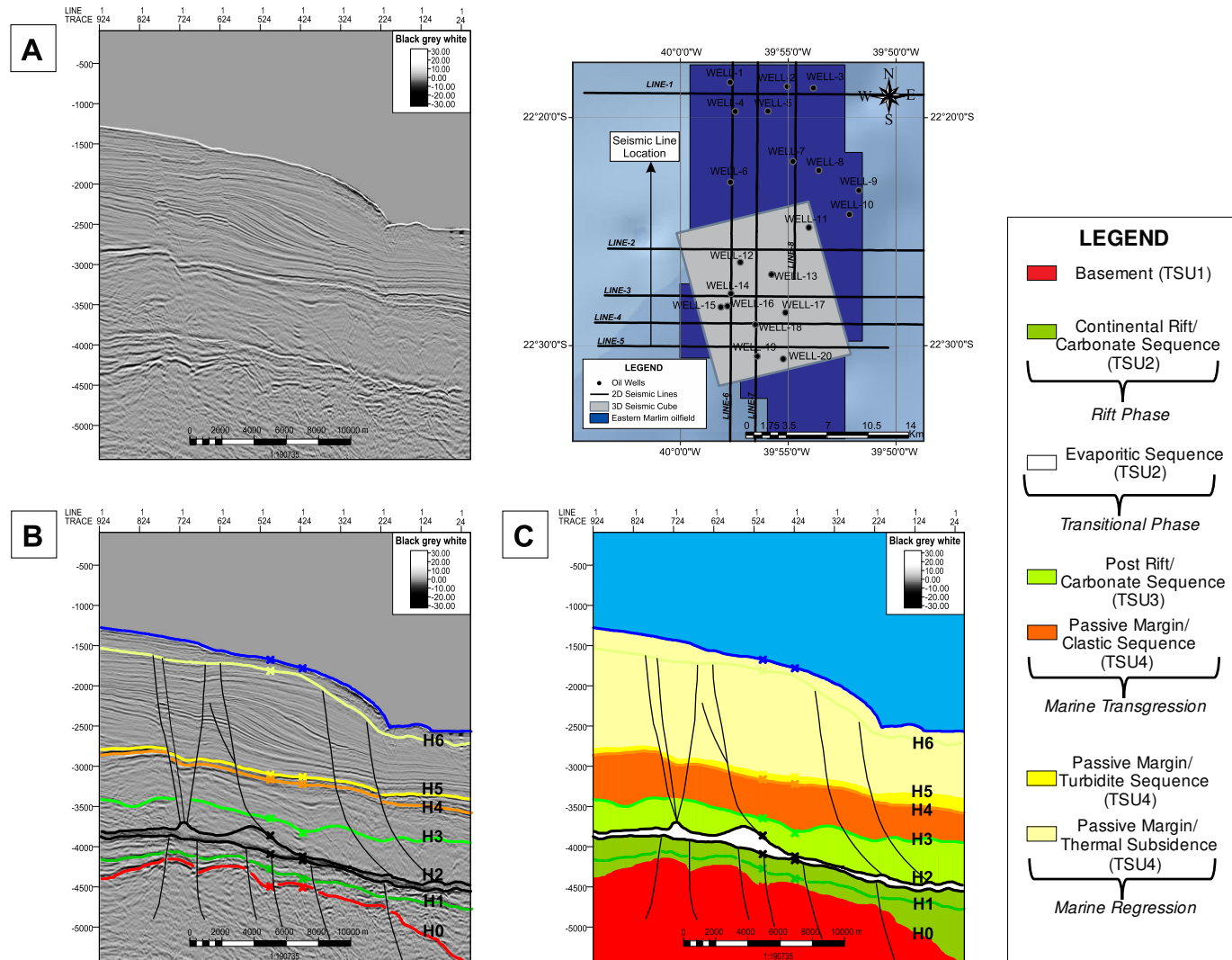


Figure 51. Seismic interpretation of the seismic line 5 (normal phase/Black-Gray-white color scale) in the Eastern Marlim oilfield. A) Seismic Line in blank, B) Interpreted seismic horizons and faults, C) Interpreted tectonostratigraphic units, faults and depositional surfaces.

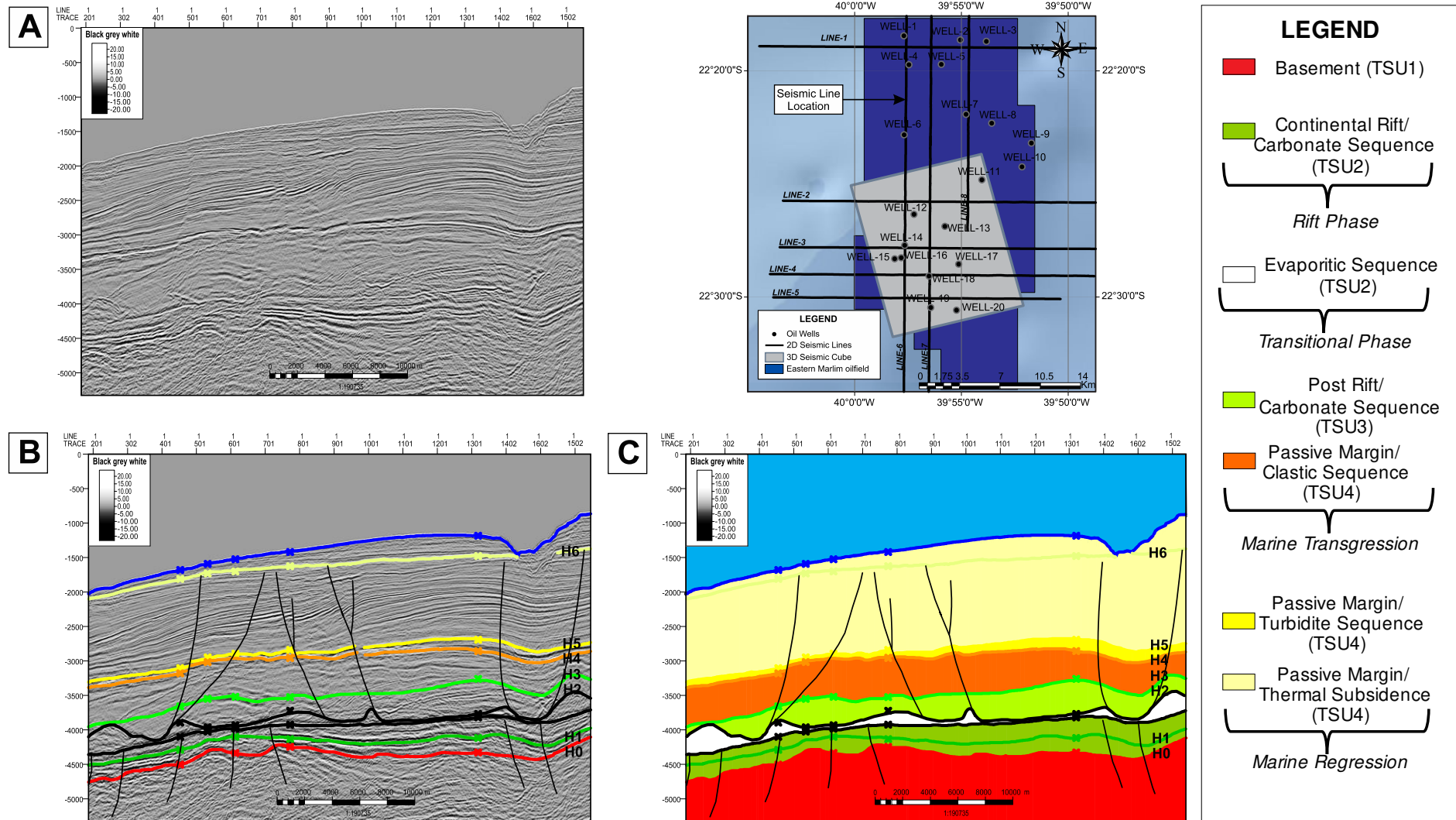


Figure 52. Seismic interpretation of the seismic line 6 (normal phase/Black-Gray-white color scale) in the Eastern Marlim oilfield. A) Seismic Line in blank, B) Interpreted seismic horizons and faults, C) Interpreted tectonostratigraphic units, faults and depositional surfaces.

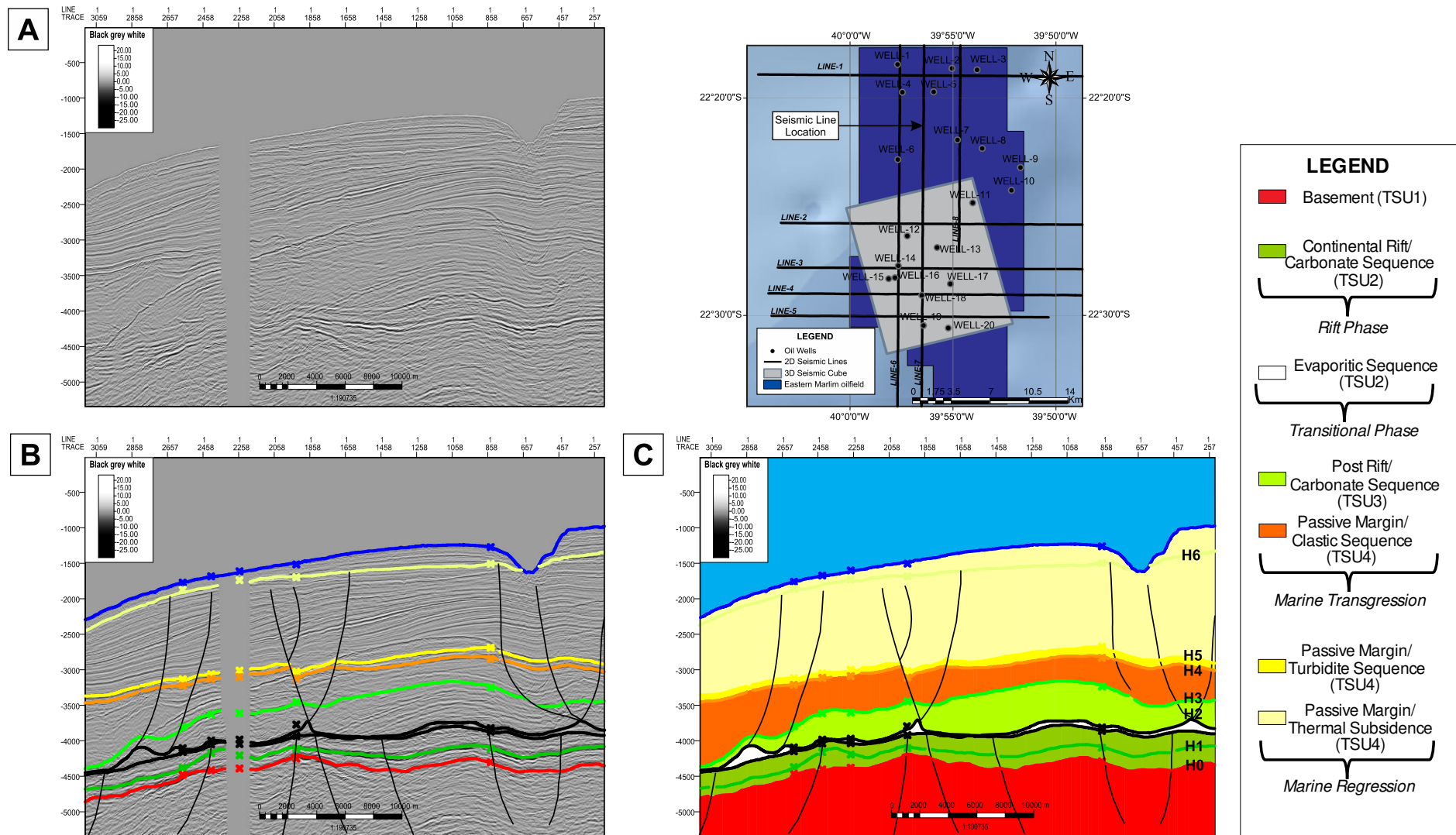


Figure 53. Seismic interpretation of the seismic line 7 (normal phase/Black-Gray-white color scale) in the Eastern Marlim oilfield. A) Seismic Line in blank, B) Interpreted seismic horizons and faults, C) Interpreted tectonostratigraphic units, faults and depositional surfaces.

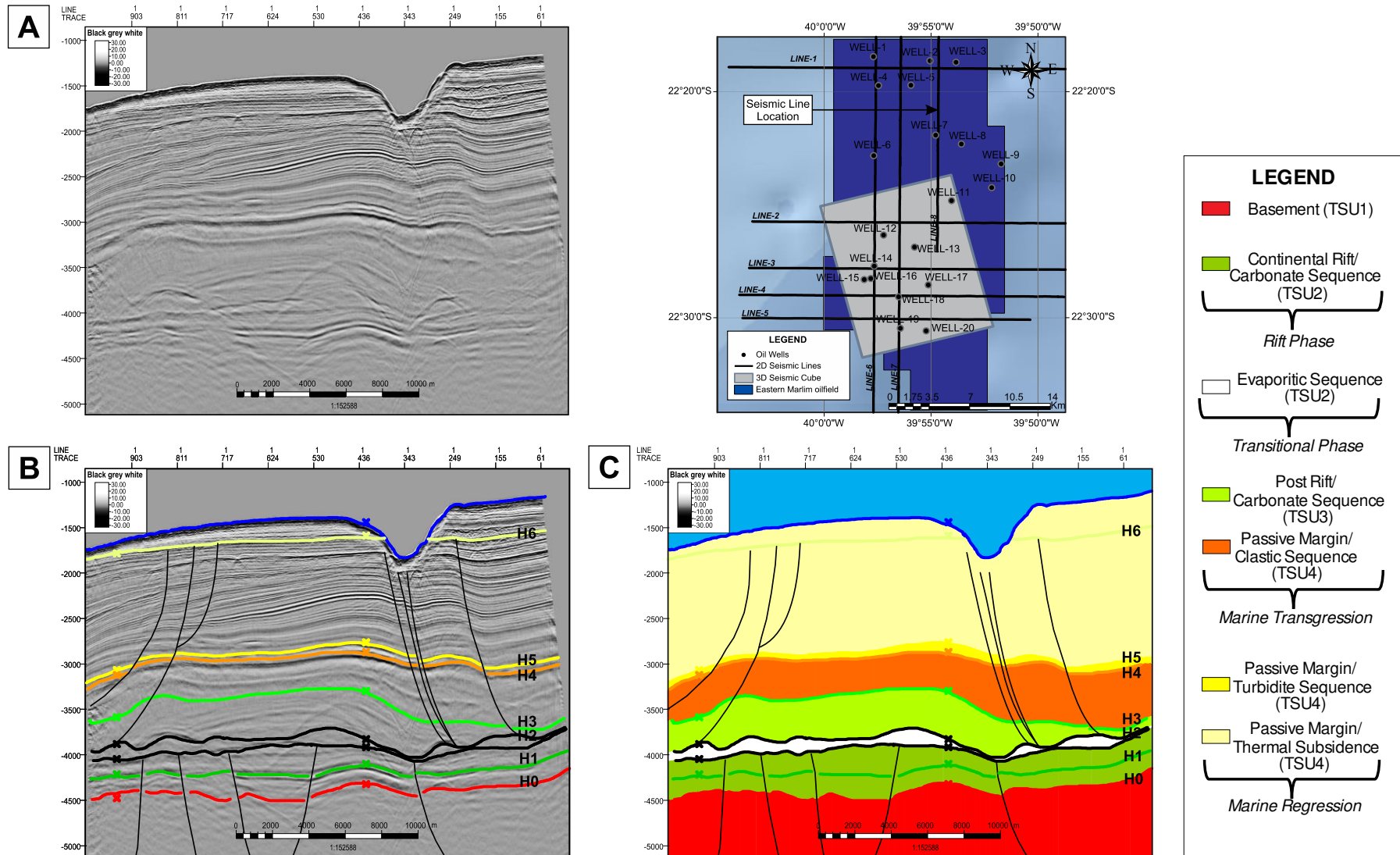


Figure 54. Seismic interpretation of the seismic line 8 (normal phase/Black-Gray-white color scale) in the Eastern Marlim oilfield. A) Seismic Line in blank, B) Interpreted seismic horizons and faults, C) Interpreted tectonostratigraphic units, faults and depositional surfaces.

The clinoforms (Fig. 55) show a complete Triassic succession where the bounding surfaces mark a significant change in depositional conditions. The boundaries are represented by unconformities and their correlative conformities. The base of the tectono stratigraphic unit 4 (TSU4) marks the change from predominantly carbonate to clastic deposition in the entire Campos Basin.

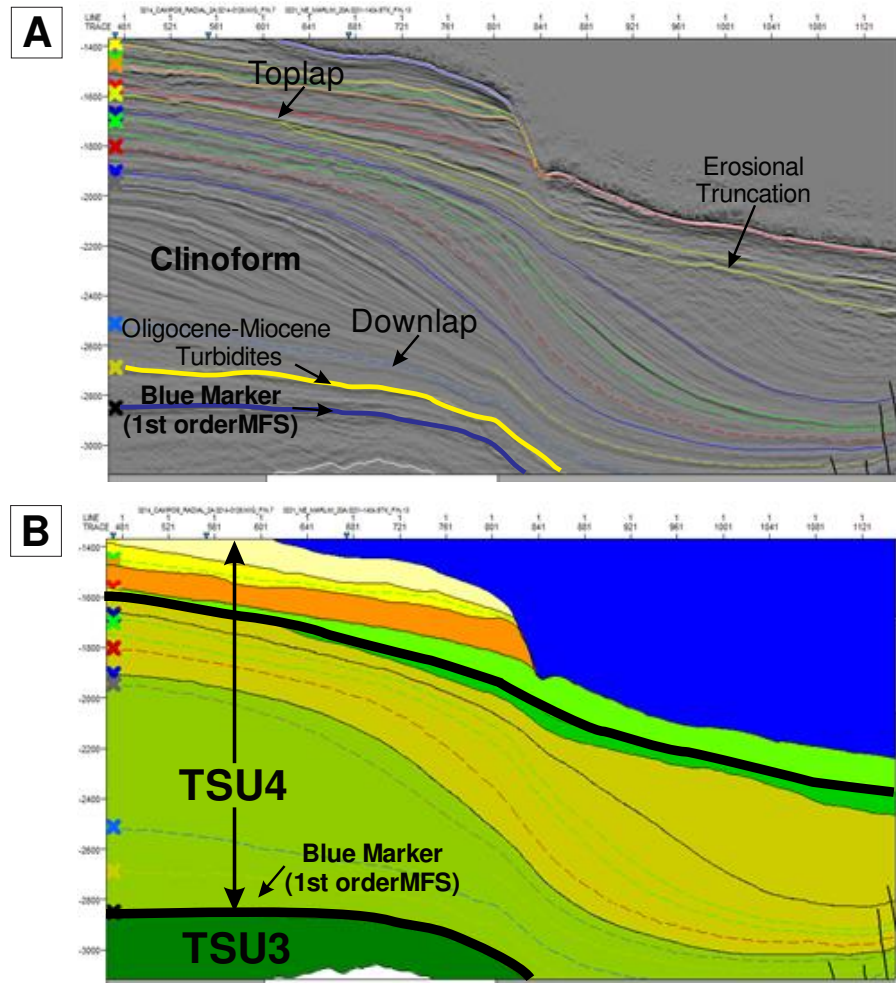


Figure 55. Semi-regional seismic line (Line 1) showing A) the prograding clinoforms successions found at multiple stratigraphic levels in the study area, and B) the moment of change from predominantly carbonate to clastic deposition in the entire Campos Basin (shift between the TSU3 to TSU4)..

The mentioned interpretations allowing to identify the spatial configuration of the recognized tectonostratigraphic units in the study area, showing the architectural arrangement of depositional systems during the filling of the basin, indicating the moments of change. The seismic and sequence stratigraphic surfaces were essential in building the tectonostratigraphic framework for the sedimentary succession analysis.

6.7 STRUCTURAL AND FAULT MODELING

Discussion of the Oligocene-Miocene interval of the Carapebus Formation in this research is fundamentally restricted to subsurface data (Fig. 21). In this way, aiming to perform the structural and fault modeling of the Eastern Marlim oilfield different structural correlations were developed based on the accompanying seismic interpretation (2D and 3D surveys) (Fig. 56).

Additionally, well log information, cuttings and core descriptions were taking into account to improve the structural model. Through the interpretation of the mentioned information, different geological faults were identified varying from normal to listric normal faults associated with a distensive regime affected by salt tectonics.

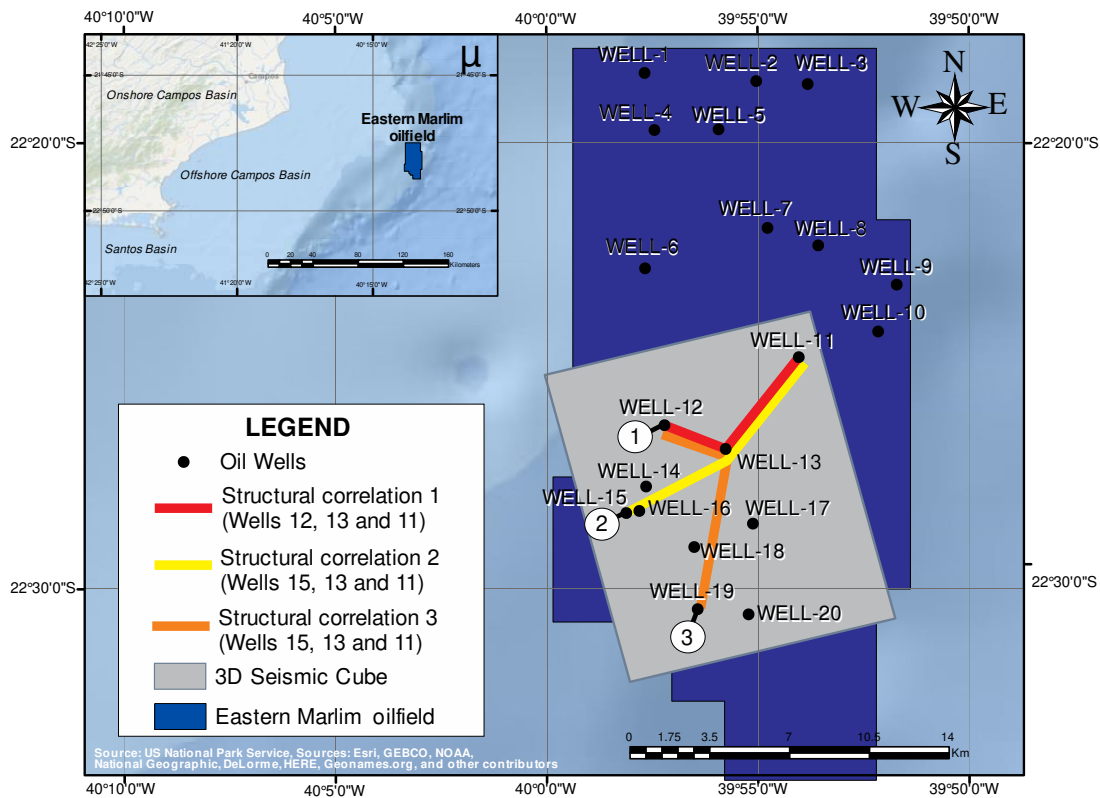


Figure 56. Location map of the developed structural correlations based on the 3D seismic cube that displays the better quality and describes the principal characteristics of the Oligocene-Miocene reservoirs at seismic scale in the study area.

6.7.1 Structural Correlations:

Three associated schematic structural correlations were developed aiming to understand the structural framework of the research area and improving the final 3D reservoir modeling of the Oligocene-Miocene turbidite system in the Eastern Marlim oilfield (Figs. 57, 58, and 59). Based on the different faults interpreted in the seismic data, the developed schematic structural correlations displays at least four main reservoirs (Miocene, Oligocene, Eocene and Cretaceous sandstones) belonging to the Carapebus Formation of the Campos Group of the Campos Basin in the Eastern Marlim oilfield.

In that way, the schematic structural correlation-1 shows a negative flower structural style associated with a salt pillow, which causes normal faulting into deep-waters (Fig. 57). On the other hand, the schematic structural correlation-2 displays an echelon structural style as well associated with normal faulting and salt tectonics (Fig. 58). Finally, the schematic structural correlation-3 confirms a negative flower structural style associated as well with halokinesis activity (Fig. 59).

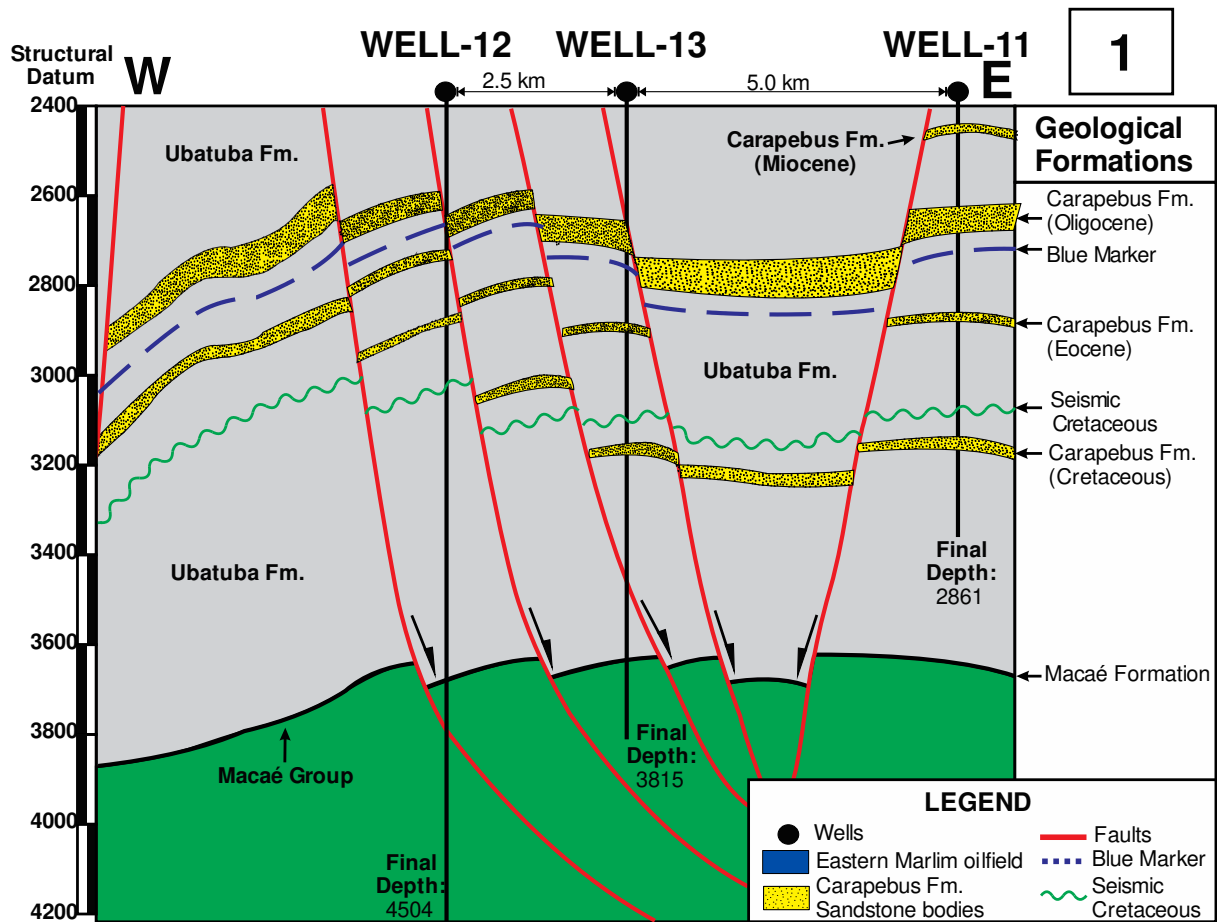


Figure 57. Schematic structural correlation 1 developed in the Eastern Marlim oilfield.

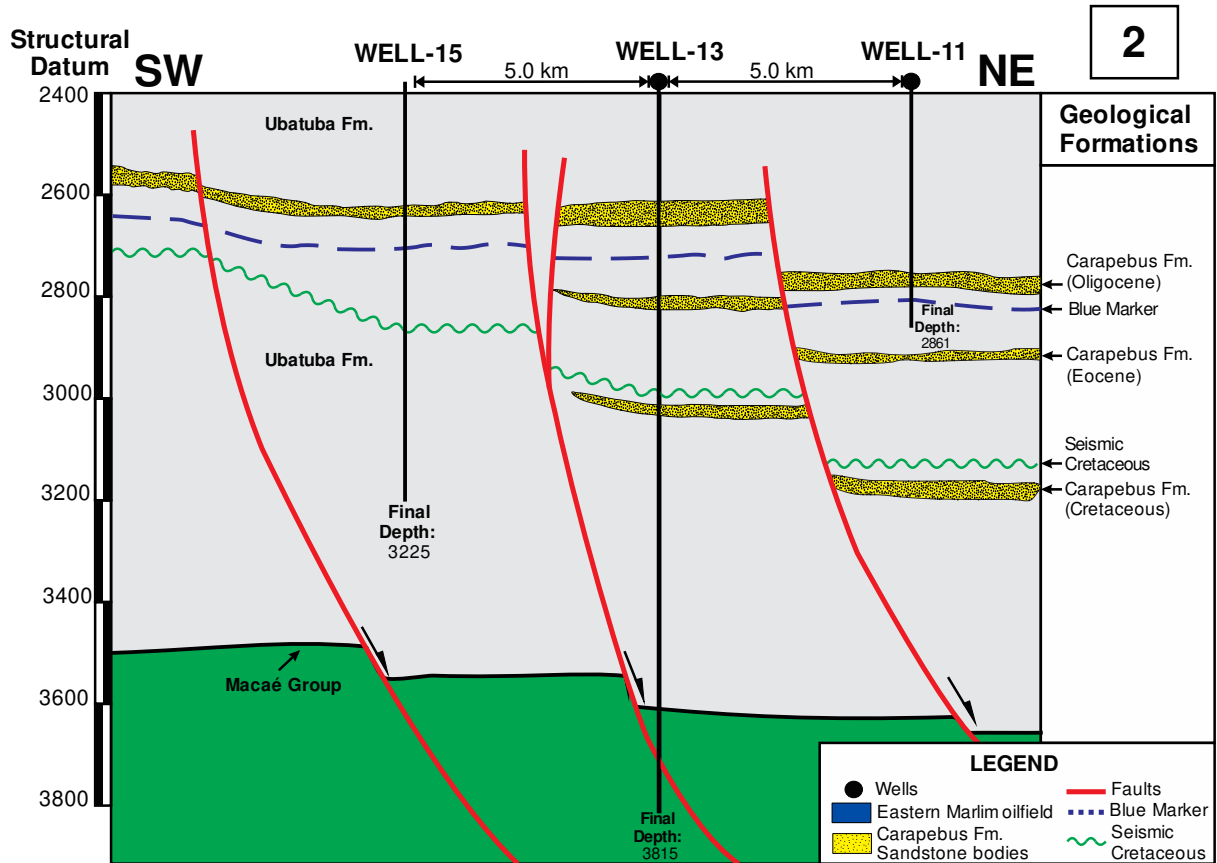


Figure 58. Schematic structural correlation 2 developed in the Eastern Marlim oilfield.

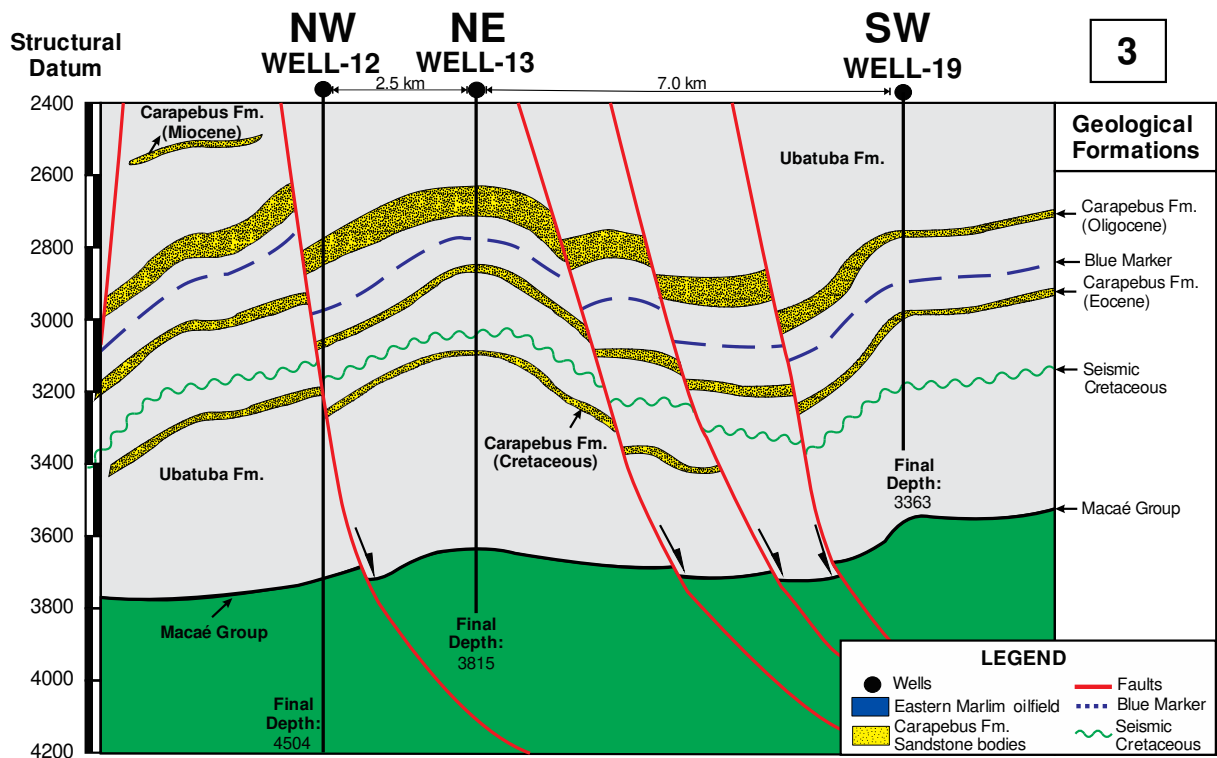


Figure 59. Schematic structural correlation 3 developed in the Eastern Marlim oilfield.

The oilfield is divided into two main blocks by a normal fault with NW-SE strike direction and SW sense dip, caused by the movement of a saline wedge that raised the NW block in relation to the SE block (Figs. 60). Secondary blocks occur due to synthetic subordinate faults and antithetical related with the main normal faults, arranged in standard in negative flower and echelon structural styles.

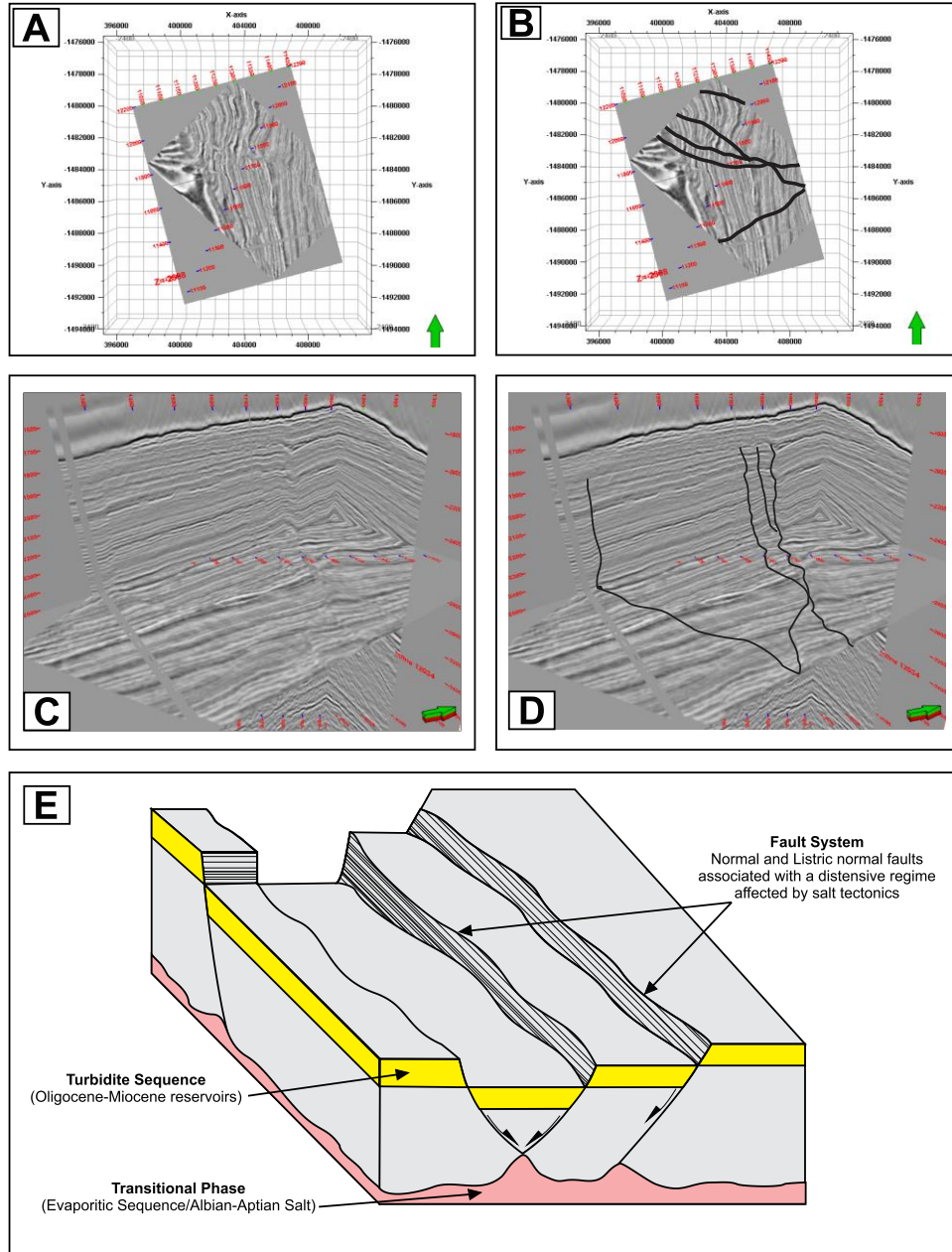


Figure 60. Principal faults affecting the geometry of the 3D seismic cube in the study area. A) Time slice of the seismic cube without fault interpretation. B) Time slice of the seismic cube with fault interpretation. C) Cross-line and Strike-line seismic cube visualization without fault interpretation. D) Cross-line and Strike-line seismic cube visualization with fault interpretation. E) Structural and fault schematic model of the Eastern Marlim oilfield displaying a normal and listric normal fault system associated with a distensive regime affected by salt tectonics.

6.8 3D GEOLOGICAL MODELING (STATIC MODEL)

The generation of a static model is considered the last step in the development of a 3D integrated model in reservoir characterization. The 3D geological modeling workflow in this study consisted of the sequential methodology proposed in the present research (Fig. 27) and, lastly summarized into nine steps (Fig. 61), ranging from the time-depth conversion to the development of probabilistic models for hydrocarbon volumetric calculations. An important task before the geological modeling is to create the stratigraphic and structural model of the reservoir, meaning the geometry (architecture) of the reservoir, as well as the petrophysical modeling. The stratigraphic model is related to the depositional modeling and reservoir heterogeneity based on lithological, sedimentological and stratigraphical proxies (Chapter 6.2). On the other hand, the structural model includes the position and characteristics of main stratigraphic horizons and faults (Chapter 6.7). Lastly, the petrophysical modeling was developed through the petrophysical analysis based on lithotypes proposed in the current study (Chapter 6.4). Finally, all the mentioned information was merged for the development of the current geological modeling aiming to understand the framework and heterogeneities of the Oligocene-Miocene section at reservoir scale in the Eastern Marlim oilfield, Campos Basin, Brazil.

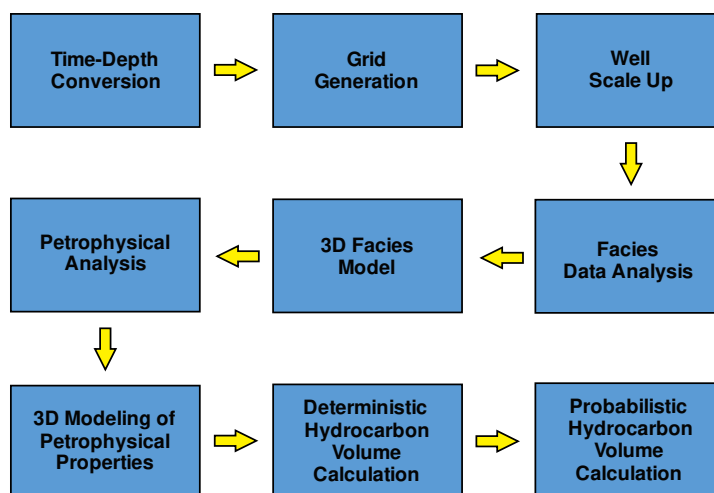


Figure 61. 3D static model workflow developed in the current case study.

Therefore, the first step in the mentioned workflow is to perform the time-depth conversion, in which constant velocities are used by zones (tops of geological formations). These velocities were calculated from check shots and time-depth tables of the available wells. In figure 62, an example of the time-depth conversion can be observed, where the average velocity have a good correlation with the interval velocity in the Well-12 in the study area.

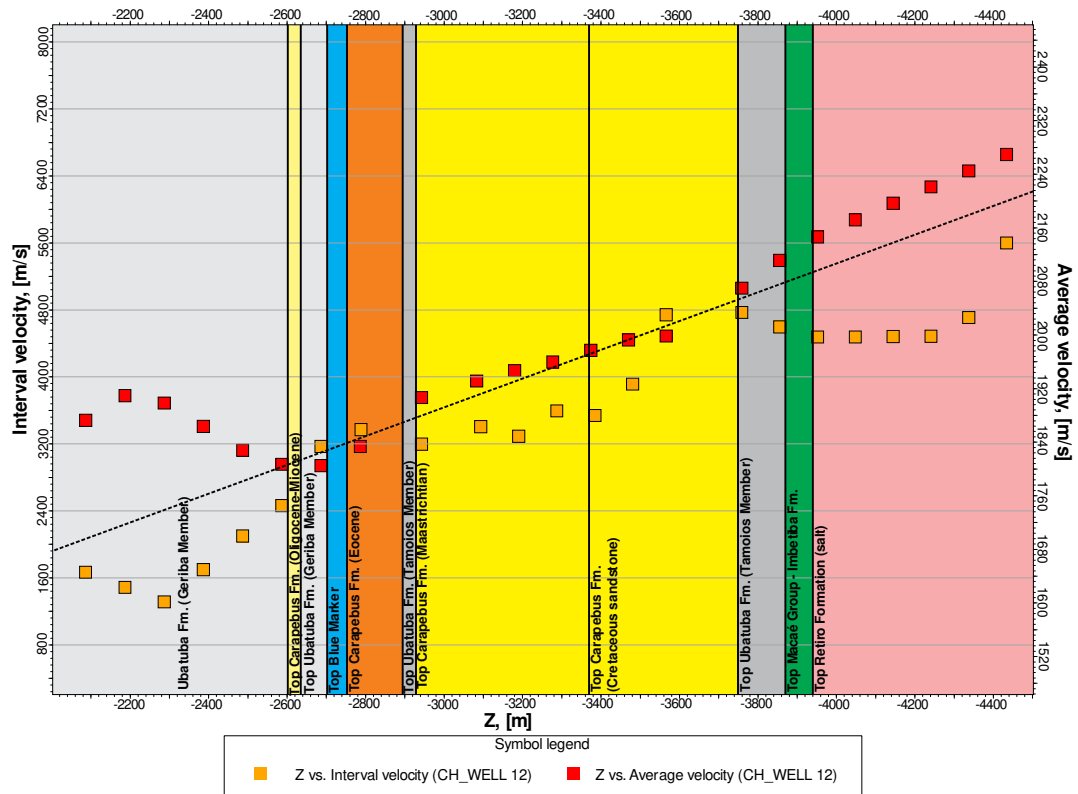


Figure 62. Time-Depth conversion (average velocities vs interval velocities).

As a final point, the time-depth conversion process finished when the construed geological surfaces of the Oligocene-Miocene interval of the Carapebus Formation interpreted in the available 2D and 3D seismic lines in time, are now, transformed into depth units, showing a respectable fit between them. In figure 57, a visualization of the surfaces in time (Fig. 63, A), which correspond to the top and base of the mentioned interval, displayed a very good correlation with the new surfaces migrated into depth units (Fig. 63, B).

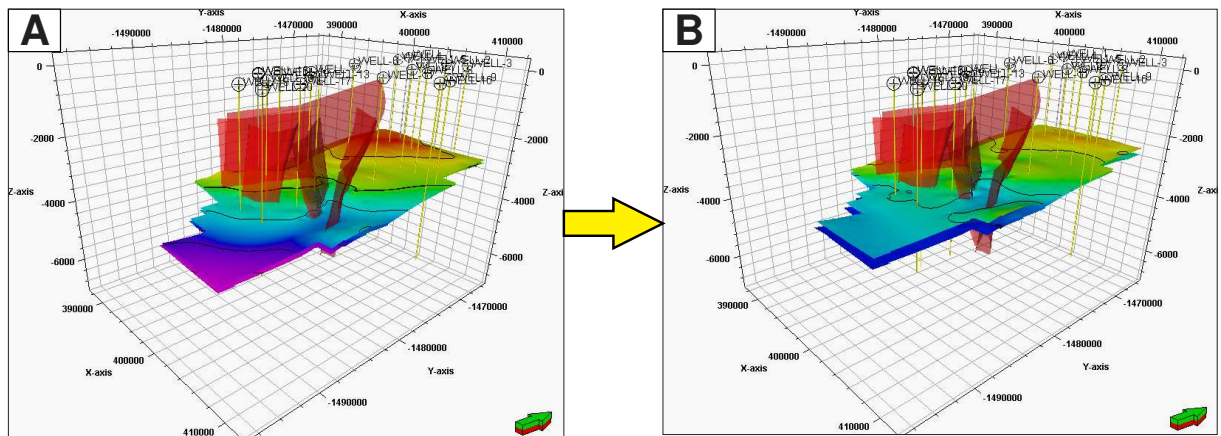


Figure 63. Time-Depth conversion of the Oligocene Miocene interval of the Carapebus Formation in the Eastern Marlim oilfield.

In figure 64, an excellent match between the generated surfaces in time transformed into depth units, with the tops of the geological formations in depth in meters, can be observed; showing a very good time-depth conversion in the study area. It is important to highlight that a special treatment was developed for the top and base of the Oligocene-Miocene interval of the Carapebus Formation in the study area, taking into account is the scope of the current research project.

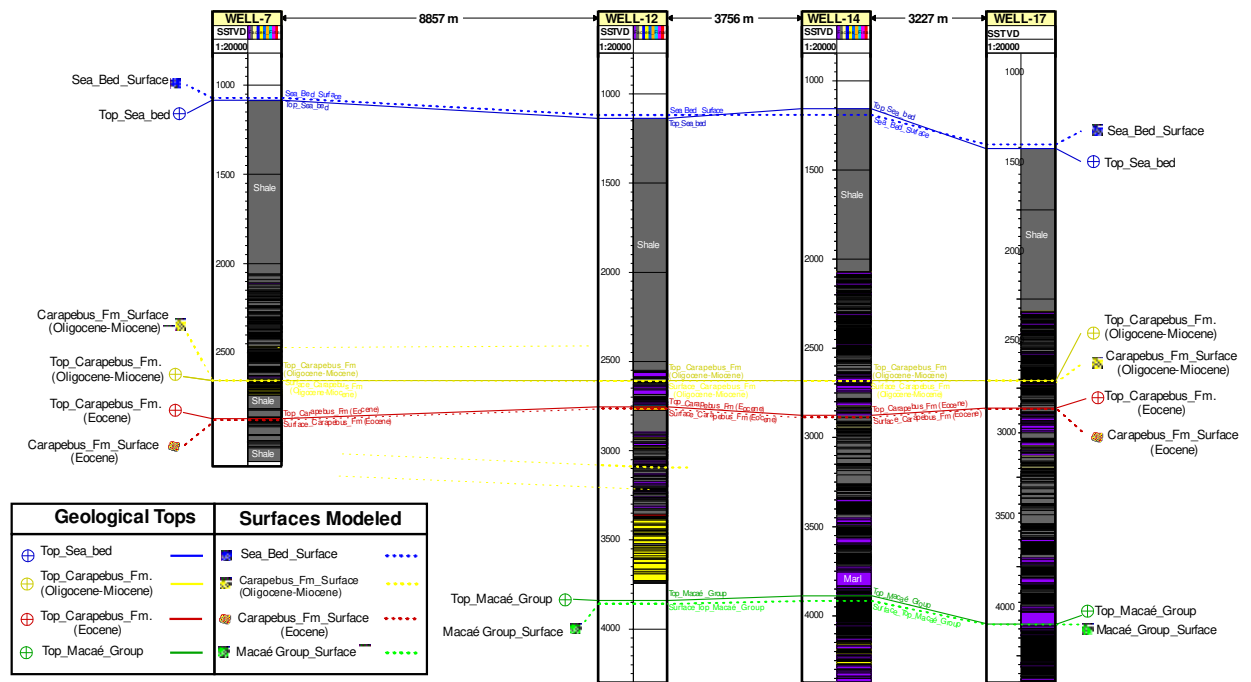


Figure 64. Time-Depth conversion match between the geological surfaces generated in time and transformed into depth units, versus the geological tops in depth of the formation of interest in the study area.

Subsequently, the static framework of the model can be generated. Then, a division between the different zones is developed in order to give a vertical resolution to the model; this process is known as layering. The scale up of the well logs was made on the generated grids, which consists in taking the logs of each well and assigning them to the corresponding cells in the static model. In this step, it is very important to take into account that the resolution of the well logs is different from the resolution of the gridded data that can be modified or displaced, so different methods must be applied to obtain the best fit between the gridded well logs and the original data. In figure 65, a very good match between the generated grids and the original data can be observed giving a respectable confidence to the model.

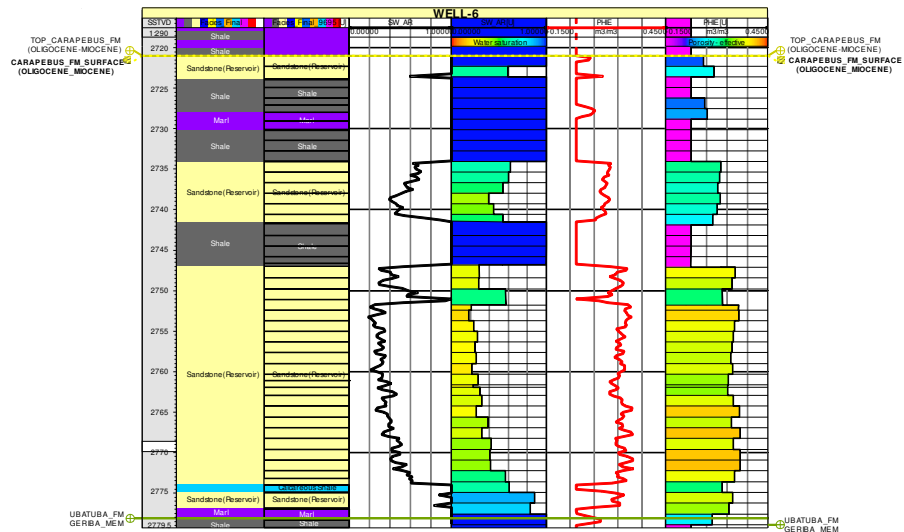


Figure 65. Example of the well scale up processing in the Well-6 in the study area.

After the well scaled up processing, it is mandatory to perform the data analysis, starting with the facies or lithological model. Initially the analysis of the vertical distribution to each lithological facies is performed. In this way, the data analysis consists in observing if the proportion of a given facies exists and have a good correlation with certain layer, in order to see the variation that each facies has in the vertical resolution of the model (Fig. 66, A). Considering the mentioned information, it is required to perform the horizontal and vertical distribution analysis using the variogram technique (Fig. 66, B, C, and D).

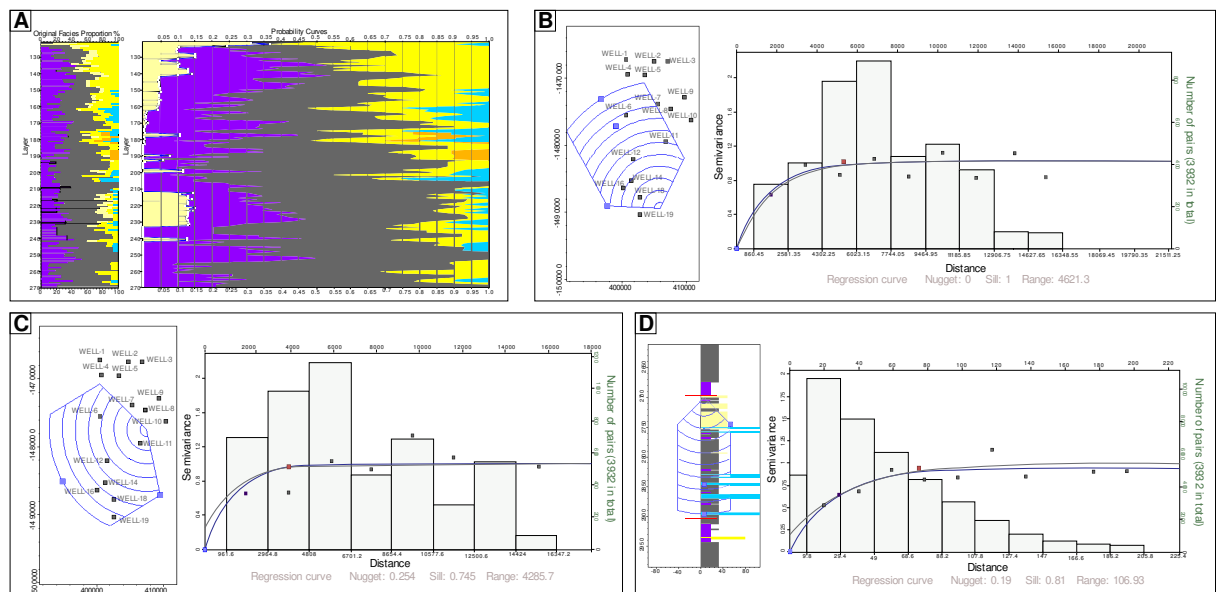


Figure 66. Data analysis of the lithological facies in the distribution of the 3D model. A) Curve of vertical proportion. B) Variogram in principal direction. C) Variogram in minor direction. D) Variogram in vertical direction.

In this stage, the analysis of different trends observed in the data is developed, and it is mandatory to have an excellent correlation between them, calculating the values of nugget, sill, rank and main direction for each lithological facies (Fig 66, B, C and D). With this analysis, the 3D lithological model is generated in which the sequential indicator simulation (Gslib) is used displaying a distribution of the lithological facies of the Oligocene-Miocene interval in the study area (Fig. 67).

Initially, at least 10 lithological facies varying from siliciclastic to volcanic and igneous rocks were codified (Fig 68, A). Then, for the Oligocene-Miocene section of the Carapebus Formation in the Eastern Marlim oilfield, a zone partition was developed. The task of dividing in zones has the objective to have better control during the modeling process, because it is performed separately. The criteria to divide the stratigraphic intervals were based in the cluster of horizons as a coherent way, meaning that the zones must have a homogeneous thickness respect each other. The practical aspect to create zones is related to avoid the mixing of bodies or beds from different stratigraphic horizons during the application of the simulation methodologies.

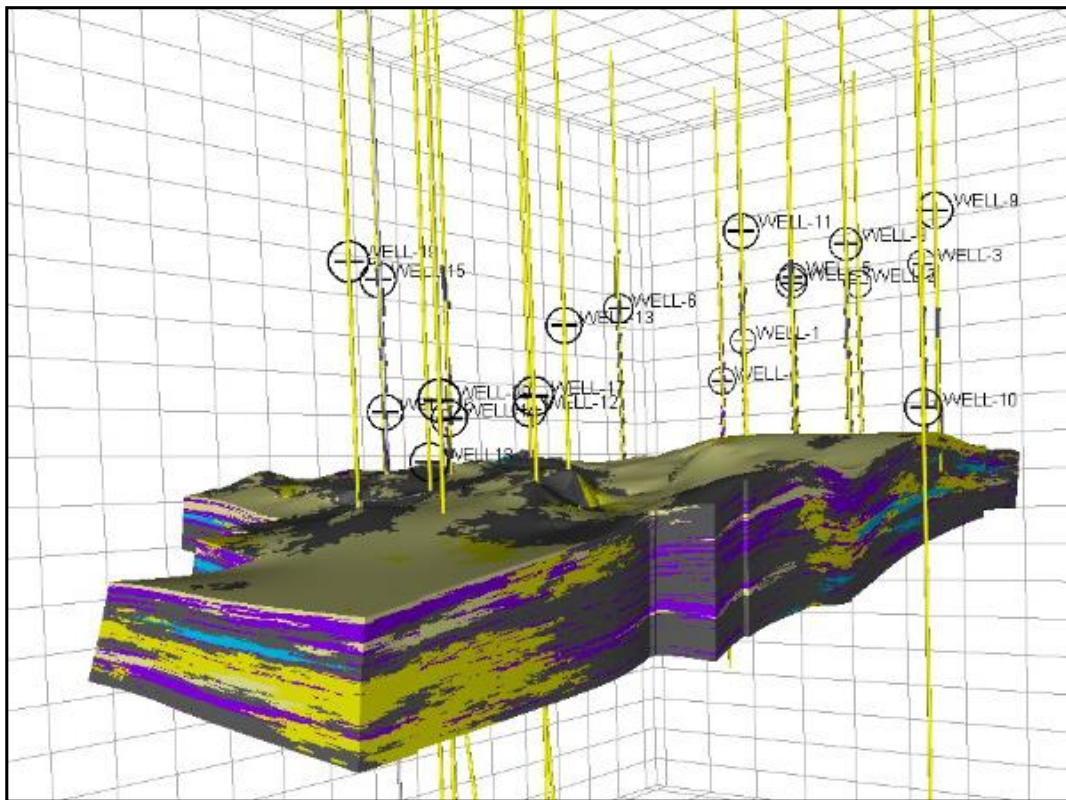


Figure 67. 3D facies modeling using the sequential indicator simulation (Gslib) method for the Oligocene-Miocene interval of the Carapebus Formation in the Eastern Marlim oilfield.

Then, for the interval of study, only five facies were taken into account for the modeling process (Fig. 68, B). In this way, for the mentioned facies an exhaustive data analysis were made using the variogram method. Thus, five lithologies were identified in the entire reservoir interval of study, and then four distribution maps were built aiming to understand the geological features of the research area (Fig. 69).

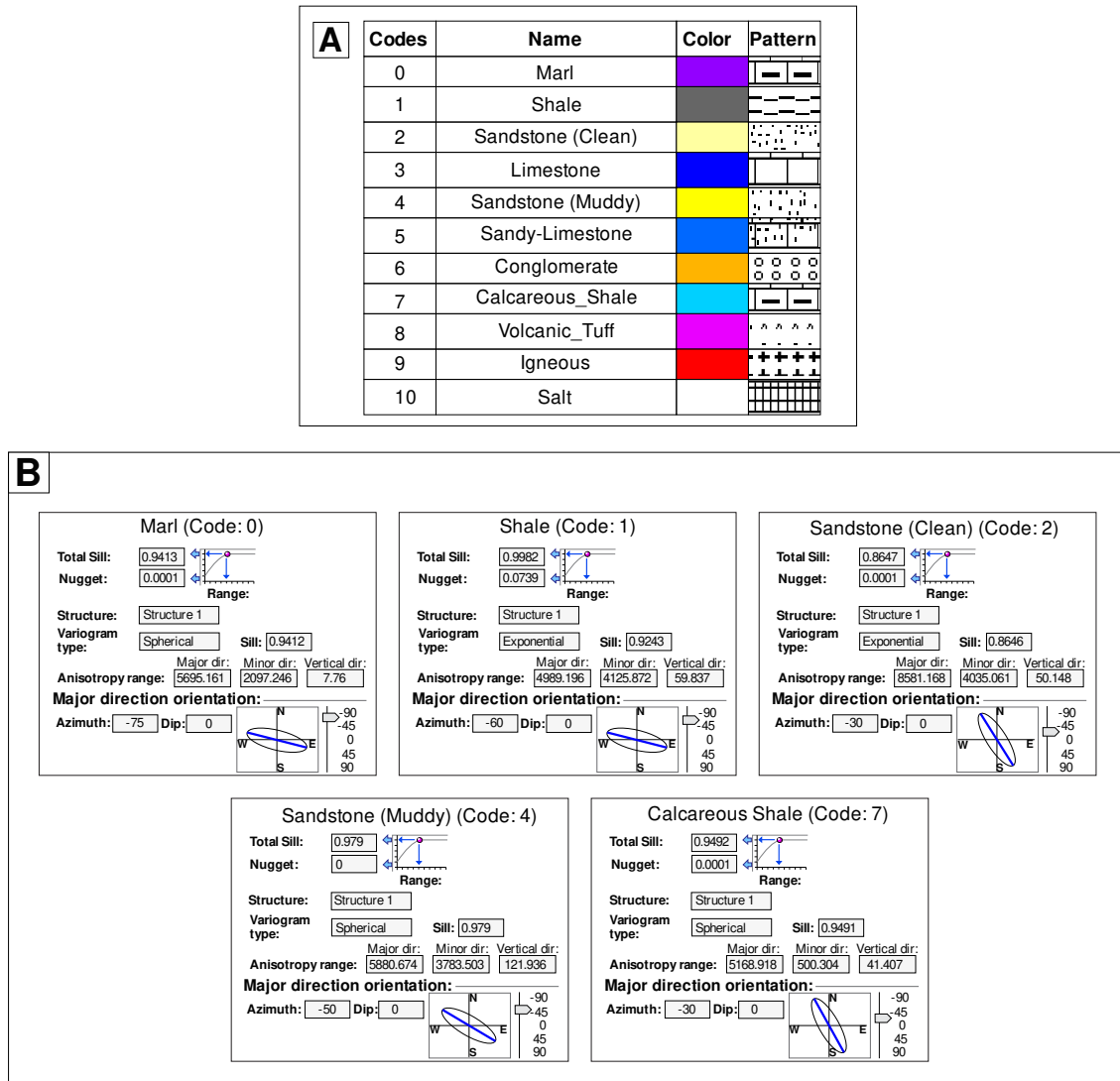


Figure 68. Facies codification and data analysis of the lithological facies observed in the interval of study in the current research. A) Facies codes of all interpreted facies. B) Variograms of the analyzed facies in the Oligocene-Miocene interval of the Carapebus Formation.

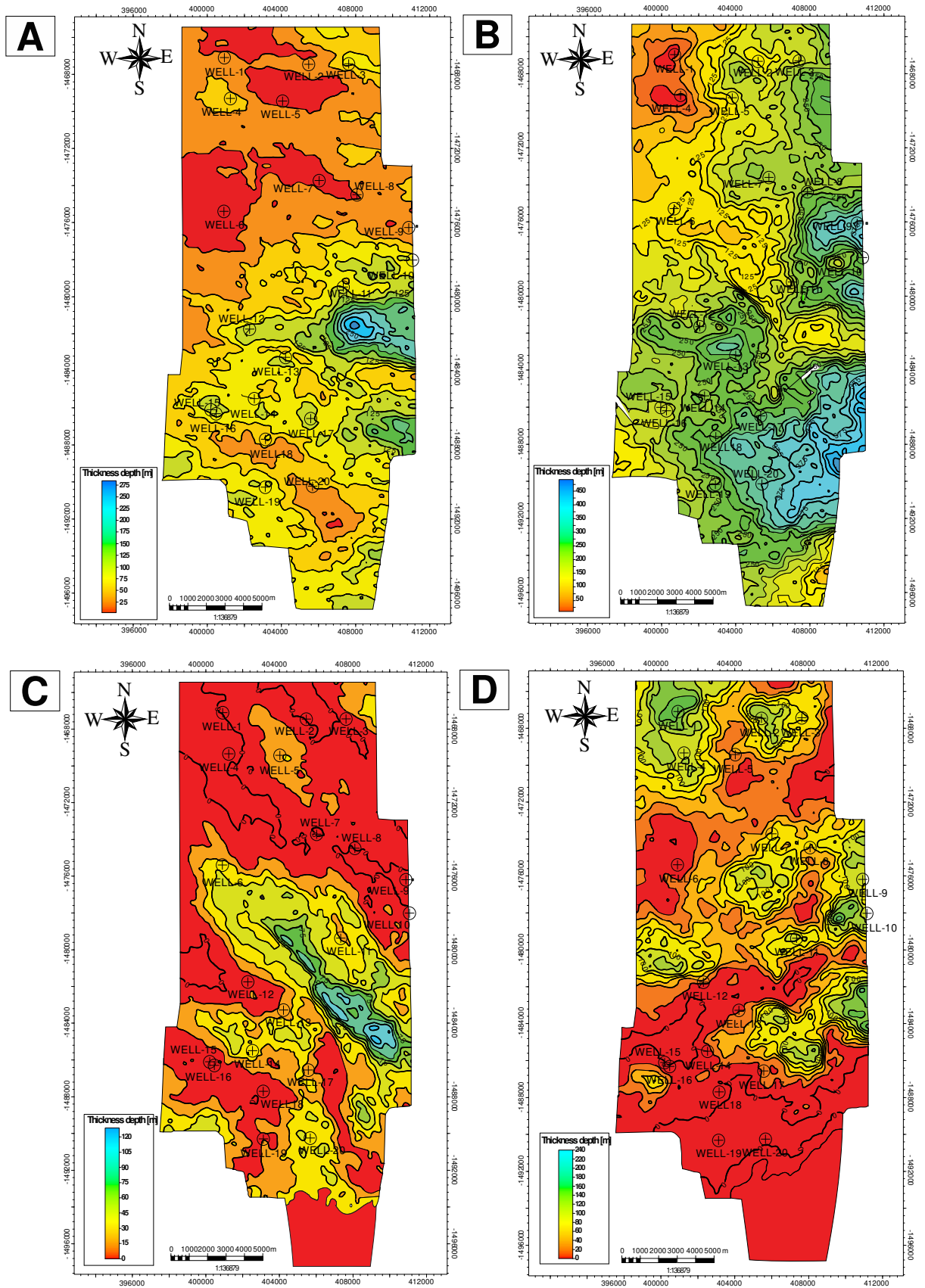


Figure 69. Distribution maps for the major lithological facies observed in the research area. A) Marl, B) Shale, C) Sandstone (clean), and D) Sandstone (muddy).

The previous maps display a very good correlation with the stratigraphic model proposed in the current research following the NW-SE regional trend of sediment accumulation perceived in the Eastern Marlim oilfield. Besides, a fence diagram was developed following the style of the developed chronostratigraphic correlations (Chapter 6.2.1). In that way, a very good lateral and vertical continuity of the sandstone layers of the Oligocene-Miocene section in the study area was observed, along with an increase in the non-reservoir facies to the southern portion of the research area (Fig. 70).

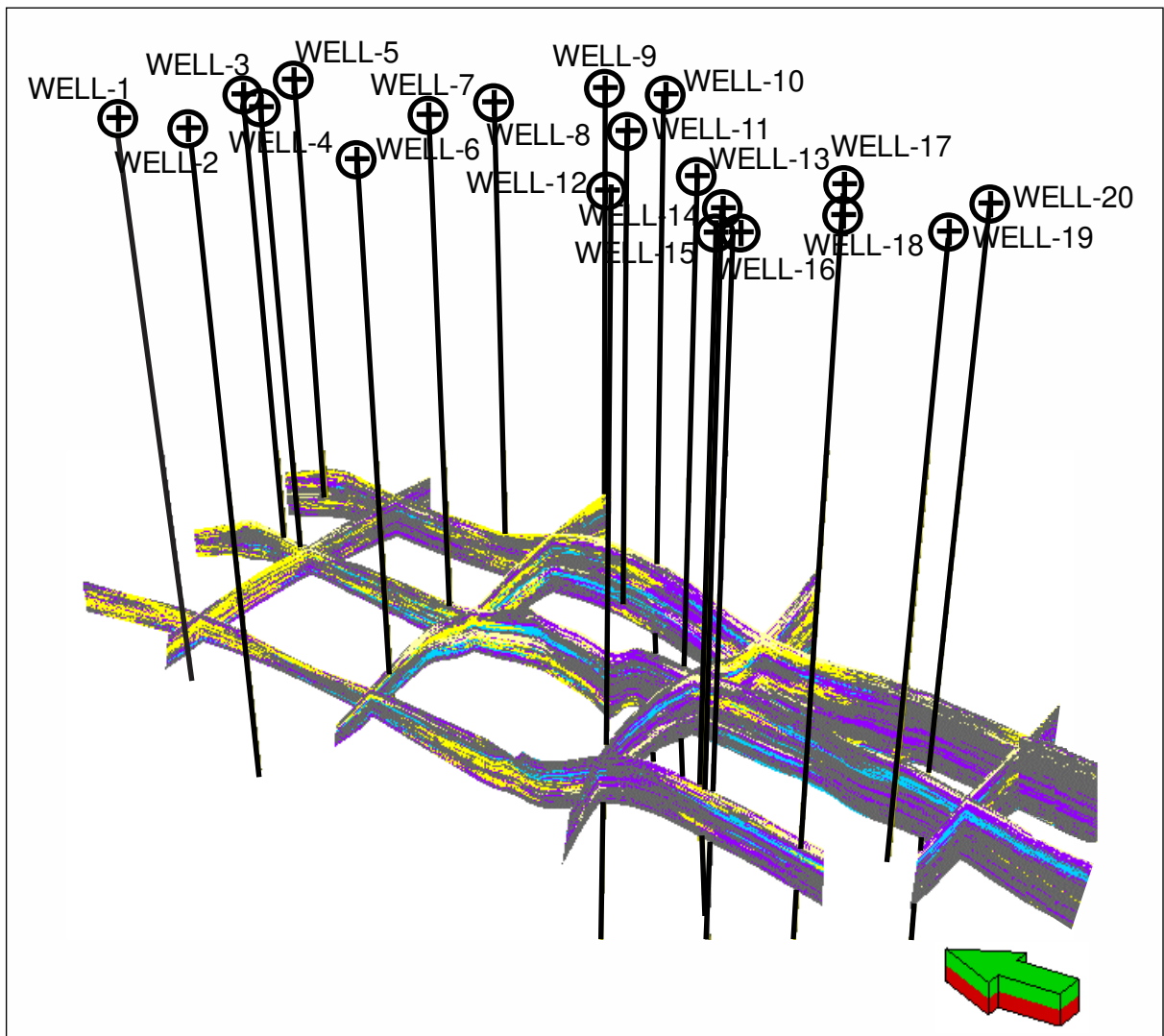


Figure 70. Fence diagram displaying a 3D view of the original facies distribution obtained using the Truncated Gaussian simulation method, following the trend of the four-chronostratigraphic sections in W-E direction and three sections in N-S direction.

With the distribution of the lithological facies in the model, the analysis of the petrophysical properties was performed. The principal objective of this analysis is to create a probability curve for each property and each facies taking into account the developed petrophysical model (Chapter 6.4). A great match between the facies model and the

petrophysical properties in the model is observe in figure 71, were the water saturation and porosity properties were modeled.

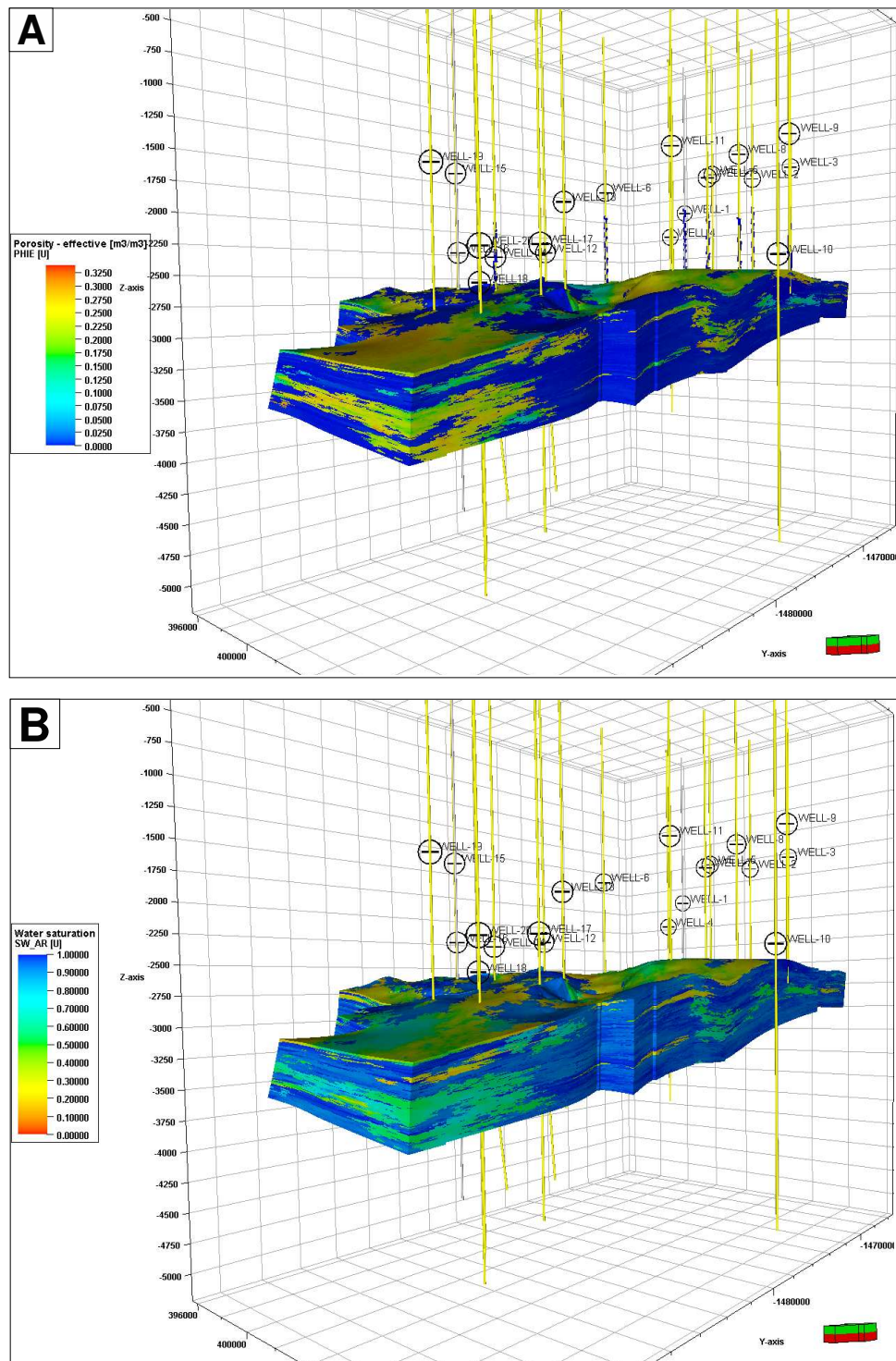


Figure 71. 3D models of the petrophysical properties. A) Porosity. B) Water saturation

Having built the models of facies and petrophysical properties is mandatory to proceed and perform the calculation of the volume of the original oil in place (OOIP). For this purpose, the Net to Gross calculation was performed, which consists in generating a volume using cutoffs on the properties previously obtained. For this step, the following parameters were used: Facies= Sandstones (clean and muddy, codes 2 and 4), Porosity $> 10\%$, and Water Saturation (SW) $\leq 65\%$, resulting in a volume consisting of values between 1 (one) and (0) zero, where if the values are equal to one (1) the condition is met and zero (0) when the condition is not met (Fig. 72).

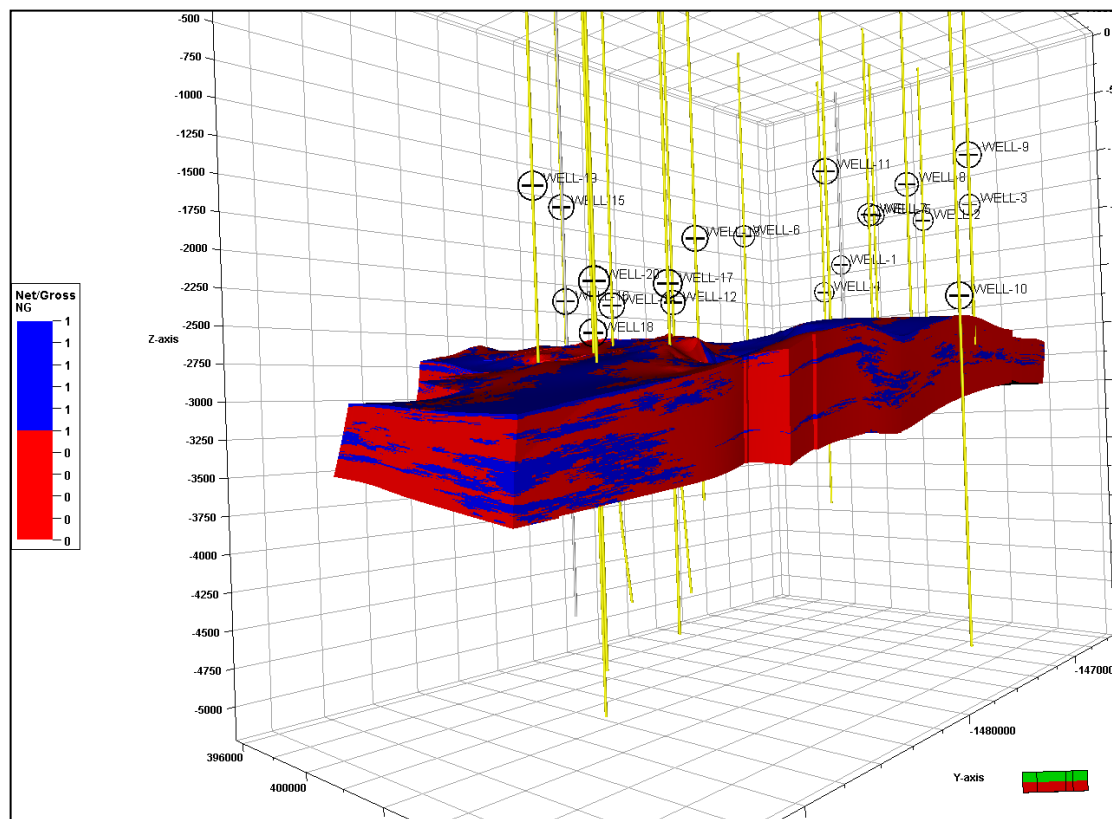


Figure 72. Net to gross process developed in the generated volume (static model).

In order to make hydrocarbon volume calculations in the Eastern Marlim oilfield, the volumes previously generated in the Volume Calculation application of the Petrel software were used to calculate the deterministic model. The mentioned model yields 3,774 billion (Bbls) (Fig. 73); having a good correlation with the proven reserves for the post-salt reservoirs of the Eastern Marlim oilfield that according to the ANP (2014) are approximately 4.1 billion (Bbls). The difference between the proven reserves of the oilfield and the deterministic result of the current investigation could have a strict relationship with reserves of oil accumulated in other minor reservoirs zones in the oilfield (Miocene, Eocene, and Cretaceous reservoirs).

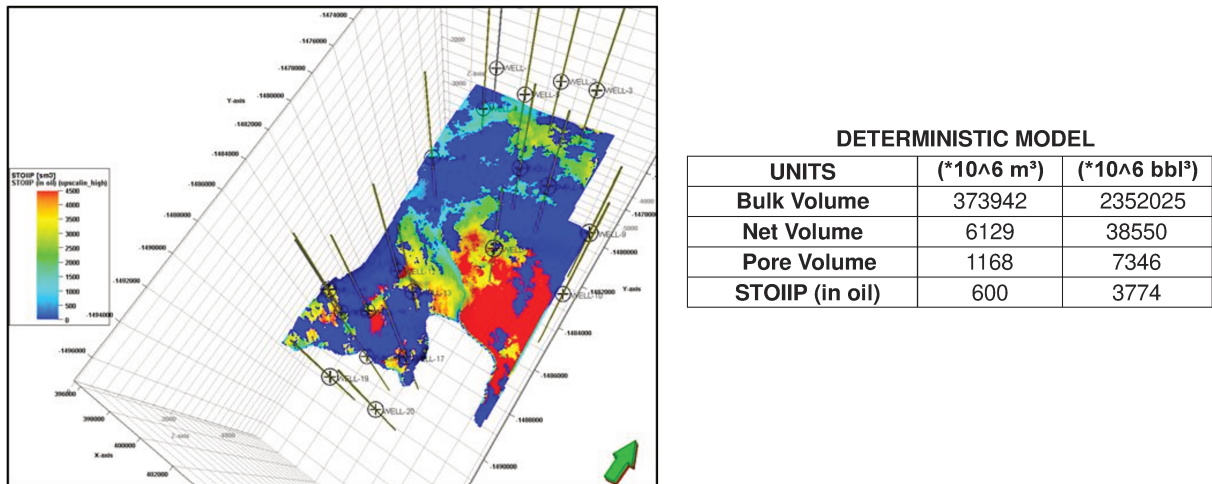


Figure 73. OOIP calculation (deterministic model) for the Eastern Marlim oilfield.

Later, in order to obtain a range of uncertainty in the current proposed static model, a probabilistic model was generated using the Monte Carlo method. For this research project, 70 models were generated, obtaining the following probabilities: P10= 3.603 (Bbls), P50= 3.678 (Bbls), and P90= 3,763 (Bbls) (Fig. 74).

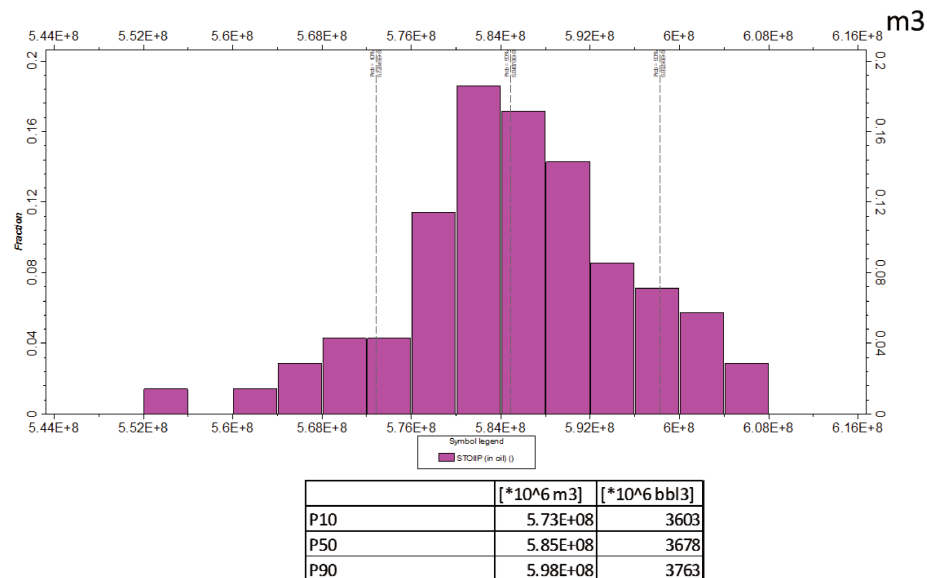


Figure 74. Probabilistic modeling for the Eastern Marlim oilfield.

In this way, all the mentioned information allowed to obtain a 3D geological modeling based on the available subsurface information provided by the ANP honoring the geological proxies of the research area and achieving a respectable and realistic reservoir static model. Finally, the current research can be used as an analog methodology, aiming to enhance the quantity and quality of information of simulation data in siliciclastic reservoir studies in the petroleum geology field.

7. FORWARD MODELING LIMITATIONS

The principal limitations involved in the current research project were related to the available dataset and software modeling restrictions.

7.1 STRATIGRAPHIC FRAMEWORK

The lack of cores and thin slides descriptions to strengthen the results, restricted to make broader and more rigorous conclusions.

7.2 PETROPHYSICAL MODELING

A small number of wells with petrophysical information measured in the oilfield (wells 4-7-13-15-19) limited a deeper approach in the development of the current research project.

7.3 SEISMIC INTEGRATION

The lack of a 3D seismic volume that occupies the entire area of the Eastern Marlim oilfield limited the generation of a comprehensive 3D geological modeling, and thus improving the visualization and understanding of the study area.

7.4 3D GEOLOGICAL MODELING

The most important limitation was not having the appropriate hardware (PC) that would help to bring about a more robust modeling ("Layering and Gridding" in more detail), through more powerful simulations that could have provided a better result.

8. DISCUSSION

8.1 STRATIGRAPHIC AND DEPOSITIONAL MODEL

The interval of study in the current research correlates to the E74 sequence proposed by Winter et al. (2007). The mentioned sequence includes the Ubatuba (Geribá Member), Carapebus and Emborê (São Tomé and Grussaí Members) formations. According to Winter et al. (2007), this sequence contains sandstones deposits that occur amalgamated on the Blue Marker into deep-waters. These affirmations had a very good correlation with our results where Oligocene-Miocene sandstones bodies of the Carapebus Formation were deposited above the Blue Marker. According to Winter et al. (2007), the mentioned geological marker occurs practically in the entire basin, composed of calcilutites rich in nanoplankton, representing an important flooding event in the basin (MFS). In addition, he stated that these layers of rocks, originated by phytoplankton deposits were developed under specific ecological conditions of explosive growth, called phytoplanktonic flowering. The event that resulted in the formation of this particular sedimentary deposit was virtually instantaneous, in a geological time scale, and extremely comprehensive in area, characteristics of a true geological marker (Winter et al., 2007). Moreover, as stated by Winter et al. (2007), the other rocks that make up the mineral suite of this sequence follow the pattern of the Tertiary package with sandstones resulting from dense turbidite flows or mixed turbidite systems, siltstones and shales, in addition to diamactites and marls, subordinately. Along these lines, the observations previously stated have a very good correlation with the current outcomes, where the studied Oligocene-Miocene reservoirs have an essential relationship with high-density turbiditic flows related to amalgamated sandstones bodies resulting in a submarine lobe complex following the regional pattern of the Tertiary turbiditic deposition.

8.2 PETROPHYSICAL MODELING

Other studies developed in the adjacent Marlim Oilfield located in the center and western portion of the Marlim Complex; demonstrating a very good match with the presented findings. According to Milani & Araújo (2003), the Marlim reservoirs consists of a series of unconfined, coalescing submarine lobes, resulting in a relatively homogeneous and massive sandstone body of medium to fine particle size, and porosity values about 25%, with an average thickness of 47m, almost unconsolidated. In this way, the mentioned information has an excellent match with our results, associated with the reservoir facies found in the Eastern Marlim oilfield, characterized by the Sm and Smcf lithofacies and Ss1 and Ss2 petrophysical

lithotypes. These reservoirs are in general massive unconsolidated to semi-solid cohesive whitish cream sandstones with average particle size, sub-round rounding, regular selection, minor calciferous/major feldspathic composition, good porosity (15-25% average), and recurrent light brown oil stains with total fluorescence and immediate cut. These facies represent different stages of deposition of bipartite turbidite flows, resulting in lateral and vertical extent amalgamated sandstones bodies, with an average thickness of 50m approximately. Furthermore, in the same cited work, Milani & Araújo (2003) stated that in the western and northeastern portions of the Marlim oilfield, deposits of elongated geometry appear, recording sandy facies attached to distal lobes feeding channels. Hence, the mentioned findings have a strict relationship with the Middle Sandstone (MS) identified in our research, which record coarsest sediments that become finer towards the top, that are observable in the developed chronostratigraphic correlations and distribution maps, displaying channel features deposits attributed to high-density turbidity flows. As well, according to Milani & Araújo (2003), the compositional analysis of the Marlim sandstones revealed an arcossian composition, with about 30% of feldspars, mainly potassic. The mentioned authors identified that the alteration rate of these minerals is low when is compared to other tertiary reservoirs in the Campos Basin, which reduces the presence of kaolinite and other clay minerals that potentially impair flow during production. The mentioned stated findings have once again a very good correlation with the existing results since the reservoir facies of the Eastern Marlim oilfield shows in general a minor calciferous/major feldspathic composition. Moreover, the best reservoir features were observed in the Sm lithofacies or Ss1 petrophysical lithotype (Clean Sandstones), and fair to good characteristics for the Smcf lithofacies or Ss2 petrophysical lithotype (Muddy Sandstones) taking into account the calciferous/feldspathic composition of the last one.

8.3 STRUCTURAL MODELING

As stated by Tinoco and Corá (1991) the Marlim Complex itself embraces a similar stratigraphic and structural context. In this way, the principal differences in the oil complex are eminently structural. According to the cited authors, towards the western, northern and southern directions of the Marlim complex, the trap is eminently stratigraphic given by the pinch out of the reservoirs against the shales that surrounded the sandy deposits, in contrast to the eastern part, where the accumulation ends against a normal listric fault. In summary, the different findings achieved in the adjacent Marlim oilfield have a very good correlation with the results obtained in the current research in the Eastern Marlim oilfield

taking into account their similar nature of deposition. Regarding the structural model developed in the current research, the Eastern Marlim oilfield follows the structural style of the basin, which according to Milani & Araújo (2003) is predominantly subject to a distensive regime, causing normal faults with listric geometry associated with salt tectonics, which have an excellent correlation with the obtained results.

8.4 3D GEOLOGICAL MODELING (STATIC MODEL)

Regarding the 3D geological modelling developed in the current research; other authors have made approximations related to this issue. The variability of the facies and petrophysical properties as well as the consequent heterogeneity of the reservoir proved to be consistent with the context of the Southeast Brazilian margin and the type of turbidite reservoirs proposed by Bruhn et al. (2003). It is possible to establish a comparison between the achievements of the proposed lithological facies model developed in the current research and the sand distribution map of Peres (1993). According to Peres (1993), the further development of sands of the turbidite system of the Campos Basin shows a NW-SE direction, having an excellent correlation with the current results. In addition, as cited in the same study, in the Marlim Complex the sands reach a thickness of 150m with greater development for SE (where is located the Eastern Marlim oilfield), which is very consistent with the information provided in the present study. Furthermore, it is possible to establish relationships between the directions of development of the deposits corresponding to the reservoir and non-reservoir lithofacies, which in general follow the general pattern of deposition proposed by Peres (1993). Concerning the porosity models, the present outcomes display porosities varying between 15% and 35% with an average of 25%. These results can be compared to the measurements of Bruhn (2001) in samples of turbiditic reservoirs of Oligocene-Miocene age in the Campos Basin. The mentioned author obtained two values of porosities according to granulometric and selection trends. Then for coarse and poorly selected deposits, the mentioned author obtained 31.8%, and for finer and better-selected deposits, he obtained 26.3% porosity values, displaying again a good correlation with the results obtained in the petrophysical modeling. Besides, according to Machado et al. (2004), the geometry of the Carapebus Formation in the proximal portion of the Campos Basin has a lobe feature, with layers deposited in several events. In the Eastern Marlim oilfield, a lobe complex depositional framework was observed having a strict relationship with the mentioned features observed by the mentioned authors; where these lobes are considered the best reservoirs of the Campos basin.

Finally, the ANP (2016) stated that the Eastern Marlim oilfield comprises sandstone reservoirs of the Carapebus Formation, dating from Miocene to Oligocene-Miocene age. Additionally, it can be found calcareous-sandstone reservoirs in the Quissamã Formation of the Albian Macaé group (known as Jabuti); and calcareous reservoirs of predominantly microbial origin in the Macabu Formation of the Aptian Lagoa Feia group. The primary mechanism of production is gas in solution, and, in some areas, there is the action of aquifers. Water injection is used as a reservoir pressure maintenance mechanism in the Oligocene-Miocene reservoirs. The average API grade of the produced oil in the oilfield is 20.7°. Furthermore, as cited by the ANP (2014), at least 4.1 billion barrels of oil (Bbls) are accumulated in the post-salt reservoirs of the Eastern Marlim oilfield, in Oligocene-Miocene reservoirs respectively. In addition, the ANP (2016) calculated 5.8 billion barrels of oil (Bbls) in the entire oilfield, assuming all the respective accumulations in all the mentioned reservoirs. In this manner, the hydrocarbon volume calculations developed by the ANP (2014) for the post-salt reservoirs of the Eastern Marlim oilfield (specifically the Oligocene-Miocene reservoirs of the Carapebus Formation) have a very good correlation with the current outcomes; where the deterministic model indicate at least 3,774 billion barrels of oil (Bbls), and the probabilistic models yields possibilities varying from 3.603 (P10), 3.678 (P50), and 3,763 Bbls (P90), respectively. The dissimilarity between the mentioned results could have a relationship with reserves of oil accumulated in other minor reservoirs zones in the oilfield (Miocene reservoirs), which were not taken into account in the current study.

9. CONCLUSIONS

The Oligocene-Miocene section studied in this research belongs to the E74 sequence (second-order sequence in the present investigation) of Winter et al. (2007), which, in turn, is part of the first-order HST of the Campos Basin. Turbiditic sandstones bodies deposited in a deepwater setting in the Eastern Marlim oilfield represent most of this time interval. Four principal lithofacies were identified in the entire section through stratigraphic and sedimentological interpretations, where two are eminently reservoir facies associated with sandy facies (Sm and Smcf lithofacies) and the remaining lithofacies are evidently non-reservoir facies represented by shaly and calcareous deposits (Sh and M lithofacies). The environmental interpretation of the reservoir lithofacies are related to transport through long distances in the basal layer of a turbulent flow and rapid mass deposition (Sm) and mass deposition from the residual suspended load of a concentrated turbulent flow (Smcf), representing different stages of deposition of bipartite turbidite flows, resulting in lateral and vertical extent amalgamated sandstones bodies. Regarding the non-reservoir facies (Sh and M), they were interpreted as the product of slumps and/or cohesive debris flows, slip deposits or canyon flank in the study area.

Three different major zones were identified, called as Lower sandstone (LS), Middle sandstone (MS), and Upper sandstone (US), recognized from the developed lithofacies characterization and chronostratigraphic correlations taking into account correlatable electric and/or lithological markers. In this way, the Lower Sandstone (LS) marks the early stages of an entire HST cycle, deposited after the deposition of the maximum flooding surface (MFS) associated with the regional Blue Marker. Regarding the MS, this zone display laterally and vertically amalgamated channel features deposits attributed to high-density turbidity flows marking the principal stages of the HST. Lastly, the US zone, represented by laterally amalgamated sandstones, which pinch out toward the middle and eastern portion of the field, marking the final stages of the HST. The sand proportion and distribution maps of the mentioned zones exhibit lobe-shape features and discrete channelized structures. Along the axis of the channels, a thickest distribution of sandstones is present, representing distal lobes feeding channels.

The petrophysical analysis based on lithotypes demonstrated to be a powerful tool to enhance the lithofacies characterization in the study area. At least, five petrophysical lithotypes were identified displaying an excellent correlation with the developed lithofacies characterization in the Eastern Marlim oilfield. Like this, each petrophysical lithotype

defined specific features of petrophysical properties that allows to classifying them as reservoir (Ss1 and Ss2), retardant (Ss-Lm) or seal-cemented rocks (Lm and Sh). As a result, the reservoirs facies (Ss1 and Ss2) have and strict relationship with the Sm and Smcf lithofacies, displaying good porosities values and petrophysical and lithological characteristic to be consider as excellent reservoir rocks, as expected. In addition, the mentioned reservoir facies were identified in the US, MS and LS zones, observing an increase of oil shows in the US and MS in contrast to the LS. We concluded through the developed petrophysical analysis that the US display oil accumulations in the Smcf lithofacies or Ss2 petrophysical lithotype (Muddy Sandstones), but with a decrease in their petrophysical properties related with their compositional nature. On the other hand, the MS displays the principal accumulations in the study area associated with the Sm lithofacies or Ss1 petrophysical lithotype (Clean Sandstones), with excellent features considered as the best reservoir zone in the Eastern Marlim oilfield. Unlikely, although the LS exhibited some clean sandstones (Sm lithofacies and Ss1 petrophysical lithotype) it is unusual to find hydrocarbon shows in the study area. This is explained because the LS is located just below the oil/water contact (OWC) in best part of the Eastern Marlim oilfield, pointing towards to find water accumulations in the majority of this zone. However, the LS had some sandstone layers located close to the MS, where oil accumulations were found, situated above the OWC. Finally, with reference to the retardant (Ss-Lm) and seal-cemented rocks (Lm and Sh) petrophysical lithotypes, they had a tremendous correlation with the identified Sh and M lithofacies, considered as non-reservoir rocks in the entire section of study. In addition, taking into account the lack of measures of petrophysical conditions in the studied section the developed petrophysical characterization improved and enhance the understanding of the Oligocene-Miocene reservoirs at reservoir scale in the Eastern Marlim oilfield.

The development of the 3D geological modeling of the research area demonstrated good correspondence with previous studies. The lithological and petrophysical models generated and integrated in the developed static model displaying values that are in accordance with the studies developed for the turbiditic deposits of the Campos Basin in Brazil (Peres, 1993, Bruhn, 2001, Machado et al. 2004, and, Correia, 2015), indicative of the heterogeneity and complexity of these types of reservoirs. In addition, the hydrocarbon volume calculations developed in the current research have a very good match with the proven hydrocarbon reserves calculated by the ANP (2014, 2016).

Lastly, integrating the entirely mentioned results, the 3D geological modeling of the Oligocene-Miocene section of the Eastern Marlim oilfield displays the application and

integration of different parameters such as seismic and well log interpretation, lithofacies and petrophysical analysis, chronostratigraphic correlations, stratigraphic and depositional modeling, structural and fault modeling, etc.

To conclude, different methods were used and can be suggested aiming to characterize these kind of deepwater turbidite strata that could be applied in different academic and/or industrial purposes. Different mathematical and statistical approaches are used in a static reservoir modeling, displaying excellent outcomes taking into account that the mentioned disciplines are powerful geological modeling tools, but they need to be mixed with a geological background, aiming to firmly support the subsurface framework and achieve a more realistic approach.

10. REFERENCES

- Abreu V., 2010. Sequence stratigraphy of siliciclastic systems: the ExxonMobil methodology, Atlas of exercises. SEPM. Tulsa, 226 pp.
- ANP. Plano de Desenvolvimento Aprovado, Reunião de Diretoria nº 785 de 23/12/2014 Resolução nº 1311/2014, 2014.
- ANP. Plano de Desenvolvimento Aprovado, Reunião de Diretoria nº 785 de 23/12/2014 Resolução nº 1311/2014, 2016.
- Asquith G. and Krygowski D., 2004. Basic Well Log Analysis, 2nd edition. AAPG Methods in Exploration Series, pp 28-244.
- Azevedo, L., 2009. Atributos sísmicos na caracterização de reservatórios de hidrocarbonetos. 2009. 165 f. Dissertação (Mestrado em Geociências) - Universidade de Aveiro, Aveiro. 2009.
- Azevedo, L.; Pinheiro, L.M.; Kaschaka, A.; Abbassi, H., 2010. Caracterização de reservatórios de hidrocarbonetos utilizando atributos sísmicos. Congresso nacional de geologia, geotéc – sociedade geológica de Portugal, 8. Ed –Terra, Rev. Elec. Ciências da Terra, 10 (11).
- Bacoccolli G., and Toffoli L.C., 1988. The role of turbidites in Brazil's offshore exploration – a review. Offshore Tech. Conf. Proc. 5659, p. 379-388.
- Bacoccolli G., Morales R.G., Campos O.A.J., 1980. The Namorado Oil Field: A major oil Discovery in the Campos Basin, Brazil. *In*: Halbouty M.H. (eds). Giant oil and gas fields of the decade: 1968-1978. Am. Assoc. Petrol. Geol. Mem. 30, p. 329-338.
- Baldissera, P.R. Modelagem Estocástica de Fácies para Caracterização da Distribuição Espacial das Heterogeneidades de Reservatório. Dissertação (Mestrado em Geoengenharia de Reservatório) – Universidade Estadual de Campinas, Faculdade de Engenharia Mecânica, Instituto de Geociências. 1992. 2000
- Banco de dados de exploração e produção, BDEP Webmaps. Available in: <http://app.anp.gov.br/webmaps/>. Accessed in April 20 of 2016.
- Bessa F., 2004. Reservoir characterization and reservoir modeling in the northwestern part of Hassi Messaoud field Algeria. Thesis Submitted to the Graduate Institute at the Departement of Earth Sciences of the University of Hamburg, Hamburg, Germany, 93 pp.

Bohling G., 2007. Introduction to geostatistics. In *Hydrogeophysics: Theory, Methods, and Modeling*. Boise State University. Kansas Geological Survey, Boise, Idaho, U.S.A.

Brown A.R., 2004b. Flat Spots Are Not Always Flat. *AAPG Search and Discovery*, Article #40119.

Bruhn C.H.L.; Gomes J. A.T.; Lucchese C.D.; Johann P.R. Campos Basin: reservoir characterization and management – Historical overview and future challenges. OTC 15220. *In: Offshore Technology Conference*, Society of Petroleum Engineers, Houston, Texas, USA. 2003.

Bruhn C.H.L. Contrasting Types of Oligocene/Miocene Giant Turbidite Reservoirs from Deep Water Campos Basin, Brazil. *AAPG Distinguished Lecture*. 2001.

Caetano, H., 2012. Integration of Seismic Information in Reservoir Models: Global Stochastic Inversion, In: GOMES, J.S. (ed.). *New Technologies in the Oil and Gas Industry*. Publisher: Intech,. p. 119-150. <http://dx.doi.org/10.5772/52308>

Cainelli, C. & Mohriak, W. U. 1999. Some remarks on the evolution of sedimentary basins along the eastern Brazilian continental margin. *Episodes*, 22(3):206-216.

Carminatti M., 1987. Relações entre a Evolução Estrutural e a Ocorrência de Campos Gigantes de Hidrocarbonetos na Área Nordeste da Bacia de Campos. *In: Rio de Janeiro-Espírito Santo Symposium*, p. 43-56.

Casar-González, R. Díaz-Viera, M.A., Murillo-Muñetón, G., Velasquillo-Martínez, L., García-Hernández J. & Aguirre-Cerda, E., 2012. Chapter 9: A 3D geostatistical model of Upper Jurassic Kimmeridgian facies distribution in Cantarell oil field, Mexico. In *Multiphysics Modeling, Volume 6. Mathematical and Numerical Modeling in Porous Media: Applications in Geosciences*. Editors Martín A. Díaz Viera, Pratap N. Sahay, Manuel Coronado and Arturo Ortiz Tapia, ISSN: 1877-0274

Catuneanu, O., et al., 2006. Towards the standardization of sequence stratigraphy: *Earth-Science Reviews*, v. 92, p. 1–33, DOI:10.1016/j.earscirev.2008.10.003.

Cazzola, C, Mutti, E., and Vigna, 8., 1985: Cengio turbidite system, Italy, in A.H. Bouma, W.R. Normark, and N.E. Barnes, eds., *Submarine fans and related turbidite systems*; Springer-Verlag, New York, p. 179-183.

Correia, M.G., 2014. Representação de Reservatórios Carbonáticos Naturalmente Fraturados em Simulação de Reservatórios. 163f. Tese (Doutorado em Ciências e Engenharia de Petróleo) – Universidade Estadual de Campinas, Faculdade de Engenharia Mecânica, Instituto de Geociências.

Correia U. M., 2015. Integração de dados sísmicos e de poços para a modelagem de reservatórios siliciclásticos da Bacia de Campos, Brasil. Tese (Mestrado em Geociências) – Universidade Estadual de Campinas, Instituto de Geociências. Campinas, 2015

Cosentino, L. Integrated Reservoir Studies. Editions Technip, 2001. 310p.

Darcy, H., 1856. Les Fontaines Publiques de la ville de Dijon, Dalmont, Paris.

De Gasperi, A. & Catuneanu, O., 2014. Sequence stratigraphy of the Eocene turbidite reservoirs in Albacora field, Campos Basin, offshore Brazil. AAPG Bulletin, v. 98, no. 2, pp. 279–313, DOI: 10.1306/07031312117

De Jager G., 2012. The influence of geological data on the reservoir modelling and history matching process. PhD Thesis, Delft University of Technology.

Delgado L., 2017. Petroleum Geochemical Characterization and Petroleum Systems Modeling of the Eastern Marlim Oilfield, Campos Basin, Brazil. Master Thesis, Geosciences Institute, University of Campinas, 101 p.

Doligez, B.; Beucher, H.; Lerat, O.; Souza, O., 2007. Use of a Seismic Derived Constraint: Different Steps and Joined Uncertainties in the Construction of a Realistic Geological Model. Oil & Gas Science and Technology – Rev. IFP, v. 62, n. 2, pp. 237-248. <http://dx.doi.org/10.2516/ogst:2007020>

Doll H. G., 1948. The SP log, theoretical analysis and principles of interpretation: Trans., AIME, v. 179, p.146-185.

Dupuit, J., 1857. Mouvement de l'eau a travers le terrains permeables, C. R. Hebd. Seances Acad. Sci., 45, 92 – 96.

Elliott, T., Apps, G., Davies, H., Evans, M., Ghibaudo, G., and Graham, R.H., 1985: A structural and sedimentological traverse through the Tertiary foreland basin of the external Alps of southeast France, in P. Allen, P. Homewood, and G. Williams, eds., International Symposium on Foreland Basins, Fribourg, Switzerland; Excursion Guidebook, p. 39-73.

Fainstein, R., Jamieson, G., Hannan, A., Biles, N., Krueger, A. and Shelander, D., 2001. Offshore Brazil Santos basin exploration potential from recently acquired seismic data: Presented at 7th International Congress of the Brazilian Geophysical Society.

Fancher G. H., Lewis J. A, and Barnes K. B., “Some Physical Characteristics of Oil Sands,” The Pennsylvania State College Bull. (1933), 12, 65.

Farre, J.A., McGregor, B.A., Ryan, W.B.E, and Robb, J.M., 1983: Breaching the shelf-break: passage from youthful to mature phase in submarine canyon evolution; in O.J. Stanley and G.T. Moore, eds., *The shelfbreak: Critical interface on continental margins*; Soc. Econ. Paleont. Mineral. Spec. Publ. 33, p. 25-39.

Guardado L. R., Gamboa L. A. P., Lucchesi C. F. 1989. Petroleum geology of the Campos Basin, Brazil: a model for producing Atlantic type basins. In Edwards J. D. and Santogrossi P. A., eds., *Divergent/passive margin basins*, *AAPG Memoir*, **48**: 3–80.

Guardado, L. R., Spadini, A. R., Brandão, J. S. L., Mello, M. R. 2000. Petroleum system of the Campos Basin. In Mello M. R. and Katz B. J., eds., *Petroleum systems of South Atlantic margins*, *AAPG Memoir*, 73: 317–324.

Hagen, R.A., Bergersen, D.D., Moberly, R. and Coulbourn, W.T. 1994. Morphology of a large meandering submarine canyon system on the Peru-Chile forearc. *Marine Geology*, 119, 7–38.

Haldorsen, H.H., Chang, D.M., 1986. Notes on stochastic shales- from outcrop to simulation model. In: Lake, L.W., Carroll, H.B. (eds.). *Reservoir characterization*: London, Academic Press, p. 445 - 485.

Hardage B.; Remington R.L.; Murray P.E., 2006. Chronostratigraphic Surfaces and Seismic Reflections. *AAPG Search and Discovery*, Article #40212.

Jackson M.P.A., and Talbot C.J., 1986. External shapes, strain rates, and dynamics of salt structures. *Geol. Soc. Am. Bull.*, v. 97, p. 305-323.

Kendall, C. & Alnaji, N. S, 2002. Carbonate Response to Changing Base Level: Case Histories and Comparisons from the Permian of West Texas and the Jurassic of Saudi Arabia, Abstracts American Association of Petroleum Geologists. Annual Convention, Houston, p. A91-92.

Kuenen, P.H., and Migliorini, C.I. 1950. Turbidity currents as a cause of graded bedding. *Journal of Geology*, 58 (2), 91-127.

Kuenen, P.H. 1957. Sole markings of graded greywacke beds. *Journal of Geology* , 65, 231-258.

Larionov, V. V. (1969), *Radiometry of boreholes* (in Russian), NEDRA, Moscow.

Lastras, G., Canals, M., Urgeles, R., Amblas, D., Ivanov, M., Droz, L., Dennielou, B., Fabr s, J., Schoolmeester, T., Akhmetzhanov, A., Orange, D. and Garc a-Garc a, A. 2007. A walk down the Cap de Creus Canyon, Northwestern Mediterranean Sea: Recent processes inferred from morphology and sediment bedforms. *Marine Geology* , 246, 176-192.

Lee, S.-Y., Carle, S.F., Fogg, G.E., 2007. Geologic heterogeneity and a comparison of two geostatistical models: Sequential Gaussian and transition probability-based geostatistical simulation. *Advances in Water Resources*, v. 30, p. 1914–1932. <http://dx.doi.org/10.1016/j.advwatres.2007.03.005>

Leverett M. C. and Lewis W. B., 1941. Steady Flow of Oil-Gas-Water Mixtures through Unconsolidated Sands,” *Trans. AIME* , **142**, 107.

Lucia F.J., 2007. *Carbonate Reservoir Characterization. An Integrated Approach*. Springer, Berlin Heidelberg, 341 pp.

Matheron G., 1970. La théorie des variables régionalisées et ses applications. Cahiers du centre de morphologie mathématique, Fascicule 5. School of mines of Paris. Translation, The theory of regionalized variables and its applications.

May J.A., Warme J.E., Slater R.A., 1983. Role of submarine canyons on shelfbreak erosion and sedimentation; modern and ancient examples. *In: Stanley D.J., Moore G.T (Eds). The shelfbreak; critical interface on continental margins. Soc. Econ. Paleon. Mineral. Spec. Public. No. 33, p. 315-332.*

Mello, M. R., Koutsoukos, E. A. M., Mohriak, W. U., Bacocoli, G., 1994. Selected petroleum systems in Brazil. *Memoirs. American association of petroleum geologists*, 60: 499-512.

Miall, A.D., 1985. Architectural element analysis: A New Method of Facies Analysis Applied to Fluvial Deposits; *Earth Sciences. Rev. Vol. 22; pp. 261-308.*

Machado L.C.R.; Kowsmann R.O.; Almeida W.; Murakami C.Y.; Schreiner S.; Miller D.J.; Orlando P.; Piaulino V. Geometria da porção proximal do Sistema turbidítico moderno da Formação Carapebus, Bacia de Campos; modelo para heterogeneidades de reservatório. *B. Geoci. Petrobras, Rio de Janeiro*, v. 12, n. 2, p. 287 – 315, 2004.

Mallet J. L., Jacquemin P., and Cheimanoff N., 1989. GOCAD project: Geometric modeling of complex geological surfaces, *SEG Expanded Abstracts* 8, 126.

Mata-Lima, H. Geostatistic in Reservoir Characterization: From Estimation to Simulation Methods. *Estudios Geol.*, v. 61, p. 135-145, 2005.

Milani, E. J. & Araújo, L. M., 2003. Recursos minerais energéticos: petróleo. *In: Bizzi, L. A.; Schobbenhaus, C.; Vidotti, R. M. & Gonçalves, J. H. (eds.). Geologia, tectônica e recursos minerais do Brasil, Brasília, CPRM*, p. 541-576.

Mitchum, R. M., Jr., 1977. Seismic stratigraphy and global changes of sea level, part 11: glossary of terms used in seismic stratigraphy. In: Payton, C. E. (ed.), *Seismic Stratigraphy – Applications to Hydrocarbon Exploration*. American Association of Petroleum Geologists Memoir 26, 205–212.

Mohriak W. U., Mello M. R., Dewey J. F., Maxwell J. R., 1990. Petroleum geology of the Campos Basin, offshore Brazil. *Geological Society Special Publications*, 50: 119-141.

Mutti E., 1985. Turbidite systems and their relations to depositional sequences. In: Zuffa G.G. (ed). *Provenance of arenites*. Reidel, Holland, p. 65-93.

Mutti E. & Normark. W.R., 1987. Comparing modern and ancient turbidite systems: Problems and concepts. In: Legget J., Zuffa G.G (Eds). *Marine and clastic sedimentology: concepts and case studies*. Graham and Trotman, London, p. 1-38.

Nascimento T. M., Menezes P. T. L., Braga I. L., 2014. High-resolution acoustic impedance inversion to characterize turbidites at Marlim Field, Campos Basin, Brazil. *Interpretation, Society of Exploration Geophysicists and American Association of Petroleum Geologists*, Vol. 2, No. 3, pp. T143–T153

Nelson, M.P., Hart, S.L., Cavette, G.1., and Zienianski, WP., 1988: Geology and development of the Pitas Point Gas Field; *Am. Assoc. Petrol. Geol. Bull.*, v. 72, p. 390-391 (abstr.).

Nilsen, T.H., 1990: Santonian, Campanian, and Maestrichtian depositional systems, Sacramento Basin, California, in R.Y. Ingersoll and T.H. Nilsen, eds., *Sacramento Valley Symposium and Guidebook*; *Pac. Sect. Soc. Econ. Paleon. Mineral. Field Trip Guidebook*, v. 65, p. 95-132.

Normark W.R., 1980. Modern and ancient submarine fans. *Am. Assoc. Petrol. Geol. Bull.*, v. 64, p.1108-1112.

Normark W.R., Piper D.J.W., Hess G.R., 1979: Distributary channels, sand lobes, and mesotopography of Navy submarine fan, California Borderland. With applications to ancient fan sediments; *Sedimentology*, v. 26, p. 749-774.

Normark W.R., Piper DJW., Stow D.A.Y., 1983: Quaternary development of channels, levees, and lobes on middle Laurentian Fan; *Am. Assoc. Petrol. Geol. Bull.*, v. 67, p. 1400-1409.

Overeem I., 2008. Course: "Geological Modeling: Introduction"Community Surface Dynamics Modeling System, the University of Colorado at Boulder.

Peres W.E., & Arso L.P., 1986: O uso da sísmica na delimitação de acumulações de hidrocarbonetos na Bacia de Campos-Brasil; *Boletim Tecnico APREL*, v. 15, p. 101-115.

Peres, W. E., 1993, Shelf-fed turbidite system model and its application to the Oligocene deposits of the Campos Basin, Brazil: AAPG Bulletin, 77, 81–101.

Petrel E&P 2013. Software of Schlumberger.

Posamentier, H.W.; Kolla, V. Seismic Geomorphology and Stratigraphy of Depositional Elements in Deep Water Settings. SEPM Journal of Sedimentary Research, v. 73, n. 3, p. 367–388, 2003. <http://dx.doi.org/10.1306/111302730367>

Pratson, L.F. & Coakley, B.J. 1996. A model for the head ward erosion of submarine canyons induced by downslope-eroding sediment flows. Geological Society of America Bulletin, 108 (2), 225-234.

Qi, L., Carr, T.R. & Goldstein, R.H., 2007. Geostatistical three-dimensional modeling of oolite shoals, St. Louis Limestone, southwest Kansas. AAPG Bulletin, 91 (1), 69–96.

Rangel H. D.; Martins F. A. L.; Esteves F. R.; Feijó F. J., 1994. Bacia de Campos. Boletim de Geociencias. Petrobras, Rio de Janeiro, v. 8, n. 1, p. 203 – 217.

Ravenne, C.; Galli, A.; Doligez, B.; Beucher, H.; Eschard, R., 2002. Quantification of facies relationships via proportion curves. In: Armstrong, m.; Hettini, C.; Champigny, N.; Galli, A.; Remacre, A. (eds.) Geostatistics rio 2000. Dordrecht, Kluwer academic press, p. 19-39.

Ravenne, C., 2002a. Stratigraphy and oil: a review. part 1. exploration and sequence stratigraphy: observation and description. oil & gas science and technology – rev. ifp, v. 57, n. 3, p. 211-250, <http://dx.doi.org/10.2516/ogst:200201682>

Ravenne, C., 2002b. Stratigraphy and oil: a review. Part 2. Characterization of reservoir and sequence stratigraphy: quantification and modeling. Oil & Gas science and technology – rev. ifp, v. 57, n. 4, p. 311 340, 2002b. <http://dx.doi.org/10.2516/ogst:2002021>

Remacre, A.Z.; Normando, M.N.; Sancevero, S.S., 2008. Krigagem das proporções utilizando a krigagem da média: uma ferramenta auxiliar na modelagem de reservatórios. Revista Brasileira de Geociências, v. 38, n. 1 – suplemento, p. 82-77, 2008.

Rider M., 1996. The Geological Interpretation of Well Logs. Gulf Pub. Co, 280 pp.

Ricci Lucchi, E. & Valmori, E., 1980: Basin-wide turbidites in a Miocene, over-supplied deep-sea plain; a geometrical analysis; Sedimentology, v. 27, p.241-270.

Robert, L. & Slater T, 2003. Reservoir quality of the coastal basins of southeast Brazil. Robertson research international limited. Report No. CL046.

Robinson A., Griffiths P., Price J., Hegre J., Muggeridge A., (Eds.), 2007. *The future of geological modeling in hydrocarbon development*. The Geological Society, London, 217 pp.

Seismic data interpretation. Available in: <http://www.open.edu/openlearncreate/mod/page/view.php?id=41010>. Accessed in August 15 of 2016.

Serra, O. 1986. Fundamentals of well-log interpretation. 2. The interpretation of logging data. Developments in Petroleum Science. 684 pp.

Schaller H., 1973. Estratigrafia da bacia de Campos. Congresso Brasileiro de Geologia. Sociedade Brasileira de Geologia, v. 27, p. 247-258.

Schlumberger, 1972. Log interpretation/Charts. Houston, Schlumberger Well Services, Inc.

Schon J., 2015. *Physical Properties of Rocks*. Elsevier, Amsterdam, 496 pp.

Terry R. E. & Rogers J. B, 2014. Applied Petroleum Reservoir Engineering, 3rd Edition. Prentice Hall.

Theis, C. V., 1935. The relation between the lowering of the piezometric surface and the rate and duration of discharge of a well using groundwater storage, Eos Trans. AGU, 2, 519.

Tigre, C.A., Corá, C.A.G., Candido, A., 1990. Campos de petróleo em águas profundas na costa brasileira – privilégio da Bacia de Campos? In: PETROBRAS, Seminário de Geologia de Desenvolvimento e Reservatório, 4, Natal, Anais, 478-489.

Tinoco, P.M.B. & Corá, C.A.G., 1991. Campo de Marlim: contexto geológico e estratégia de produção. In: PETROBRAS, Seminário de Engenharia de Reservatórios, 4, Cabo Frio, Anais, 321-327

Vail, P. R., Todd R.G., and Sangree J.B., 1977, Seismic stratigraphy and global changes of sea level, part 5 — Chronostratigraphic significance of seismic reflections, in C. E. Payton, ed., Seismic stratigraphy: Applications to hydrocarbon exploration: AAPG, 99–116

Varhaug M., 2016. Basic Well Log Interpretation. *Oilfield Review*, Schlumberger.

Walker, R.G., 1980: Modern and ancient submarine fans: reply; Am. Assoc. Petrol. Geol. Bull., v. 64, p. 1101-1108.

Weimer, P., Link, M. H.(eds.), Seismic facies and sedimentary processes of submarine fans and turbidite systems. Springer-Verlag, New York, p. 323–347.

Winter W.R., Jhanert R.J., França A.B., 2007. Bacia de Campos, Boletim de Geociências da Petrobras, 15: 511-529. Cartas estratigráficas.

Wyckoff R. D., Botset H. G., Muskat M., and. Reed D. W, 1934. Measurement of Permeability of Porous Media, AAPG Bulletin, 18, No. 2, p. 161.

Wyckoff R. D. & Botset H. G., 1936. The Flow of Gas-Liquid Mixtures through Unconsolidated Sands, *Physics*, 7, 325.

Worthington P.F., 2007. Specialized well logging topics. In: Holstein E.D., Lake L., (Eds)., 2007. Petroleum Engineering Handbook. Society of Petroleum Engineers, United States of America, 74 pp.

Yarus, J.M. & Chambers, R.L., 1994. Stochastic Modeling and Geostatistics: Principles, Methods, and Case Studies. American Association of Petroleum Geologists. U.S.A.